UNIVERSITY OF CALIFORNIA SAN DIEGO

Mechanisms of prion aggregate spread and synaptic toxicity

A dissertation submitted in partial satisfaction of the
requirements for the degree
Doctor of Philosophy

in

Biomedical Sciences

by

Jessica Anne Lawrence

Committee in charge:

Professor Christina Sigurdson, Chair
Professor JoAnn Trejo, Co-Chair
Professor Xu Chen
Professor Jonathan Lin
Professor Gentry Patrick
Professor Jerry Yang

2020

The dissertation of Jessica Anne Lawrence is approved, and it is acceptable in quality and form for publication on microfilm and electronically:

_____

_____

_____

_____

_____
Co-Chair

_____
Chair

University of California San Diego

2020

DEDICATION

To:

My supportive parents, who inspired me to never work in the tech industry, which brought me to science. And my siblings, Jo and Jamie, who constantly remind me that I am the nerd of the family. I would not be where I am now without your encouragement.

TABLE OF CONTENTS

LIST OF FIGURES

ACKNOWLEDGEMENTS

This body of work is the result of my graduate school efforts to become a neurobiologist and expert in prion diseases. I am incredibly appreciative for the mentorship and training from my thesis advisor, Christina Sigurdson. Christina has patiently guided me over the years, providing me with stimulating scientific conversations that resulted in groundbreaking ideas and novel ways to tackle challenges. She has supported my goals and provided me with extensive opportunities. She has trusted me to develop my projects and ideas to completion, regardless of my pace and setbacks along the way, guiding me to be the scientist I have become, and for that I am grateful. I am thankful for my committee members, Dr. JoAnn Trejo, Dr. Xu Chen, Dr. Jonathan Lin, Dr. Gentry Patrick, and Dr. Jerry Yang, who have provided valuable input on my work and extraordinary mentorship, and all of which whom have been incredible collaborators. My success has been made possible by our tightknit community of lab members, past and present, who have supported me through all of these years and answered my endless questions. I would like to especially thank Patricia Aguilar-Calvo, a postdoc who has been in the lab as long as I have and provided me with so much guidance throughout the years; Tim Kurt for training me and believing in my potential when I first joined the lab; Taylow Winrow for managing the lab so smoothly and her encyclopedia of mouse knowledge; Cyrus Bett, who left such a legacy in the lab, as well as a beautiful project for me to finish; Patricia Gaffney for her mathematical mind; Alex Sevillano for his insight on protein structure; Julia Callendar for her introduction to cell signaling; Nazilla Anderson for her scientific enthusiasm; and the undergraduates Thu Nam and Helen Khuu for all of their hard work. I cannot speak enough to the incredible community at UCSD, and all of the professors, colleagues, and friends who have helped me along the way. I'm grateful for the Cores at UCSD who have put so many hours

into teaching me and helping with my projects; Don Pizzo in Pathology; Timo Meerloo, Ying Jones, and Vanessa Goodwill in EM; Jennifer Santini and Marcy Erb in Microscopy; Eric Griffis and Daphne Bindels at the Nikon Center. And most importantly, I am thankful for the support of my family, Mum, Dad, Jo, and Jamie, throughout my life, and my partner Scott Rosenberg throughout grad school because without any of you, I would not be the scientist I am today. To everyone apart of my PhD endeavor, thank you.

Chapter 2, in full, is a reprint of material as it appears in: Bett C*, **Lawrence J***, Kurt TD, Orru C, Aguilar-Calvo P, Kincaid AE, Surewicz WK, Caughey B, Wu C, Sigurdson CJ. Enhanced neuroinvasion by smaller, soluble prions. Acta Neuropathol Commun. 2017 Apr 21;5(1):32. doi: 10.1186/s40478-017-0430-z. The dissertation author was a first author of this paper. (*, co-first authors).

Chapter 3, in full, is a reprint of material submitted to be published in: **Lawrence, JA.**, Sigurdson C. Neuronal ESCRT-0 depletion accelerates synapse loss in prion disease.*in preparation*. The dissertation author was the primary author.

Chapter 4, in full, is a reprint of material submitted to be published in: **Lawrence, JA**, Sigurdson C. Arc and an impaired endolysosomal pathway contribute to synapse damage in early prion disease. *in preparation*. The dissertation author was the primary author.

VITA

2012	Bachelor of Science in Neurobiology, Physiology, Behavior, University of California Davis
2020	Doctor of Philosophy in Biomedical Sciences, University of California San Diego

PUBLICATIONS

Chau JY, Tiffany CM, Nimishakavi S, **Lawrence JA**, Pakpour N, Mooney JP, Lokken KL, Caughey GH, Tsolis RM, Luckhart S. Malaria-associated L-arginine deficiency induces mast cell-associated disruption to intestinal barrier defenses against nontyphoidal Salmonella bacteremia. Infect Immun. 2013 Oct;81(10):3515-26. doi: 10.1128/IAI.00380-13.

Dail M, Wong J, **Lawrence JA**, O'Connor D, Nakitandwe J, Chen SC, Xu J, Lee LB, Akagi K, Li Q, Aster JC, Pear WS, Downing JR, Sampath D, Shannon K. Loss of oncogenic Notch1 with resistance to a PI3K inhibitor in T-cell leukaemia. Nature. 2014 Sep 25;513(7519):512-6. doi: 10.1038/nature13495.

Bett C*, **Lawrence JA***, Kurt TD, Orru C, Aguilar-Calvo P, Kincaid AE, Surewicz WK, Caughey B, Wu C, Sigurdson CJ. Enhanced neuroinvasion by smaller, soluble prions. Acta Neuropathol Commun. 2017 Apr 21;5(1):32. doi: 10.1186/s40478-017-0430-z. (*, co-first authors).

Aguilar-Calvo P, Bett C, Sevillano AM, Kurt TD, **Lawrence JA**, Soldau K, Hammarström P, Nilsson KPR, Sigurdson CJ. Generation of novel neuroinvasive prions following intravenous challenge. Brain Pathol. 2018 Nov;28(6):999-1011. doi: 10.1111/bpa.12598.

Sevillano AM, Aguilar-Calvo P, Kurt TD, **Lawrence JA**, Soldau K, Nam TH, Schumann T, Pizzo DP, Nyström S, Choudhury B, Altmeppen H, Esko JD, Glatzel M, Nilsson KPR, Sigurdson CJ. Prion protein glycans reduce intracerebral fibril formation and spongiosis in prion disease. J Clin Invest. 2020 Mar 2;130(3):1350-1362.

Lawrence, JA., Sigurdson C. Neuronal ESCRT-0 depletion accelerates synapse loss in prion disease. *in preparation*

Lawrence, JA, Sigurdson C. Arc and an impaired endolysosomal pathway contribute to synapse damage in early prion disease. *in preparation*.

ABSTRACT OF THE DISSERTATION

Mechanisms of prion aggregate spread and synaptic toxicity

by

Jessica Anne Lawrence

Doctor of Philosophy in Biomedical Sciences

University of California San Diego, 2020

Professor Christina Sigurdson, Chair
Professor JoAnn Trejo, Co-Chair

Prion diseases are sporadic and infectious neurodegenerative disorders caused by PrP^{Sc}, a misfolded and aggregated isoform of the cellular prion protein, PrP^{C}. PrP^{Sc} accumulates and spreads through the CNS, causing neurodegeneration, gliosis, and ultimately death. However, the mechanisms underlying prion transport and pathogenesis remain poorly defined. The goals of my thesis research are to uncover properties of both prions and cellular pathways that facilitate prion spread into the central nervous system (CNS). First, we analyzed the biochemical properties of prion strains that enable entry into the central nervous system from

the peripheral organs. While prion strains have identical amino acid sequences, strains differ in the incubation period to terminal disease, lesion profile, and biophysical properties, including conformational stability, depending on the strain. In this work, we found that prion strains that neuroinvade were more soluble than the non-neuroinvasive strains, and that sonicating the non-neuroinvasive strains increased the solubility as well as the neuroinvasive properties. Second, we studied cellular pathways reported to be involved in prion spread through the CNS. We found that the ESCRT (Endosomal Complexes Required for Transport) pathway contributes to prion conversion in multivesicular bodies (MVBs) in neurons and prion spread via exosomes. Surprisingly, depletion of ESCRT-0 in the neurons of prion-infected mice worsened disease by accelerating the degeneration of synapses, without detectably increasing conversion of PrP^{Sc}. In contrast, depletion of ESCRT-0 in astrocytes or microglia had no effect on PrP^{Sc} levels or survival time. Third, we investigated pathways that contribute to prion spread by analyzing the brains of mice in a longitudinal study that included genetic, histological, and biochemical approaches. We found that synaptic alterations in the hippocampus were among the earliest (40% of disease course) and coincided with accumulation of ubiquitinated protein inclusions, suggesting degradative pathways were impaired early in disease. Fourth, we manipulated endolysosomal pathways in prion-infected neuroblastoma cells to further understand the role of both the MVB in prion conversion and exosomes in prion spread. Here, we validated that knocking down Hrs reduced PrP^{Sc}, while knocking down Vps35 conversely increased PrP^{Sc}. We found that Hrs depletion caused a decrease of PrP^{Sc}. Reduction of prion conversion was not due to a decrease in PrP^{C} or an increase in autophagic degradation of PrP^{Sc}, or even a loss of spread through exosomes, but instead, a failure of PrP^{Sc} internalization into MVBs. This work has uncovered principal features of prion propagation and spread, as well as unveiled the

essential role of the ESCRT pathway in both synapse health and neurodegeneration.

Chapter 1

Introduction

1.1 The history of prion disease

Prion diseases are fatal neurodegenerative disorders caused by the misfolding of the cellular prion protein, PrP^{C}, into the infectious, aggregated conformer, PrP^{Sc}, leading to neuron death (Bolton et al., 1982; DeArmond and Prusiner, 1995; Prusiner, 1982; Prusiner et al., 1977). The deposition of prion aggregates in the brain causes profound neuron loss, spongiform change, and gliosis (astrocytic and microglial) (DeArmond and Prusiner, 1995; Prusiner and Kingsbury, 1985). Remarkably, these misfolded prion aggregates have led to epidemics, as occurred with kuru in humans and bovine spongiform encephalopathy in cattle (BSE) (DeArmond and Prusiner, 1995). There is no treatment available for prion diseases or most other neurodegenerative diseases, including Alzheimer's and Parkinson's disease, which also involve protein aggregate accumulation and spread in the brain.

The importance of PrP^{C} in the pathogenesis of prion disease has been well established. The protein-only hypothesis states that prion disease is caused by the conformational transition

of PrP^C, consisting mostly of alpha-helices, to the beta-sheet rich aggregated PrP^{Sc} conformer (Baral et al., 2019; Spagnolli et al., 2019). During disease progression, PrP^{Sc} templates the misfolding of PrP^C, resulting in self-catalytic propagation of PrP^{Sc}. The structure of PrP^{Sc} results in physiological abnormalities such as resistance to proteolytic degradation, relative insolubility, and aggregate deposition. While the structure of PrP^C is known (Liu et al., 2011), the structure of PrP^{Sc} remains controversial, but the latest research suggests a beta-solenoid structure (Spagnolli et al., 2019; Vazquez-Fernandez et al., 2016).

Prion disease was originally believed to be caused by a loss of function of PrP^C due to the conversion of PrP^C to PrP^{Sc}, but that has since been disproven, as knockout mice do not develop prion disease (Büeler et al., 1992; Manson et al., 1994). The challenge in understanding the mechanisms of prion disease in part lies in not knowing the function of PrP^C in the brain. Knockout studies have led to inconsistent conclusions, due to animal models, mouse backgrounds, and methods of gene deletion (Büeler et al., 1992; Collinge et al., 1994; Wulf et al., 2017). The overarching consensus is that the role of PrP^C in the brain is complex, and perhaps the function of PrP^C would be clarified under specific conditions, such as stress (Watts et al., 2018). PrP^C has been found to be involved in long term potentiation, memory consolidation, stem cell renewal, and neuroprotection, but exact mechanisms remain unknown (Castle and Gill, 2017; Linden, 2017; Watts et al., 2018; Wulf et al., 2017). One of the more certain conclusions from these studies is that PrP^C is necessary for the maintenance of peripheral nerve myelination in mice (Baumann et al., 2007; Nishida et al., 1999; Nuvolone et al., 2016). In vitro, one study recently showed that PrP^C is involved in the regulation of synaptic vesicle proteins and release of synaptic vesicles (Peggion et al., 2019). These studies all highlight the importance of PrP^C to the neuron and health of the brain, exhibiting how the misfolded prion protein

could cause such rapidly progressing neurodegeneration.

1.1.1 Prion disease in animals

Prion diseases, also known as transmissible spongiform encephalopathies, are naturally occurring in many animals and include chronic wasting disease (CWD) of elk and deer, scrapie of sheep and goats, and bovine spongiform encephalopathy (BSE) of cattle (Mathiason, 2017). Scrapie was first reported as in Europe in the 16th century, the first prion disease shown to be infectious and transmissible between sheep (Detwiler, 1992; Parry, 1960). CWD is a prion disease first found to affect captive cervids in the Colorado area in the late 1960s but was shortly identified in free-range deer as well and has since proven to be one of the most efficiently transmitted prion diseases. Secretions and excreta were found to be infectious, even throughout the many years of the preclinical phase of prion disease (Mathiason et al., 2006; Tamguney et al., 2009). Zoonotic transmission of CWD to humans is a concern, as deer and elk are popular to hunt in the Colorado and Wyoming areas. To date, research suggests transmission is unlikely due to the species barrier, as the human and cervid PrP sequence differ enough that conversion of human prion protein does not occur (Harrathi et al., 2019; Kurt et al., 2014; Sandberg et al., 2010). Yet Davenport and colleagues suggest that the species barrier is not as strong as one would hope (Davenport et al., 2015), which poses a concern for human health. So far, only BSE has transmitted to humans, as variant CJD, spread through ingestion or inoculation (Will et al., 1996). Classical BSE was first recognized in 1984 in the UK and was subsequently identified in cattle in at least 28 other countries (Nathanson et al., 1997; Wells and Wilesmith, 1995). Transgenic mouse lines expressing PrP^{C} from different host species has led to the development of many prion disease models and the ability to study various TSEs and mutations causing

prion disease (Chiesa et al., 1998; Houston and Andréoletti, 2018; Scott et al., 2000). Serial passaging of prion-infected tissue into wildtype mice has allowed for the generation of mouse-adapted strains, originating from scrapie in sheep and goats or from BSE in cattle (Baron, 2002; Wadsworth et al., 2010).

1.1.2 Prion disease in humans

Human prion diseases are categorized as sporadic, acquired, or genetic. Classical (sporadic) CJD is a rapidly progressing neurodegenerative disease, with clinical progression to death lasting less than 6 months on average (Collinge, 2001). While the causes of sporadic prion disease remain unknown, genetic prion diseases are caused by coding mutations in the prion gene *PRNP*. Examples of genetic prion diseases include familial Creutzfeldt-Jakob disease, Gertsmann-Straussler-Scheinker (GSS) disease, and fatal familial insomnia (Collinge, 2001; Collinge et al., 1989; Fiorino, 1996; Owen et al., 1989). Over 20 pathogenic mutations have been identified, either point mutations or insertions encoding copies of an octapeptide repeat of which the normal prion protein has five copies (Collinge et al., 1989; Owen et al., 1989). Acquired CJD can occur through exposure to BSE or iatrogenically (Nathanson et al., 1997; Prusiner et al., 1985). Kuru is another example of acquired prion disease, one that reached epidemic proportions in a subpopulation in Papua New Guinea (Alpers, 2005). Kuru was transmitted during cannibalistic ceremonies where deceased relatives were consumed by relatives and is thought to originate from one case of sporadic CJD that was rapidly recycled throughout the population (Alpers, 2005). Unfortunately, no therapies for prion disease currently exist.

1.1.3 Prion strains

Even when the primary structure of the prion protein is identical, strains with a variety of quaternary structures arise due to post-translational modifications (Fraser and Dickinson, 1968). These strains can be characterized by their incubation period to terminal disease, lesion profile, ability to spread into the brain, and biophysical properties including conformational stability (Ayers et al., 2011; Peretz et al., 2001). Strains are categorized by their ability to form long fibrils that form plaques (fibrillar strain) or their lack of fibrils and diffuse spread throughout the brain (oligomeric strain). Prions inoculated in the intraperitoneal cavity only invade the brain and cause disease if the strain is oligomeric, while the fibrillar strains are poorly able to invade the CNS from the intraperitoneal cavity (Silveira et al., 2005; Tixador et al., 2010), a process termed neuroinvasion. Thus, these differences can be used to classify the strains as either neuroinvasive or non-neuroinvasive.

Additionally, there are many other differences between oligomeric and fibrillar strains. Fibrillar strains have a longer incubation period than oligomeric strains when injected into the brain. Oligomeric strains are much less stable than fibrillar strains; they disassemble at lower temperatures into monomeric prions and are less stable in chaotropes and denaturation (Bett et al., 2012). Fibrillar strains are congophilic, meaning they bind Congo red, while oligomeric strains do not. Fibrillar strains used in mice experiments include 87V and mCWD and oligomeric strains in mice used are 22L, RML, and ME7 (Kuczius and Groschup, 1999). Yet we still do not completely understand how characteristics of prion strains enable spread and neuroinvasion in specific strains but not others.

1.2 Routes of neuroinvasion

Prions only cause clinical disease upon entering the CNS, however, most exposures to prions occur through ingestion or blood exposure and the method of neuroinvasion remains unclear. There are several possible mechanisms of neuroinvasion: across the blood brain barrier, through nerves, or cell-mediated (Heikenwalder et al., 2007). Furthermore, the mechanisms of neuroinvasion could depend on the route of inoculation. Much research supports the idea that when prions are ingested, they neuroinvade by the vagal nerve from the gastrointestinal tract to the brain (Kaatz et al., 2012; McBride et al., 2001). In addition to retrograde transport in nerves, prions could cross the blood brain barrier (Siso et al., 2010), although to date this has not been rigorously shown.

1.2.1 Nerves

Research suggests that prions travel through nerves to enter the CNS (Glatzel and Aguzzi, 2000), but no definitive mechanism has been shown. During the early events following prion exposure, PrP^{Sc} traffics from extraneural entry sites into the central nervous system via peripheral nerves (Beekes and McBride, 2000), likely by retrograde axonal transport (Bartz et al., 2003). Rodents inoculated orally with prions develop prion aggregates in the myenteric plexi, vagal nerve, and the dorsal motor nucleus of the vagus in the brain (Kaatz et al., 2012; McBride et al., 2001), spreading through neuroanatomically connected routes consistent with retrograde axonal transport from the gastrointestinal tract. Interestingly, not all prion strains, or conformational variants, spread from peripheral entry sites into the CNS (Siso et al., 2010).

1.2.2 Blood brain barrier

The blood brain barrier (BBB), while more impassible than other endothelial barriers in the body, provides an opportunity for pathogens to enter the brain. The endothelial cells of the brain form the walls of the blood vessels in the brain, creating highly sophisticated barrier with the tight junctions and reduced transcytosis. Pericytes, the vascular smooth muscle cells, surround the endothelial cells. Astrocytes, an important glial cell, extend endfeet that almost completely enclose the vessel (Daneman and Prat, 2015).

A single brain perfusion study suggested that PrP^{Sc} has the ability to cross the BBB (Banks et al., 2004). This study was performed immediately after the mice had been anesthetized and were infused with radioactive PrP^{Sc}, showing that without disrupting the integrity of the BBB, PrP^{Sc} crossed the entire capillary wall to enter the brain parenchyma.

The role of the hematogenous route in the neuroinvasion of prions has become highly relevant to public health. One study of scrapie in sheep revealed that blood transfusions efficiently transmit prion disease (Houston et al., 2008). Another study shows that PrP^{Sc} aggregates appear in the circumventricular organs, a region in the brain where the BBB is absent, when sheep were inoculated by the IV route (Siso et al., 2009), indicating alternative entry points into the brain through the blood. An important human study has found that 1 in 2000 people in the UK are subclinical carriers of prions, by analyzing the appendices of 32,441 people across 41 hospitals (Gill et al., 2013). The high frequency of subclinical prion carriers highlights the risk of blood transfusions in the UK, and the potential for prion disease spread due to the known ability of prions to neuroinvade from the IV route. Understanding properties that enable prion neuroinvasion will be important to identifying risks and to prevent prion disease spread.

1.3 Cellular mechanisms of prion spread

Prions and prion-like aggregates, including α-synuclein, tau, and amyloid-β, spread through neuroanatomically connected regions of the brain via unknown mechanisms (Frost and Diamond, 2010). In vitro, prions spread cell-to-cell via exosomes and tunneling nanotubes (TNT) (Gousset et al., 2009; Guo et al., 2016), whereas in vivo prions spread through synaptosomes, GPI-painting, or direct PrP^{Sc} release from the plasma membrane as additional possible routes, illustrated in Figure 1-1. Mechanisms that underlie how protein aggregates disseminate through the CNS in neurodegenerative disease are unclear, yet fundamental to understanding disease progression.

Prions have been isolated from exosomes derived from infected Mov cells, PrP-expressing RK13 cells, N2a cells, and GT1-7 cells (Fevrier et al., 2004; Guo et al., 2015; Vella et al., 2007; Vilette et al., 2015). Exosomes containing infectious prions have also been isolated from serum of infected hamsters (Properzi et al., 2015). Furthermore, electron microscopy of neurons from infected mouse brains show that prion-filled exosomes are found in multivesicular bodies (MVBs) (Arnold et al., 1995). Isolated prion-filled exosomes harvested from infected immortalized cells inoculated intracerebrally into mice were infectious, causing prion disease (Mattei et al., 2009). Additionally, protein aggregates from other neurodegenerative diseases have been isolated from exosomes, such as α-synuclein in Parkinson's disease (Hasegawa et al., 2011), amyloid-β in Alzheimer's disease (Perez-Gonzalez et al., 2012), and tau in many experimental mouse models of tauopathies (Saman et al., 2012).

Prion aggregates are internalized from the extracellular space via macropinocytosis and enter multivesicular bodies (Bett et al., 2012; Yim et al., 2015). Multivesicular bodies (MVBs) are the sites of vesicle generation within the cell and are a major site of prion conversion in

the cell (Yim et al., 2015). Cells release these nanovesicles containing miRNA, DNA, and proteins, known as exosomes, as a mechanism of intercellular communication. MVBs are formed from endosomes by budding off the limiting membrane internally, followed by severing the neck. Endosomal sorting complexes required for transport (ESCRT) proteins direct the sorting of endosomes and their internalized cargo (Hurley, 2015; Stuffers et al., 2009). Four ESCRT complexes, 0, I, II, and III, function sequentially to localize membrane proteins and lipids to the limiting endosomal membrane and sever the inward buds, as illustrated in Figure 1-2. When Hrs, a component of ESCRT-0, is knocked down in cells, exosomal production is severely impaired (Vilette et al., 2015). Hrs depletion markedly decreases PrP^{Sc} levels in N2a cells and SMB models (Yim et al., 2015) and in Mov127S cells (Vilette et al., 2015), through unclear mechanisms, possibly due to decreased prion conversion in MVBs. These exciting results indicate a pathway that could profoundly affect both prion conversion and release.

Another proposed mechanism of prion spread, nanotubes, have been observed to serve as a conduit for prion spread between neurons in vitro (Gousset et al., 2009). However, exosomes can also be transported through nanotubes, so these hypotheses are not mutually exclusive. Additionally, one study has recently shown exosomes to be the main pathway of prion release in vitro (Arellano-Anaya et al., 2015). Furthermore, specific cell pathways that contribute to prion spread are unknown yet could be a potential therapeutic target in neurodegenerative diseases.

1.4 Prions at the synapse

Synaptic abnormalities present some of the earliest and most severe changes in prion disease (Belichenko et al., 2000; Clinton et al., 1993; Cunningham et al., 2003; Hilton et al.,

2013; Jeffrey et al., 2000). Morphological changes to the synapse precede synapse loss and neuron death (Brown et al., 2001; Jeffrey et al., 2000), while prions are seen surrounding synaptic sites (Belichenko et al., 2000; Campeau et al., 2013), leading to the hypothesis that prions induce toxicity through the synapse. Furthermore, ultrastructural pathology is observed in synapses in the prion affected brain (Siskova et al., 2009).

1.4.1 Prions at the post-synapse

PrP^C has been reported to interact with many receptors found at the post-synaptic membrane, such as NMDA receptors, AMPA receptors, kainate, and mGluRs, believed to contribute to intracellular signaling (Castle and Gill, 2017). In this regard, it is plausible that PrP^C mediates neurotoxicity upon binding with PrP^{Sc} since no neurotoxic effects are seen from PrP^{Sc} when PrP^C is not expressed (Brandner et al., 1996; Mallucci et al., 2003).

Evidently, studies of the misfolded prion protein have revealed significant and rapid effects on the post-synapse. Treatment of primary neurons with PrP^{Sc} results in rapid retraction of dendritic spines (Fang et al., 2016). Extensive studies indicate controversy on the mechanism. PrP^{Sc} is thought to activate a signaling cascade through NMDA receptors, consequentially leading to a calcium influx, stimulation of p38 MAPK, resulting in collapse of the actin cytoskeleton and consequentially dendritic spines (Fang et al., 2018). Another group illustrated that inhibition of group-I metabotropic glutamate receptors decreases the prion-induced neuron loss, both in vitro and in vivo (Goniotaki et al., 2017). Yet another group working with organotypic slices shows that prion infection causes calpain activation, reactive oxygen species production and activation of PERK (Falsig et al., 2012; Herrmann et al., 2015; Sonati et al., 2013). However, while the animal models of prion disease are reliable and consistent, in vitro systems to study

prion infection are lacking. Immortalized cells do not exhibit signs of neurotoxicity when infected with prions, and methods and sources of prion infection in primary neuron cultures vary widely, resulting in different conclusions (Le et al., 2019). Furthermore, the mechanisms of neurotoxicity at the post-synapse may not be one singular mechanism, as it has been shown that PrP^{C} interacts with a variety of post-synaptic receptors, including ionotropic and metabotropic. While there is a consensus that the N-terminus is important for the neurotoxic effects of PrP^{Sc} (Falsig et al., 2012; Fang et al., 2018), the downstream mechanisms of prion toxicity remain unclear.

1.4.2 Prions at the pre-synapse

The impact of prions at the pre-synapse is even more inconclusive. Loss of pre-synaptic proteins is one of the first changes observed in prion disease, and some attest that it is the only change in synapses during prion disease (Gray et al., 2009). Whether these changes are due to direct interactions of PrP^{C} within the pre-synapse or downstream of other interactions at the membrane remains unknown. However, PrP^{C} regulates the size and release of synaptic vesicles in Drosophila, and mutations in PrP^{C}, specifically the one found in GSS, leads to impaired synaptic vesicle release (Robinson et al., 2014). Recently, PrP^{C} has been identified as a regulator of synaptic vesicle proteins, in addition to regulating exocytosis of synaptic vesicles (Peggion et al., 2019), providing plausible evidence that prion infection could directly impair the pre-synapse during prion disease as well as the post-synapse. The investigation of role of prions at the synapse leaves many questions unanswered. The challenges in modeling prion disease in vitro are numerous and continue to not be replicated in vivo. The role of PrP^{C} in synapse health, and moreover, how PrP^{Sc} impacts the synapse during prion disease remains to be known.

1.5 Prions and the endolysosomal pathway

Endolysosomal pathway (ELP) dysfunction has proven to be involved in an array of neurodegenerative disorders, and prion disease is no exception. Enlarged Rab5- and Rab7-positive endosomes are seen in the brains of sCJD patients (Kovács et al., 2007). PrP^{Sc} is trafficked through the ELP and either recycled to the cell surface or through retrograde transport (Goold et al., 2013; Uchiyama et al., 2013), but is also found within MVBs, lysosomes, and autophagosomes (Magalhaes et al., 2005; Veith et al., 2009), illustrated in Figure 1-3. Disruption of the ELP impacts prion propagation but prion infection itself also damages the subcellular compartments of the ELP.

1.5.1 ELP as a site of prion conversion

Cells within the CNS are particularly efficient at replicating prions, but the cellular location of prion conversion is quite controversial. However, many groups propose the ELP as a major site of prion conversion. Internalization of PrP^{Sc} was first shown to be essential for prion conversion in 1992, when PrP^{Sc} synthesis was prevented by inhibiting endo-lysosomal maturation (Borchelt et al., 1992). Furthermore, prion conversion was decreased within cells that had reduced levels of Hrs or Tsg101 (Vilette et al., 2015; Yim et al., 2015). Through a series of knockdown experiments of ELP proteins in prion-infected N2a cells, the multivesicular body was shown to be a major site of prion conversion (Yim et al., 2015). An additional study identified the recycling endosome as the primary site of prion conversion, specifying Rab11, a major regulator of the recycling endosome as a necessary component in conversion (Marijanovic et al., 2009). Another study highlights that stimulation of retrograde transport toward the ER increases PrP^{Sc} levels in prion-infected cells (Beranger et al., 2002), further indicating the importance of inter-

nalization of PrP^{C} in prion conversion. In other studies, depletion of Rab7, a protein involved in the maturation of late endosomes, leads to a decrease of PrP^{Sc} in vitro (Shim et al., 2016; Yim et al., 2015). Additionally, the role of intracellular prion trafficking is further highlighted in studies showing that stimulation of autophagy pathways decreases prion conversion in vitro (Abdelaziz et al., 2019; Abdulrahman et al., 2019; Aguib et al., 2009; Heiseke et al., 2009). While the exact subcellular compartment where prion conversion occurs is not agreed upon, many groups show that intracellular trafficking is essential for prion propagation (Veith et al., 2009).

In contrast, other studies indicate the cell surface is the primary location of prion conversion (Goold et al., 2013; Heisler et al., 2018). The difference in these findings could be accounted for by the rapidity at which PrP^{Sc} is endocytosed. As Goold and colleagues showed, PrP^{Sc} is converted on the cell membrane, but PrP^{Sc} is then immediately endocytosed and trafficked through recycling endosomes and the endocytic pathway (Goold et al., 2013). Perhaps the cell membrane is the primary site of prion conversion, but endocytosis of PrP^{Sc} is important in spread and propagation. Furthermore, studies to localize cellular conversion have been restricted to in vitro models and could quite well differ among the models used or in the microenvironment of the brain. Heisler et al., identified the primary site of prion conversion using both in vitro and in vivo models. The knockdown of the endosomal regulating component, muskelin, in vitro causes an increase of surface PrP^{C} and PrP^{C} release in extracellular vesicles (Heisler et al., 2018). When muskelin knockout mice were inoculated with prions, disease was accelerated, as was prion conversion. Here, an increase in both extracellular PrP^{Sc} and total PrP^{Sc} was detected in the muskelin knockout mice, identifying the cell membrane as the primary site of prion conversion.

The location of prion conversion remains controversial, yet manipulation of the ELP

severely affects prion propagation.

1.5.2 Prions impair the ELP

While manipulation of the ELP can impact prion propagation, prions can also cause damage to the ELP. BSE-affected cattle brains examined by electron microscopy revealed excess and abnormal multivesicular bodies, perturbation of the plasma membrane, and dystrophic neurites (Ersdal et al., 2009). In neuroblastoma cells, prion infection resulted in PrP^{Sc} accumulation in recycling endosomes, causing a decrease in post-Golgi trafficking to the cell surface and consequentially a decrease in surface PrP^{C} in prion-infected mouse brain (Uchiyama et al., 2013). Additionally, lysosome degradation was impaired in prion-infected neuroblastoma cells due to reduced localization of Rab7 to membranes (Shim et al., 2016). Finally, autophagosomes accumulated in prion-infected brains late in prion disease, again suggesting an impairment to autophagic flux (Lopez-Perez et al., 2019; Lopez-Perez et al., 2020).

Questions remain, including, does the ELP enable prion spread or protect against it? How does prion infection impair the ELP? What subcellular compartments are essential for prion conversion in vivo?

1.6 How does prion disease compare to other neurodegenerative diseases?

The disruption of the ELP and spread of protein aggregates in the brain is not unique to prion disease. Neurodegenerative diseases are often characterized by the accumulation of misfolded proteins in the brain, such as amyloid-β and tau in Alzheimer's disease, α-synuclien

in Parkinson's disease, and TDP-43 in amyotrophic lateral sclerosis (ALS), all of which spread through unknown mechanisms throughout the brain. Ubiquitin aggregates, autophagosome accumulation, and lysosome dysfunction have been observed in the brains of patients with neurodegenerative diseases, suggesting impairments to the ELP (Afghah et al., 2020; Nixon, 2013).

In Alzheimer's disease, many proposed mechanisms of endolysosomal dysfunction have been reported, due to the spread and accumulation of Aβ. However, enlarged endosomes precede amyloid-β plaques in Alzheimer's disease (Cataldo et al., 2000; Ginsberg et al., 2010). Aβ42 accumulates in MVBs and disrupts degradative pathways in the cell (Almeida et al., 2006; Takahashi et al., 2002), resulting in a loss of synapses (Almeida et al., 2005; Snyder et al., 2005; Xu et al., 2016). Through both extracellular (spread) and intracellular mechanisms (increased cleavage), Aβ accumulation at the synapse has been shown to increase endocytosis of glutamate receptors, disrupt endocytosis and recycling of synaptic vesicles, and cause a loss of PSD95 at the post-synapse (Perdigão et al., 2020).

Mutations in Chmp2B, a component of ESCRT-III, are associated with fronto-temporal dementia (FTD) and ALS (Sadoul et al., 2018; Skibinski et al., 2005). Chmp2B mutations disrupt the maturation of endosomes and autophagosomes, implicating impaired endolysosomal flux in the progression of ALS and FTD (Clayton et al., 2015).

In Parkinson's disease, GWAS studies point to endolysosomal dysfunction as a cause (Vidyadhara et al., 2019). LRRK2 regulates of vesicular trafficking, and the mutations in LRRK2, the most common genetic variants in inherited PD, lead to neuronal toxicity (Deng et al., 2018). α-synuclein, involved in synaptic vesicle recycling, interacts with Chmp2B in Lewy body disease and Parkinson's disease, causing impaired lysosomal function (Spencer et al., 2016; Tanikawa

et al., 2012).

Functional synapses are essential for neurons to remain healthy. The ELP is important for proper synaptic transmission in regulating both pre-synaptic synaptic vesicle recycling and post-synaptic membrane receptor levels (Fernández-Alfonso and Ryan, 2006; Sadoul et al., 2018; Yi and Ehlers, 2007). Mutations in the ELP proteins causing damage to recycling of synaptic vesicles and synaptic proteins result in accelerated neurodegeneration (Sheehan et al., 2016; Uytterhoeven et al., 2011). However, when mutations in the ELP are countered by reduced endolysosomal flux, synapses are preserved, and neurodegeneration is reduced (Fernandes et al., 2014).

In addition to further our understanding of prion disease and protein aggregate spread, studies of prion disease will provide further understanding of neurodegenerative diseases.

1.7 Research Goals

The work presented here reveals mechanisms of prion spread and new insight into how prions drive neuronal toxicity. Specifically, Chapter 2 defines the biochemical properties of prion strains that enable prion spread into the CNS from extraneural sites. We develop biochemical assays to both evaluate and manipulate biochemical properties of fibrillar and subfibrillar prion strains. We discovered that (1) an increased solubility of prion aggregates correlates with ability to neuroinvade, (2) sonication of a fibrillar prion strain increases its solubility, and (3) sonication of fibrillar prions increases neuroinvasive capabilities. In Chapter 3, I manipulate the ESCRT pathway to investigate how it contributes to prion spread both in vivo and in vitro. By depleting the ESCRT-0 component, Hrs, in a cell-specific manner, I discovered that the ESCRT pathway contributes more to prion toxicity than spread. While depleting Hrs in cultured neurons reduces

PrP^{Sc} levels, depleting Hrs in astrocytes, microglia, or neurons in prion-infected mice has no detectable effect on prion propagation and spread. However, prion disease is profoundly accelerated when Hrs is depleted in neurons, due to contributions to the neurotoxicity at the synapse. In Chapter 4, we determined the initial changes in prion disease contributing to early pathogenesis and prion spread by performing a longitudinal study in mice, analyzing the brains of prion-infected mice by biochemical, histological, and genetic methods at seven different time points throughout disease. We found that (1) synapses are altered early in prion disease, likely due to activation of Arc, (2) endolysosomal dysfunction occurs alongside synapse remodeling at first signs of prion aggregation, and (3) inflammation in the brain occurs after these initial events, closer to when spongiform change appears when mice are showing clinical signs of prion disease. Chapter 5 is a summary of additional experiments on prion spread, including manipulation of prion conversion in prion-infected neuroblastoma (N2a) cells and spread in exosomes. In these studies, we found that depletion of retromer component Vps35 resulted in an increase of PrP^{Sc} in N2a cells, whereas Hrs depletion resulted in a decrease, both likely due to the increase or decrease, respectively, of PrP into MVBs. We discovered exosomes as a likely mechanism of prion spread, but surprisingly found that when Hrs was depleted in primary neurons, there was an increase in extracellular vesicle release. Collectively, these studies contribute to understanding mechanisms of prion pathogenesis and spread, which will ultimately provide a basis for developing therapeutics for neurodegenerative diseases.

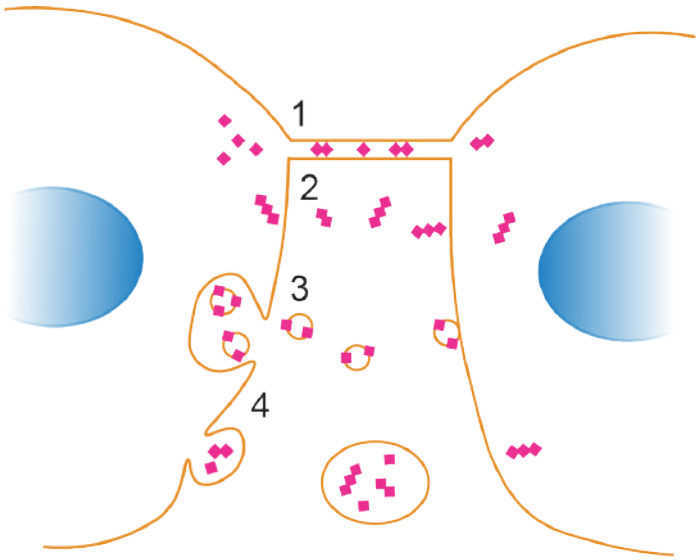

Figure 1.1: Mechanisms of cell-to-cell spread of prions. Proposed mechanisms of prion spread (pink) between cells. (1) tunneling nanotubes creating highways for prions to travel between cells, (2) GPI painting, (3) exosomes from intracellular processes, (4) macrovesicles pinching off from the cell membrane.

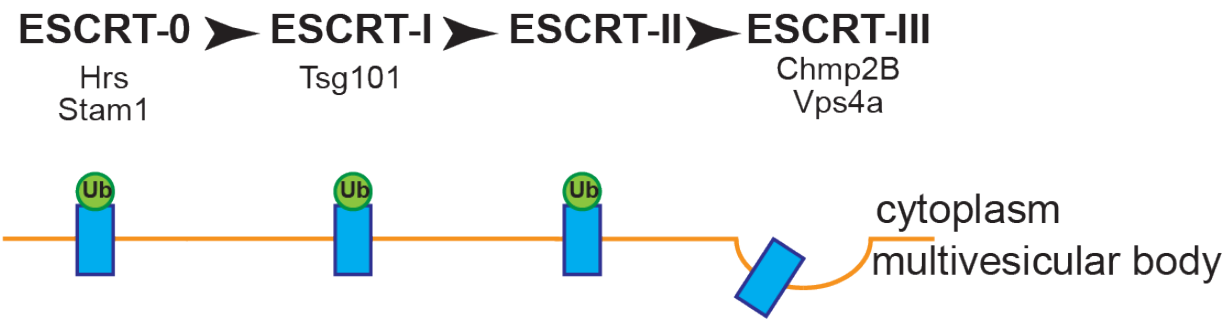

Figure 1.2: The ESCRT pathway functions sequentially to generate multivesicular bodies. Four complexes of proteins function sequentially to pass off ubiquitinated (ub – green) endosomal cargo (blue) and form invaginations of the membrane to ultimately create a multivesicular body. Proteins highlighted in these studies are associated with the complex they are written under.

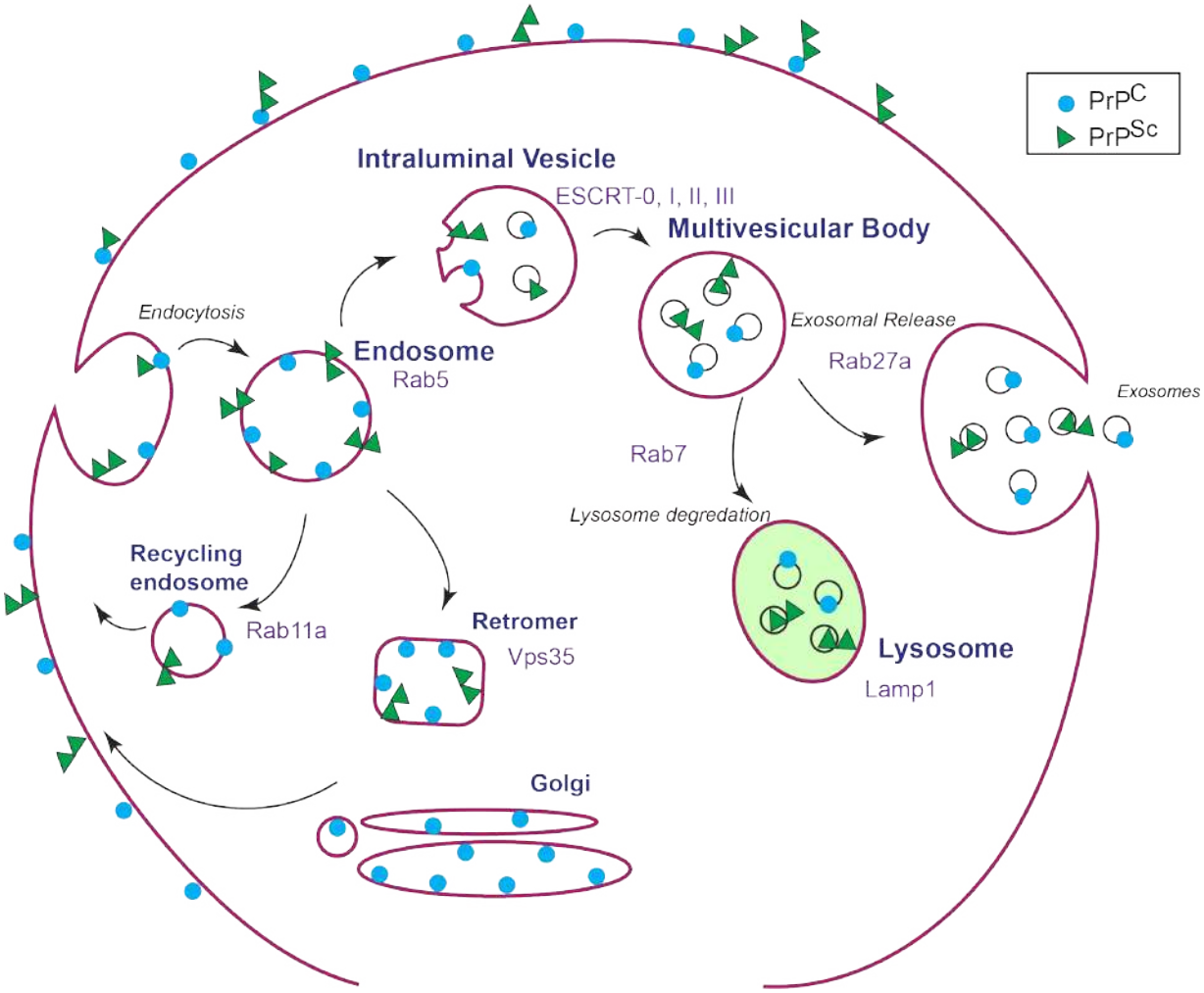

Figure 1.3: Prions are trafficking all throughout the cell, proving difficult to identify the location of prion conversion. While PrP^{C} (blue) is anchored on the cell membrane, it is found all through out the cell, endocytosed to be either recycled back to the cell surface through retromer or recycling endosomes, or trafficked through the MVB to be released in exosomes or degraded in lysosomes. Where prion conversion occurs remains controversial, as PrP^{Sc} (green) has also been identified in many of these subcellular compartments. Proteins involved in certain subcellular compartments and investigated in prion studies are shown in purple.

Chapter 2

Enhanced neuroinvasion by smaller, soluble prions

Infectious prion aggregates can propagate from extraneural sites into the brain with remarkable efficiency, likely transported via peripheral nerves. Yet not all prions spread into the brain, and the physical properties of a prion that is capable of transit within neurons remain unclear. We hypothesized that small, diffusible aggregates spread into the CNS via peripheral nerves. Here we used a structurally diverse panel of prion strains to analyze how the prion conformation impacts transit into the brain. Two prion strains form fibrils visible ultrastructurally in the brain in situ, whereas three strains form diffuse, subfibrillar prion deposits and no visible fibrils. The subfibrillar strains had significantly higher levels of soluble prion aggregates than the fibrillar strains. Primary neurons internalized both the subfibrillar and fibril-forming prion strains by macropinocytosis, and both strain types were transported from the axon terminal to the cell body in vitro. However in mice, only the predominantly soluble, subfibrillar prions, and

not the fibrillar prions, were efficiently transported from the tongue to the brain. Sonicating a fibrillar prion strain increased the solubility and enabled prions to spread into the brain in mice, as evident by a 40% increase in the attack rate, indicating that an increase in smaller particles enhances prion neuroinvasion. Our data suggest that the small, highly soluble prion particles have a higher capacity for transport via nerves. These findings help explain how prions that predominantly assemble into subfibrillar states can more effectively traverse into and out of the CNS, and suggest that promoting fibril assembly may slow the neuron-to-neuron spread of protein aggregates.

2.1 Introduction

Misfolded proteins incite cognitive and motor decline in Alzheimer's, Parkinson's, and prion disease. During a prion infection, prion aggregates, PrP^{Sc}, template the misfolding of the cellular prion protein, PrP^{C}, in an autocatalytic process that terminates in rapidly progressive and fatal neurodegeneration (Aguzzi and Falsig, 2012; Prusiner, 1982). Distinct PrP^{Sc} conformers drive PrP^{C} to misfold into a remarkable range of structural variants that correlate to profoundly different disease phenotypes (Bruce, 2003). Although most infectious prions spread from peripheral entry sites into the central nervous system (CNS), certain prion subtypes, such as variant Creutzfeldt-Jakob disease (vCJD), replicate and persist in lymphoid organs and fail to neuroinvade in mice (Beringue et al., 2008; Collis and Kimberlin, 1985). An estimated 1:2000 humans in the UK harbor vCJD prions in lymphoid tissues (Gill et al., 2013) and some individuals may remain lifelong subclinical carriers of extraneural infectious prions with no spread into the CNS. The physical properties of a prion aggregate that facilitate CNS entry and spread are unclear.

Peripheral nerves have been implicated as a major route for prion invasion of the CNS from extraneural entry sites, a process known as neuroinvasion. First, prions have been shown to spread from initial exposure sites into the brain by defined neuroanatomic pathways. For example, ingestion of prions induces early prion accumulation in the dorsal motor nucleus of the vagus and solitary tract nucleus in the brain as well as in the thoracic spinal cord, consistent with neuron-to-neuron spread via vagal and splanchnic nerve circuitry (Beekes et al., 1998; McBride et al., 2001). Second, prions replicate in lymphoid tissues in early disease, prior to CNS invasion, and manipulation of the splenic innervation also indicates nerves as a possible conduit for prion trafficking into the CNS. For example, juxtaposing splenic nerves and prion-infected follicular dendritic cells (FDCs) (Prinz et al., 2003), or increasing splenic innervation, accelerates prion spread to the brain in mouse models (Glatzel et al., 2001). Finally, sympathectomy delays or prevents scrapie in mice (Glatzel et al., 2001), again suggesting an important role for peripheral nerves in prion neuroinvasion.

There are many details of protein aggregate spread in vivo that are not yet well understood, such as which PrP^{Sc} conformers transit in nerves. An advantage to investigating prion disease in mouse models is the highly reproducible incubation period and brain regions targeted by distinct prion conformational variants (Fraser and Dickinson, 1968; Fraser and Dickinson, 1973), enabling studies linking PrP^{Sc} biophysical properties with disease phenotype. Although earlier studies demonstrated that certain prions show a limited capacity to spread via neurons into the CNS, the properties of prion aggregates that successfully traffic within nerves are unknown. We previously identified two mouse-adapted prion strains that failed to spread to the CNS following an intraperitoneal (IP) challenge of mice, and three prion strains that were highly neuroinvasive (NI) (Bett et al., 2012). Both non-NI strains formed fibrillar, congophilic plaques in

the brain after intracerebral (IC) inoculation, while the NI strains formed diffuse, noncongophilic aggregates that were less stable in chaotropes and lacked fibrils in the brain in situ, suggesting that a fibrillar structure correlated with poor neuroinvasion. Ultrastructural characterization of the fibrillar prions has been previously performed, and fibrillar prion strains were shown to form classical "kuru" type plaques composed of a central core of bundles (Bett et al., 2012; Jeffrey et al., 1994a; Jeffrey et al., 1994b; Jeffrey et al., 1996; Sigurdson et al., 2006). Interestingly, GPI-anchorless prions form large fibrillar plaques and are also poorly neuroinvasive from peripheral exposure sites; in one study, the authors suggested that the GPI-anchor on the prion protein was important for prion transport via nerves (Klingeborn et al., 2011). Although some of these data may collectively argue that fibrillar prions show inefficient neuroinvasion, there is still no consensus on the physical requirements for prion entry into the CNS. Here we investigated the biophysical requirements for prion uptake and axonal transport in vitro using primary neurons, as well as prion neuroinvasion in vivo from a highly-innervated, extraneural exposure site, the tongue.

2.2 Results and Discussion

Early entry and replication of subfibrillar prions in the brainstem after an intra-tongue prion exposure

Distinct, sequence-matched PrP^{Sc} assemblies, or strains, are associated with remarkably varied clinical and pathologic disease phenotypes (Bruce et al., 1989; Fraser and Dickinson, 1973). We first examined the ability of diverse prions to spread from the tongue to the brain using a panel of strains comprising primarily fibrillar (87V, mCWD) or subfibrillar assemblies

(amorphous oligomers or short fibrils) (22L, RML, ME7), which are defined by whether fibrils are visible ultrastructurally in the brain in situ (Bett et al., 2012; Jeffrey et al., 1994b; Jeffrey et al., 1997; Jeffrey et al., 1996; Sigurdson et al., 2006). The tongue is a natural route for prion entry through abrasions (Bartz et al., 2003), is highly innervated, and provides a direct route for prion spread to the brain via cranial nerves independent of a lymphoid replication phase (Bartz et al., 2005). WT mice (VM/DK background) and tga20 mice, which overexpress mouse PrP by 6-8 fold under the prion promoter (Fischer et al., 1996), were used to investigate prion spread (Methods detail the mice and prion strains). After an intra-tongue (IT) injection, all three subfibrillar prions induced a rapid progression to terminal disease in 100% of mice, whereas neither fibrillar strain led to efficient prion spread to the CNS, with either 0% or 11% of mice developing prion disease (Fig. 2-1, a - f). A time course revealed initial replication of subfibrillar prions in the brainstem (facial nucleus, reticular formation and deep cerebellar nuclei) (Fig. 2-1, a - b) and lateral hypothalamus by 50% of the incubation period (59 days post-inoculation), consistent with transport from the tongue to the brain via cranial nerves and spread to the hypothalamus. Clinically negative mice had no histologically or biochemically detectable prions, even following sodium phosphotungstic acid precipitation (Wadsworth, 2001) to increase the sensitivity of detection (Fig. 2-1f). The single mouse that developed prion disease following inoculation with 87V prions developed both plaques and diffuse PrP^{Sc} deposits, similar to mice inoculated by the IC route (Fig. 2-1e).

To exclude the possibility that PrP was replicating in FDCs within lymphoid tissue and then spreading to the brain, we inoculated mice that express PrP under the control of the neuron specific enolase (NSE) promoter with three prion strains by either the IT or IC route. We found that the subfibrillar prions, RML and ME7, spread from the tongue to the brain, indicating that

prion replication in lymphoid tissue was not required for brain entry. The fibrillar prion, mCWD, once again did not spread from the tongue to the brain (Fig. 2-4).

Neuronal uptake of the subfibrillar and fibrillar prion strains by macropinocytosis

To investigate the mechanism underlying the brain entry observed for the subfibrillar but not the fibrillar prion strains, we tested whether the neuronal uptake of prions correlated with the level of soluble, non-sedimenting prion particles, ie, the proteinase-K (PK)-resistant particles that remain suspended in 15% iodixanol following centrifugation. We first measured the non-sedimenting fraction of the five prion strains and found that the subfibrillar strains showed significantly more soluble, non-sedimenting particles than the fibrillar strains ($P < 0.01$) (Fig. 2-5). We next tested prion uptake by neurons. Using primary neurons, we found no difference in the internalization of subfibrillar or fibrillar prions (Fig. 2-2a; Fig. 2-6), and uptake was independent of PrP expression, consistent with previous reports (Magalhaes et al., 2005). As the mechanism of uptake may vary between the subfibrillar or fibrillar prion strains, macropinocytotic- and clathrin-mediated endocytic pathways were inhibited chemically. Macropinocytosis inhibitors markedly decreased the internalization of both subfibrillar and fibrillar prions, indicating that endocytosis of prions occurs primarily via macropinocytosis (Fig. 2-7). Inhibitors of clathrin-mediated endocytosis had less of an effect on prion uptake in primary neurons (Fig. 2-7).

Axonal transport of prions from the axon terminal to the cell body

Given that neurons endocytose both subfibrillar and fibrillar prions in vitro, yet only the subfibrillar prions efficiently spread to the brain in vivo, we reasoned that prions may differ in their capacity for axonal transport. Therefore we next used neurons to examine the transit

of prion aggregates from the axon terminals to the cell body. Neurons grown in microfluidic compartmentalized chambers were exposed to subfibrillar or fibrillar prions, or a mock control, for 48 hours (Fig. 2-2b), and two weeks later the cell bodies were analyzed for PrP^{Sc} using the highly sensitive and specific real-time quaking induced conversion (RT-QuIC) assay (Wilham et al., 2010). As a control for leakage, microfluidic chambers lacking cells were exposed to prions in the axonal compartment, and the cell body compartments were assessed for prion seeding activity. As a further control, all chambers were assessed for leakage between compartments using trypan blue dye and showed no dye into the cell body compartment. Surprisingly, both the subfibrillar and fibrillar prion strains were detected in the cell bodies in equal numbers of experimental replicates (Fig. 2-2c). No prions were detected in the mock (Fig. 2-2c) or in the prion-seeded, cell-free control samples (data not shown). Collectively, these results suggest that the fibril-forming prion strains can transit in nerves, despite rare entry into the CNS in vivo.

Increasing the particle number enhances neuroinvasion of 87V prions

Our findings indicate that the fibrillar prion strains are endocytosed and transported from the axon terminals to the neuronal cell bodies in vitro, although rarely enter the CNS in vivo. The in vitro exposure to the fibrillar strains would flood the axon terminals with small and large fibril fragments, whereas in vivo, the smaller, diffusible particles would likely travel faster through the interstitial space to the axon terminals (Reddy et al., 2006). To test the hypothesis that the level of small, diffusible prion particles impacts neuroinvasion, we exposed mice to a higher dose of 87V fibrillar prions IT (10-fold increase). We observed a 53% increase in the attack rate (number of mice developing terminal disease) and the presence of prion plaques in the cerebral cortex (Fig. 2-3, a - b), indicating that the poor neuroinvasion was not due to an absolute block

in the capacity for neuroinvasion, but that more prion particles or a higher titer, could enhance neuroinvasion of 87V prions.

Increasing prion aggregate solubility enhances neuroinvasion

We and others have found that sonication decreases prion fibril size (Chatani et al., 2009; Sun et al., 2008), shifting the fibril population from a mixture of short and long fibrils to more uniformly short fibrils (Fig. 2-3c). In addition to decreasing the fibril size, sonication also markedly increased the solubility of prion fibrils from 3% soluble to approximately 37% soluble (Fig. 2-3d). We next assessed how sonication alters the solubility of brain-derived prions using a modified disaggregation assay that does not involve PK digestion to deplete the PrP^{C} (Deleault et al., 2008). In brief, samples were subjected to ultracentrifugation and the pellet fraction was resuspended and divided into two tubes, one of which was sonicated. All samples were overlayed onto 15% iodixanol, centrifuged, and the PrP^{Sc} was measured in the supernatant and pellet fractions. We found that the soluble, non-sedimenting fraction of all strains except mCWD significantly increased post-sonication (Fig. 2-3d). In the case that the number of small particles governs neuroinvasion, sonicating the prions while maintaining the same absolute prion mass, would be expected to increase spread to the CNS. Sonicating the 87V fibrillar prions increased prions in the soluble fraction by 2.5 fold and significantly increased the attack rate, as 50% of mice developed terminal prion infection and prion plaques in the cerebral cortex (previously 11%). The mean incubation period was slightly shorter than the single mouse inoculated with the unsonicated prions (350 versus 374 days) (Fig. 2-3d). Our data suggest that a critical threshold of small, soluble particles is required for prion propagation into the CNS. Interestingly, the mCWD prions, which form exclusively large dense plaques of long fibrils (Sigurdson et al.,

2006) and primarily insoluble PrP^{Sc} aggregates, did not neuroinvade following exposure of mice to either a higher prion concentration or to sonicated prions (Fig. 2-7). Collectively, these results show that high levels of small, soluble PrP^{Sc} particles correlates with the ability of a prion to neuroinvade.

Discussion

Prion spread from tongue to brain is reported to be highly efficient, occurring rapidly and without requiring an initial replication phase in lymphoid tissue (Bartz et al., 2005; Bartz et al., 2003; Bessen et al., 2009). Consistent with these reports, we also found highly efficient, rapid spread of prions from tongue to brain for three subfibrillar strains. However, two fibrillar strains either failed to spread, or rarely spread following an intra-tongue challenge. Similar findings have been reported for other fibrillar prions inoculated into the tongue or other peripheral sites (Beringue et al., 2008; Collis and Kimberlin, 1985), including GPI-anchorless prion fibrils, which accumulate in the nerves and muscle of the tongue, but fail to spread into the brain following a tongue inoculation (Klingeborn et al., 2011).

The poor spread of fibrillar prions into the brain was unlikely due to a lack of prion uptake by neurons. In primary neurons, fibrillar prion strains were readily internalized by macropinocytosis, similar to other protein aggregates, such as SOD1 and tau (Holmes et al., 2013; Yerbury, 2016; Zeineddine et al., 2015). Consistent with our findings, Magalhães and colleagues showed prion fibrils were internalized by neurons, and uptake was independent of PrP expression (Magalhaes et al., 2005). In addition to being internalized by neurons, the fibrillar 87V prion strain could transit from the axon terminal to the cell body in vitro, indicating that concentrated 87V prions applied directly to axon terminals could be transported within a neuron. This finding was

consistent with the single mouse developing prion disease after intra-tongue inoculation, and indicates that the 87V prion strain can, in rare cases, transit into the CNS.

The failure of prion transport to the CNS in most mice exposed to 87V prions may be due to limited exposure of axon terminals to fewer small, soluble particles. When the PrP^{Sc} mass was held constant but the particle sedimentation, and presumably size, of 87V prions was reduced by sonication, prion neuroinvasion profoundly increased. Since sonication does not alter prion strain properties (Deleault et al., 2008), the initial poor neuroinvasion of the fibrillar prions was not likely due to features of the quaternary structure, surface chemistry, or other biophysical properties of the 87V prions, but instead was likely due to the low number of small, non-sedimenting particles. Simply increasing the number of smaller, non-sedimenting prion particles, while maintaining the same PrP^{Sc} mass, enhanced neuroinvasion.

Was the increase in neuroinvasion simply due to a higher prion titer post-sonication? Smaller subfibrillar prion particles have been shown to be more infectious than larger fibrils when compared by mass of PrP (Silveira et al., 2005). Additionally, sonication likely increased the titer due to increasing the particle number and "free ends" available for recruiting PrP^{C} monomers, and we observed an 18% decrease in incubation period in IC-inoculated mice, consistent with a higher titer. However, if a high titer is the primary determinant for prion neuroinvasion, then GPI-anchorless RML fibrillar prions, which develop to very high titers in blood and heart of transgenic mice (Trifilo et al., 2006), should be highly neuroinvasive, even more so than their RML counterpart. Yet this is not the case, as GPI-prions are non-neuroinvasive by the intra-tongue route (Klingeborn et al., 2011), although a requirement of a GPI-anchor for prion neuroinvasion cannot be excluded. High prion titers do not seem to strictly correlate with neuroinvasion.

Although titer does not correlate well with neuroinvasion, it is worth considering that a

higher local prion titer in the tongue may increase prion replication locally and enable prions to neuroinvade. We and others have shown that prion neuroinvasion from the tongue does not require initial replication in local or distal lymphoid tissue. Additionally, mice exposed to the sonicated 87V prions showed an incubation period very similar to the mouse that developed infection from the non-sonicated prions (0.05% difference), suggesting that there was no major change in the incubation period due to any prolonged initial local replication phase. We would argue that the enhanced neuroinvasion observed with the sonicated 87V prions was not due to the increased number of "free ends" per se that enable a heightened peripheral replication phase, but was instead due to a higher number of smaller, soluble and diffusible particles that traverse the interstitial space for nerve entry and axonal transport.

Pathogenic prions form a spectrum of small subfibrillar to highly fibrillar aggregates. The findings reported here may be most relevant to the highly fibrillar, plaque-forming prions with few low density prion particles, similar to the non-neuroinvasive mCWD strain. Bovine amyloidotic spongiform encephalopathy (BASE) is thought to originate as a sporadic prion disease of cattle and causes dense, congophilic, fibrillar plaques in the brain (Casalone et al., 2004). BASE prions are highly infectious to cattle after an IC exposure (Lombardi et al., 2008). Interestingly, an oral exposure of 16 cattle with 1-50 g of BASE prion-infected brain, containing 106.9 LD50 / g, infected only one animal that had been exposed to 50 g of prion-infected brain (6% of exposed cattle) (Okada et al., 2017). In this animal, there were fine and coarse PrP^{Sc} aggregates in the neuropil, but no fibrillar plaques in any brain section examined. Neither the second animal challenged with 50 g of brain, nor any other animal, developed clinical disease or any detectable PrP^{Sc}. These findings suggest very rare entry of BASE prions into the CNS from an extraneural site, and only when the dose is exceedingly high. Similarly, variant CJD in 129M tg650 mice

formed fibrillar plaques in the brain following IC inoculation, yet prions did not spread to the brain following intraperitoneal inoculation, despite early and persistent prion replication in the spleen (Beringue et al., 2008). Together with our findings, these studies suggest that fibril-rich, plaque-forming strains are inefficient at neuroinvasion. Since at least some plaque forming strains replicate in peripheral lymphoid tissues, the lack of neuroinvasion of such subtypes may lead to persistent subclinical carriers of infectious prions.

Taken together, these findings support a model in which small, soluble prion particles shuttle between extraneural organs and the CNS via peripheral nerves. Slowly sedimenting prion particles were previously found to be highly infectious and a feature of strains that induce a rapidly lethal disease (Tixador et al., 2010). Future studies may indicate whether an abundance of small, more soluble particles distinguishes the highly infectious prions from amyloids such as amyloid-β and α-synuclein, which transit poorly from the eye or tongue into the CNS, respectively (Breid et al., 2016; Eisele et al., 2009). These findings also suggest that therapeutic strategies designed to stabilize fibrils (Herrmann et al., 2015a; Margalith et al., 2012) may hinder the neuronal transport of prions, and more generally other protein aggregates, thereby slowing the progression of neurodegenerative disease.

2.3 Materials and Methods

Prion inoculation of mice with diverse strains

WT (VM/Dk) or tga20 (Sv129/C57BL/6) mice (groups of 4-10 male and female mice, 2-3 months old) were inoculated intracerebrally into the left parietal cortex or intra-tongue with 10% or 1% prion-infected brain homogenate prepared from the brains of terminally ill mice. Tga20

mice express the Prnpa sequence variant and develop prion disease after a short incubation period, for example, after IC inoculation, mCWD prions induce disease in 160 days in tga20 mice, but more than 500 days in WT mice. VM/DK mice express the Prnpb sequence variant (Moore et al., 1998) and are highly susceptible to 87V fibrillar and 22L subfibrillar prion strains. Mice expressing PrP under the NSE promoter, as well as *Prnp*-/- mice, were a kind gift from Dr. Adriano Aguzzi. NSE-PrP mice on a *Prnp*-/- background express more than 1.5-fold higher PrP^{C} than WT in cerebral hemispheres (Haybaeck et al., 2011). Mice were maintained under specific pathogen-free conditions on a 12:12 light/dark cycle (2 – 5 mice per cage) and were monitored three times weekly.

Strains 22L and ME7, as well as RML, are mouse-adapted prions originally derived from sheep scrapie that have different cellular targets in the brain and plaque morphologies (Carroll et al., 2016), and were kind gifts from Drs. Michael Oldstone and Adriano Aguzzi, respectively. Mouse-adapted CWD (mCWD) was derived from fifth passage of deer CWD in tga20 mice (Sigurdson et al., 2006).

TSE was diagnosed according to clinical criteria including ataxia, kyphosis, stiff tail, hind leg clasp, and hind leg paresis. Mice were sacrificed at early timepoints (50 and 75% of the incubation period) or at the onset of terminal disease. The brain was halved, and one hemi-brain was formalin-fixed for 2-3 days, then immersed in 96% formic acid for 1 hour, washed in water, and post-fixed in formalin for 2-4 days. Brains were then cut into 2 mm transverse sections and paraffin-embedded for histological analysis. The remaining hemi-brain was cut and a 2-3 mm transverse section at the level of the hippocampus/thalamus was embedded in OCT and immediately frozen on dry ice. The remaining brain sections were frozen for biochemical analyses. No mice were excluded from the analysis.

Histopathology and immunohistochemical stains

Four μm sections of brain were cut onto positively charged silanized glass slides and stained with hematoxylin and eosin or immunostained using antibodies for PrP (SAF84). For PrP staining, sections were deparaffinized and incubated for 5 min in 96% formic acid, then washed in water for 5 min, treated with 5 μg/ml of proteinase-K for 7 min, and washed in water for 5 min. Sections were then placed in citrate buffer (pH 6) and heated in a pressure cooker for 20 min, cooled for 5 min, and washed in distilled water. Sections were incubated with anti-PrP SAF-84 (SPI bio; 1:400) for 45 min followed by anti-mouse biotin (Jackson Immunolabs; 1:250) for 30 min, followed by streptavidin-HRP (Jackson Immunolabs; 1:2000) for 30 min. Sections were then incubated with DAB reagent and an enhancer (Invitrogen), and then were counterstained with hematoxylin.

Paraffin-embedded tissue (PET) blot

Five-μm thick sections were collected onto 0.45 μm nitrocellulose membranes (Biorad), dried at room temperature overnight, and heated at 55 0C for 30 min. Membranes were then incubated in xylene and serially rehydrated in 100%, 70% isopropanol, and distilled water with 0.1% Tween-20 for 10 min each. To improve tissue adherence, membranes were dried. After a brief rinse with TBST [10 mM Tris-HCl (pH 7.8), 100 mM NaCl, 0.05% Tween-20], membranes were incubated in 50 μg/ml of PK in 10 mM Tris-HCl (pH 7.8), 100 mM NaCl, 0.1% Brij-35 at 56 0C for 16 hours, washed twice in TBST, incubated in 4M guanidine isothiocyanate in 10 mM Tris-HCl for 30 min, and washed in TBST. Membranes were blocked in casein (Sigma-Aldrich) and immunolabelled with anti-PrP monoclonal antibody SAF84 (Cayman Chemical) for two hours, biotinylated goat anti-mouse IgG (Jackson Immunolabs) for one hour, streptavidin-

HRP (Jackson Immunolabs) for 30 min, and DAB substrate for 5 min. Color development was stopped by immersing briefly in distilled water and then membranes were dried overnight.

Western blotting and sodium phosphotungstic acid precipitation

Brain tissue was homogenized in PBS using a Beadbeater^{TM} tissue homogenizer. Homogenates in a Tris-based lysis buffer (10 mM Tris-HCl, 150 mM NaCl, 10 mM EDTA, 0.5% NP40, 0.5% DOC; pH 7.4) were digested with 50 μg/ml proteinase K at 37 °C for 30 min and the reaction stopped by boiling samples for 5 min in LDS loading buffer (Invitrogen). Samples were electrophoresed in 10% Bis-Tris gel (Invitrogen) and transferred to a nitrocellulose membrane by wet blotting. Membranes were incubated with monoclonal antibody POM19 (discontinuous epitope at C-terminal domain, amino acids 201–225 (Polymenidou et al., 2008), a kind gift from Dr. Adriano Aguzzi) followed by incubation with an HRP-conjugated anti-mouse IgG secondary antibody (Jackson Immunolabs). The blots were developed using a chemiluminescent substrate (ECL detection kit, ThermoScientific) and visualized on a Fuji LAS 4000 imager. Quantification of PrP^{Sc} glycoforms was performed using Multigauge V3 software (Fujifilm).

PrP^{Sc} was concentrated from 87V and mCWD mouse brain samples by performing sodium phosphotungstic acid (NaPTA) precipitation prior to western-blotting (Wadsworth, 2001). Briefly, 100 μl aliquots of 10% brain homogenate in an equal volume of 4% sarkosyl in PBS were incubated for 30 min, then digested with an endonuclease [Benzonase^{TM} (Sigma)] followed by treatment with 100 μg/ml proteinase K at 37 °C for 30 min. After addition of NaPTA, MgCl2, and protease inhibitors (Complete TM, Roche), extracts were incubated at 37 °C for 30 min, and centrifuged at 18,000 g for 30 min at 37 °C. Pellets were resuspended in 0.1% sarkosyl prior to electrophoresis and blotting.

Prion uptake by primary neurons

Prions were partially purified by lysis in Tris buffered saline containing 2% sarcosyl, then were digested with an endonuclease for 30 min at 37 °C, and centrifuged at 18,000 g for 1 hour. The pellets were washed and resuspended in PBS. Primary cortical neurons (200,000 cells) from E18 WT or Prnp-/- mouse embryos were cultured for a minimum of 6 days (in neurobasal media, 2% B27, and 1X GlutaMAX^{TM}) (Zhao et al., 2016; Zhao et al., 2014). In brief, the cerebral cortices were dissected, dissociated with 0.25% trypsin at 37 °C for 20 min, treated with DNase, and triturated. Debris was removed by passing the cells through a 40 μm cell strainer. Cells were then centrifuged for 5 min and resuspended in neurobasal media with 2% B27, 1X GlutaMAX^{TM}. Following several days in culture, neurons were then exposed to partially purified prions for timepoints from 0 - 48 hours. At each timepoint, neurons were washed three times with cold PBS, treated with 0.25% trypsin for 3 min, centrifuged for 5 min at 2000 g, washed in cold PBS, and centrifuged again prior to cell lysis (10mM Tris-HCl, 150 mM NaCl, 1% sarcosyl). Total protein concentration was measured and equal protein amounts were assessed at each timepoint by western blot for analysis of prion uptake. Immunoblot signals were quantified using Multigauge V3 software (Fujifilm). To calculate the percent uptake, the signal at each timepoint was divided by the signal at the final timepoint, which was considered 100%. A minimum of three experimental replicates were performed.

Exposure of neurons to compounds interfering with internalization

Cortical neurons from E18 mouse embryos were cultured for 7 days. Dynasore (80 μM), cytochalasin D (2 μM), amiloride (200 μM), 5-(N-ethyl-N-isopropyl)amiloride (EIPA) (50 μM), rottlerin (30 μM), chlorpromazine (5 μg/ml) in media were added to neurons for 30 min. Prions

were then added to the neurons for 3 hours, and then cells were washed three times with cold PBS and treated with 0.25% trypsin for 3 min to remove surface PrP^{Sc}. Media was added and cells were collected and washed with PBS prior to lysis with lysis buffer (Tris-HCl, 150 mM NaCl, and 1% sarcosyl) and endonuclease treatment. Protein concentration was measured and proteins were normalized prior to proteinase K digestion and immunoblotting. Six experimental replicates were performed for all compounds except EIPA (3 replicates).

Retrograde axonal transport using microfluidic chambers

Cortical neurons were cultured from wild type (C57BL/6) mouse E18 embryos. The cerebral cortices were dissected, dissociated with 0.25% trypsin at 37 $^{\circ}$C for 20 min, treated with DNase, and triturated. Debris was removed by passing the cells through a 40 μm cell strainer. Cells were then centrifuged for 5 min and resuspended in neurobasal media with 10% FBS, 2% B27, 1X GlutaMAX^{TM}. Approximately 25,000 neurons were loaded into the cell body compartment of the polydimethylsiloxane microfluidic chamber for protein biochemistry assays (Weissmiller et al., 2015). After 5 min, the remaining compartments were filled with media. Cells were maintained in maintenance medium (neurobasal media with 2% B27 and 1X GlutaMAX^{TM}). The neurons were grown in the microfluidic chambers for 6 days or until neuronal projections extended into the axon compartment. Subfibrillar or fibrillar prions were added to the axon terminal compartment for 48 hours. Prions were removed after 48 hours by washing, and cell bodies and axons were collected 2 weeks later. The axons and somas were each washed three times with PBS. The soma chamber was washed by placing the chamber with the soma compartment in a vertical position and passing PBS through the somal well. The somas were collected first by similarly holding the chamber vertically and applying lysis buffer

(10mM Tris-HCl, 150 mM NaCl, 1% sarcosyl, benzonase^{TM}, MgCl2) to the well and collecting the lysate. Axons were next collected by adding lysis buffer to the axon chamber. All chambers were assessed after use for leakage using trypan blue dye.

RT-QuIC assay

RT-QuIC reaction mix was composed of 10 mM phosphate buffer (pH 7.4), 130 mM NaCl, 0.1 mg/ml recombinant mouse prion protein (residues 23-230 rPrPSen), 10 μM Thioflavin T (ThT), 1 mM ethylenediaminetetraacetic acid tetrasodium salt (EDTA), and 0.001% SDS. Aliquots of the reaction mix (98 μl) were loaded into each well of a black 96-well plate with a clear bottom (Nunc) and seeded with 2 μl of a 10-1 dilution of 22L, 87V or WT mouse brain exposed neuronal lysates (somas or axons). The plate was sealed (plate sealer film, Nalgene Nunc International) and incubated at 42 $^{\circ}$C in a BMG FLUOstar Omega plate reader with cycles of 1 minute shaking (700 rpm double orbital) and 1 minute rest. ThT fluorescence measurements (450 +/- 10 nm excitation and 480 +/- 10 nm emission; bottom read) were taken every 45 min. To compensate for minor differences in baselines between fluorescent plate readers and across multiple experiments, data sets were normalized to a percentage of the maximal fluorescence response (260,000 rfu) of the plate readers after subtraction of the baseline and plotted versus reaction time. Reactions were classified as RT-QuIC positive based on a threshold set by 1.5 standard deviations from the average of the wild-type control brains at 30 hours (approximately 10% of ThT emission).

Prion solubility assay of PrP^{Sc}

Brain homogenates were solubilized in 1% sarcosyl in PBS and digested with 50 μg/ml of proteinase K (final) (WT) or 100 μg/ml (tga20) for 30 min at 37 °C. Protease inhibitors were added (Complete TM™), and samples were layered over 15% Optiprep™ and centrifuged at 18,000 g for 30 min at 4 °C. Supernatants were removed and pellets were resuspended in PBS in a volume equivalent to the supernatant. Supernatant and pellet fractions were immunoblotted using anti-PrP antibody POM19 and PrP signals were captured and quantified using the Fuji LAS 4000 imager and Multigauge V3.0 software. Brain samples from 3-5 mice were measured per strain.

PrP^{Sc} disaggregation assay

The protocol was adapted from Deleault et al., 2008 (Deleault et al., 2008). In brief, 10% brain homogenate was solubilized in 1% sarcosyl in PBS for 30 min at 37 °C. 1% Triton X-100 in PBS was added and samples were ultracentrifuged at 100,000 g for 1 hour at 4 °C. The supernatant was discarded and pellets were resuspended in 1% Triton X-100 and incubated for 2 hours at 37 °C. After 2 hours, samples were subjected to sonication bursts of 10 seconds on and 30 seconds off at 80% power in a high intensity sonicator bath (Misonix™ horn sonicator) for a total sonication time of 3 min. Samples (700 μl) were then layered over 15% Optiprep™ (300 μl) and centrifuged at 10,000 g for 30 min at 4 °C. Pellets were resuspended in 0.2% sarcosyl in PBS. PrP^{Sc} in the supernatants was concentrated by sodium phosphotungstic acid (NaPTA) precipitation (Wadsworth, 2001). Samples were immunoblotted using the anti-PrP POM19 antibody, an HRP-conjugated anti-mouse IgG secondary antibody, and a chemiluminescent substrate, and signals were captured on the Fuji LAS 4000 Imager and measured using

the Multi Gauge V3.0 software. Brain samples from 4-6 mice were measured per strain.

Assessing the size of recombinant PrP fibrils

Recombinant PrP fibrils were prepared by expression and purification of mouse PrP (amino acids 23-144) followed by fibrillization as previously described (Jones and Surewicz, 2005). Fibrils were sonicated the same way as the brain homogenates: 80% power, 10 seconds on, 30 seconds off, for a total of 3 min of sonication time. Negative stain electron microscopy was performed to compare the unsonicated and the sonicated fibril length. Fibrils were loaded onto a 100 mesh copper grid, washed with PBS, and stained with 2% uranyl acetate. Grids were imaged using transmission electron microscopy on a Tecnai G2 Spirit BioTWIN transmission electron microscope equipped with an Eagle 4k HS digital camera (FEI). For quantification, 8-12 isolated fibrils from 12 images (93 and 147 unsonicated and sonicated fibrils, respectively) were measured using ImageJ software (NIH). Sonicated and unsonicated fibril lengths were compared using a Student's t-test.

Prion fibril solubility assay

Fibrils were diluted to 0.4 mg/ml in PBS. Sonicated and unsonicated fibrils were layered over 15% Optiprep^{TM} and centrifuged at 18,000 g for 30 min at 4 $^{\circ}$C. Supernatants were removed and pellets were resuspended in PBS in a volume equivalent to the supernatant. Supernatant and pellet fractions were immunoblotted using anti-PrP antibody POM1 and PrP signals were captured and quantified using the Fuji LAS 4000 imager and Multigauge V3.0 software.

Statistics

Data are presented as mean +/- SEM unless otherwise indicated with group differences tested using standard parametric methods (Student's t test, 2-tailed). P values of less than 0.05 were considered statistically significant.

2.4 Acknowledgements

The authors thank Nazilla Alderson, Katrin Soldau, Carlitos Chen, Don Pizzo, Timo Meerloo, and Jennifer Santini for providing outstanding technical support. We thank Drs. Steven Edland for discussions, and Adriano Aguzzi for the anti-PrP POM antibody. We are grateful for the excellent care provided by the animal caretakers at UC San Diego.

Chapter 2, in full, is a reprint of material as it appears in: Bett C*, **Lawrence J***, Kurt TD, Orru C, Aguilar-Calvo P, Kincaid AE, Surewicz WK, Caughey B, Wu C, Sigurdson CJ. Enhanced neuroinvasion by smaller, soluble prions. Acta Neuropathol Commun. 2017 Apr 21;5(1):32. doi: 10.1186/s40478-017-0430-z. The dissertation author was first author of this paper.

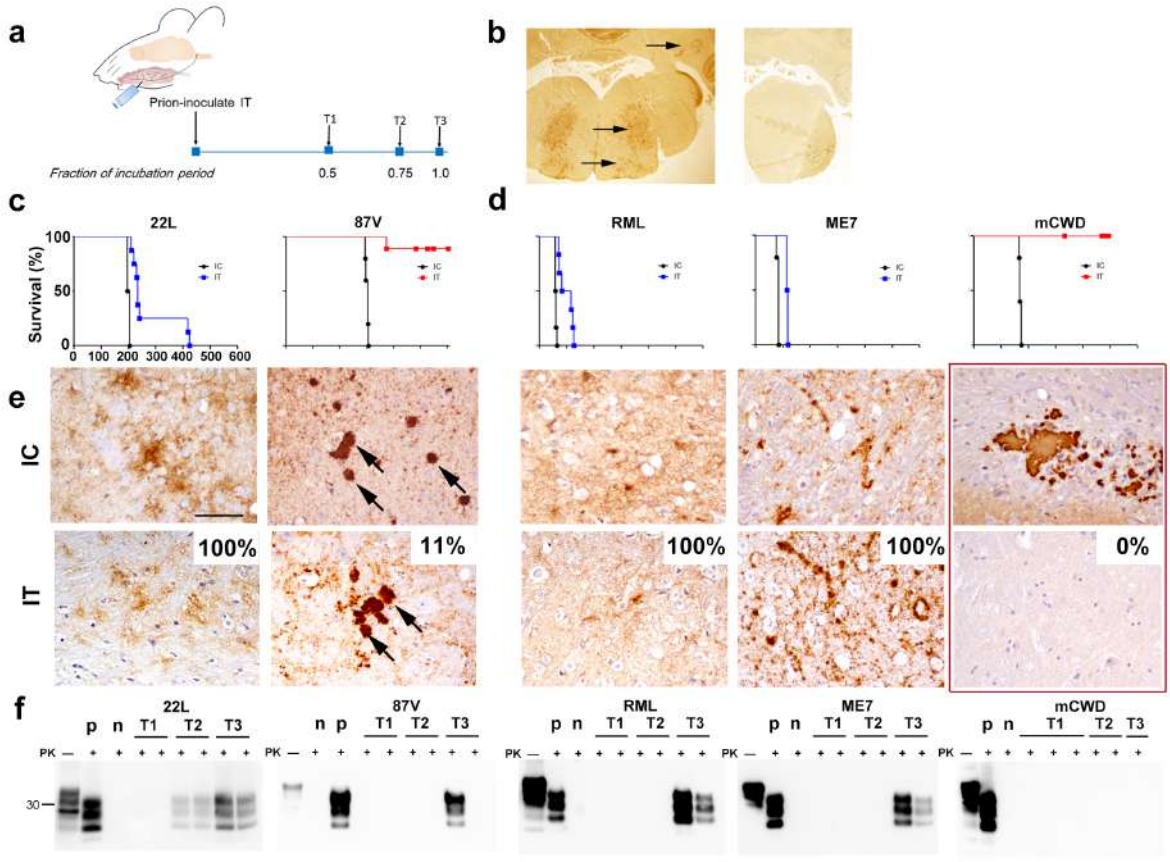

Figure 2.1: Fibrillar prion strains rarely neuroinvade following intra-tongue inoculation. (a) Schematic of time course experiment following IT exposure. T1, and T2: 50% and 75% of the expected incubation period; T3: terminal disease. (b) Paraffin-embedded tissue (PET) blot of brainstem (T2 timepoint) shows subfibrillar prions in the facial, reticular, and deep cerebellar nuclei (strain RML, left panel, arrows), whereas fibrillar prions were not detected at any early timepoint (strain 87V, right panel). (c) Survival curves of WT or (d) tga20 mice (overexpress mouse PrP^C) inoculated IT or IC with subfibrillar (blue - 22L, RML, ME7) or fibrillar (red - 87V, mCWD) prion strains. (e) Brain immunolabelled for PrP shows diffuse prion aggregates or large dense plaques in mice exposed to highly or poorly neuroinvasive prions, respectively. No plaques were detected in mice inoculated with mCWD IT. Percentage of IT-inoculated mice that developed terminal prion disease is noted. (WT: 8-9 mice; tga20: 5-6 mice per group). Brain regions shown are as follows: cerebral cortex (IC: 22L); corpus callosum (IC: mCWD); thalamus (IC: 87V, RML, ME7; IT: 22L); hypothalamus (IT: ME7); brainstem (IT: 87V, RML, mCWD). (f) Immunoblots of brain from T1, T2, and T3 timepoints post IT inoculation. “p” and “n” refer to prion positive and negative brain samples (controls), and PK indicates proteinase K treatment. For IC inoculated mice, n = 4 (22L), 5 (87V, ME7, mCWD), or 6 (RML). For IT inoculated mice, n = 8 (22L), 9 (87V), 6 (RML), 4 (ME7), or 5 (mCWD). Scale bar = 100 μm

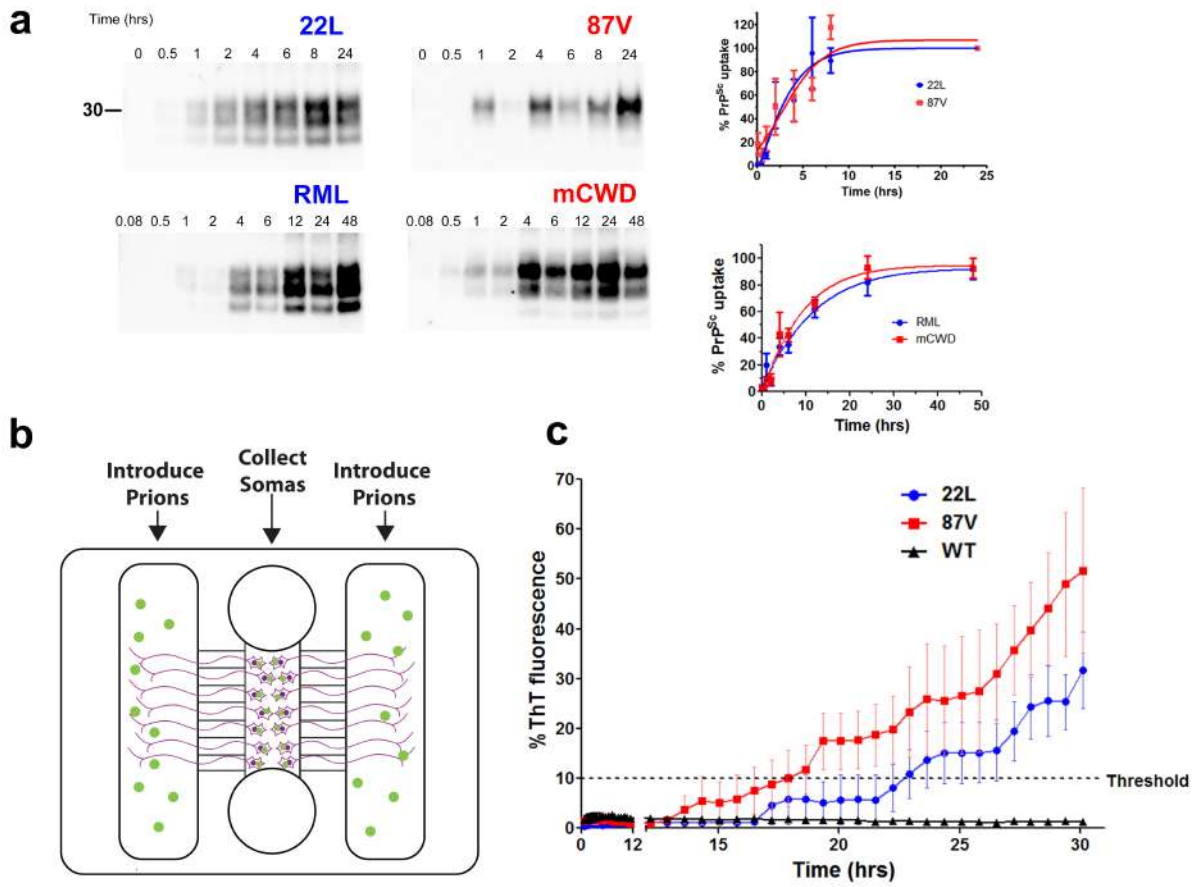

Figure 2.2: Subfibrillar and fibrillar prion strains are internalized and transported from the axon terminal to the soma. (a) Representative western blot shows subfibrillar (22L, RML) or fibrillar (87V, mCWD) prion internalization over time. Mean and SE from four (22L, 87V) or three (RML, mCWD) independent experiments. (b) Schematic of the microfluidic chamber in which the cells bodies reside in a large chamber and axons grow through fine grooves into side chambers where prions are introduced. (c) RT-QuIC analysis reveals PrP^{Sc} in the soma of neurons whose axons were exposed to subfibrillar (22L) or fibrillar (87V) prions, but not uninfected WT brain (WT). Shown are the mean and SE thioflavin T fluorescence signal for the positive cell body samples collected two weeks after prion exposure (4 of 8 positive samples per strain). The 87V prions were detected by RT-QuIC at slightly earlier times, which is not indicative of differences in the prion levels. Dashed line represents the threshold for positivity (see Methods).

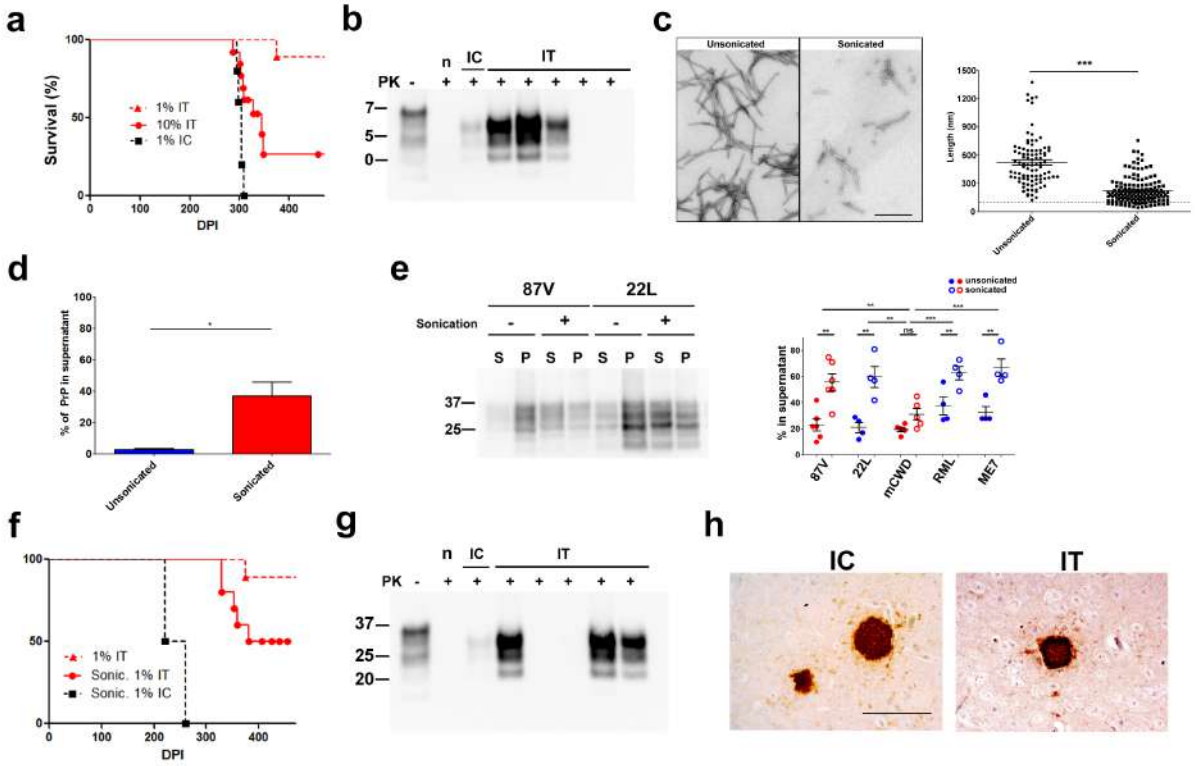

Figure 3

Figure 2.3: Increasing PrP^{Sc} concentration or sonicating prions increases neuroinvasion of fibrillar prion strain 87V. (a) Survival curves of mice inoculated with a 10-fold higher concentration of fibrillar 87V prions (high dose: solid red line) (10% IT: n=13; 1% IT: n=9; 1% IC: n=5) (1% IC and 1% IT mice are the same shown in Fig. 2-1c). (b) Representative western blot of brain shows proteinase-K (PK) resistant PrP^{Sc} in 3 of 5 mice exposed IT to high dose 87V prions. (c) Representative images of recombinant PrP fibril ultrastructure show that sonication results in short homogenous fibrils (mean length of unsonicated = 524 nm versus sonicated = 222 nm; P $<<$ 0.0001, Student's t test). (d) Solubility assay on sonicated and unsonicated fibrils shows that sonication increases the solubility of the fibrils. (e) Disaggregation assay. Western blots show the increase of PK-resistant 22L and 87V prions in the supernatant following sonication of prion-infected brain homogenate. Quantification shows the results of all strains. (f) Survival curve of mice inoculated with sonicated, low dose (1%) fibrillar 87V prions. n = 10 (1% sonic. IT), 9 (1% IT), 4 (1% sonic. IC). The 9 mice inoculated 1% prions IT are also shown in panel a and Fig. 2-1c. (g) Representative western blot of brain from mice exposed IT to sonicated fibrillar 87V prions shows PK-resistant PrP^{Sc} in 3 of 5 mice. (h) PrP^{Sc} shows large dense plaques in the brains of mice (cerebral cortex) exposed IC or IT to sonicated 87V prions. "n": mock-inoculated brain control. Scale bar = 500 nm (panel C) and 100 μm (panel G)

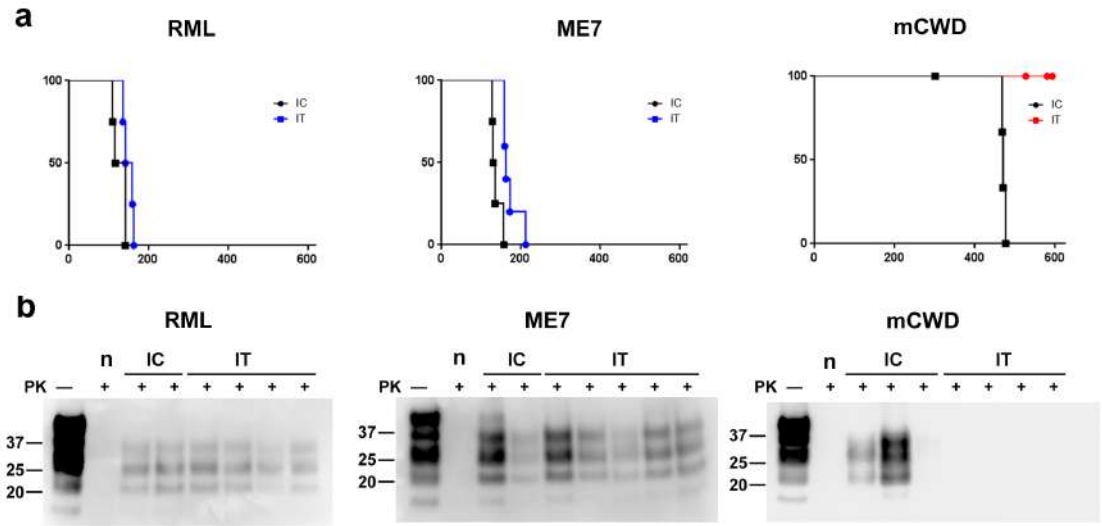

Figure 2.4: mCWD is a non-neuroinvasive strain. (a) Survival curves of tg(NSE-PrP) mice inoculated IC or IT with RML, ME7, or mCWD prions. N = 4 mice per group for all groups except ME7 and mCWD IT where n = 5 mice. (b) Immunoblots from RML-, ME7-, and mCWD-inoculated Tg(NSE-PrP) mice. “n”: uninfected brain control. PK: proteinase K

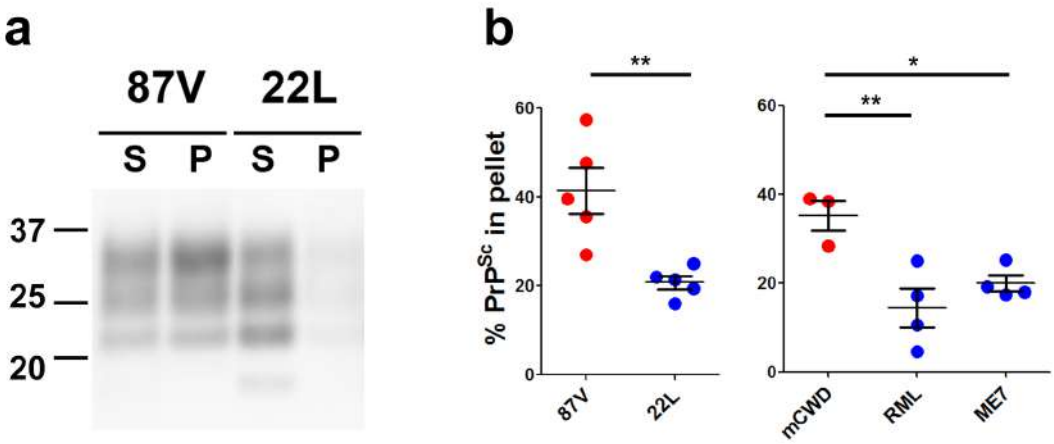

Figure 2.5: Subfibrillar strains are more soluble than fibrillar strains. (a) Western blots show the solubility of two prion strains, 22L (subfibrillar) and 87V (fibrillar). S: supernatant and P: pellet. (b) Quantification of the pellet fraction for all five strains: 87V and 22L in WT mice (n = 5 mice each) and mCWD, ME7, and RML in tga20 mice (n = 3 (mCWD) or 4 mice (ME7, RML). *P $<$ 0.05 and **P $<$ 0.01 for 87V versus 22L prions (Student's unpaired, 2-tailed t-test) and for tga20 mice (one way ANOVA followed by Tukey multiple comparison test).

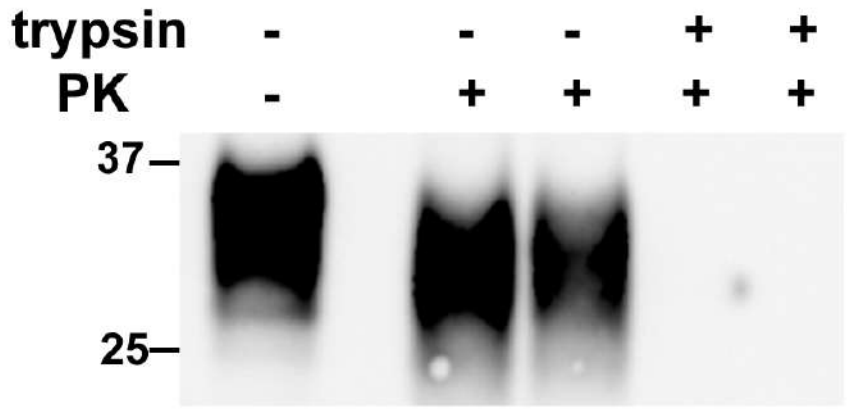

Figure 2.6: No difference in prion uptake in N2a cell. Membrane bound prions are removed by trypsin. Uninfected N2a cells were cooled to 4 °C for 10 min and then exposed to partially purified 87V prions for 45 min at 4 °C. Cells were then washed three times with cold PBS, exposed to 0.25% trypsin for 3 min, centrifuged for 5 min at 2000 g, and washed three times in cold PBS prior to cell lysis, proteinase K digestion, and immunoblotting for prion protein.

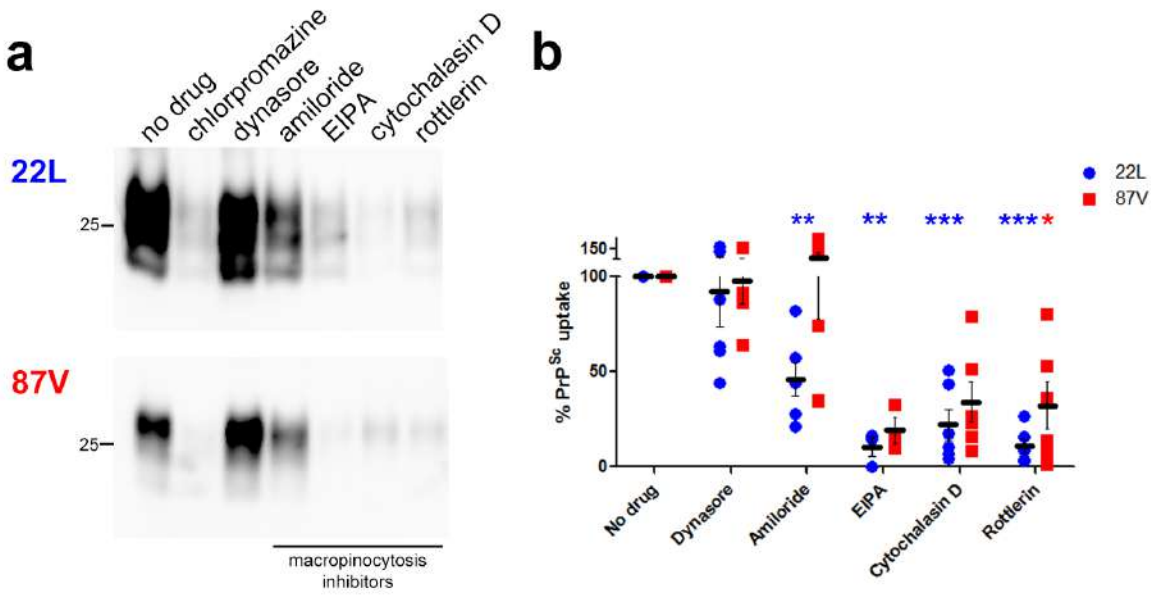

Figure 2.7: Prion uptake in neurons occurs primarily by macropinocytosis. Primary neurons were exposed to prions after chemically inhibiting macropinocytotic- (amiloride, EIPA, cytochalasin D, rottlerin) and clathrin-mediated (dynasore) endocytic pathways. (a) Western blot shows very low PrP^{Sc} in cells in which the macropinocytotic pathways were inhibited. Note that dynasore, an inhibitor of clathrin-mediated uptake, had little effect on 22L or 87V prions. (b) Quantification of PrP^{Sc} uptake relative to the no drug control. Chlorpromazine was toxic to the cells and was not quantified. ***P $<<$ 0.0001 for 22L and *P $<$ 0.05 for 87V, repeated measures one way ANOVA. Results from the Tukey multiple comparison on the raw data are shown on the figure. Six experimental replicates were performed for all inhibitors except for EIPA, which had three replicates.

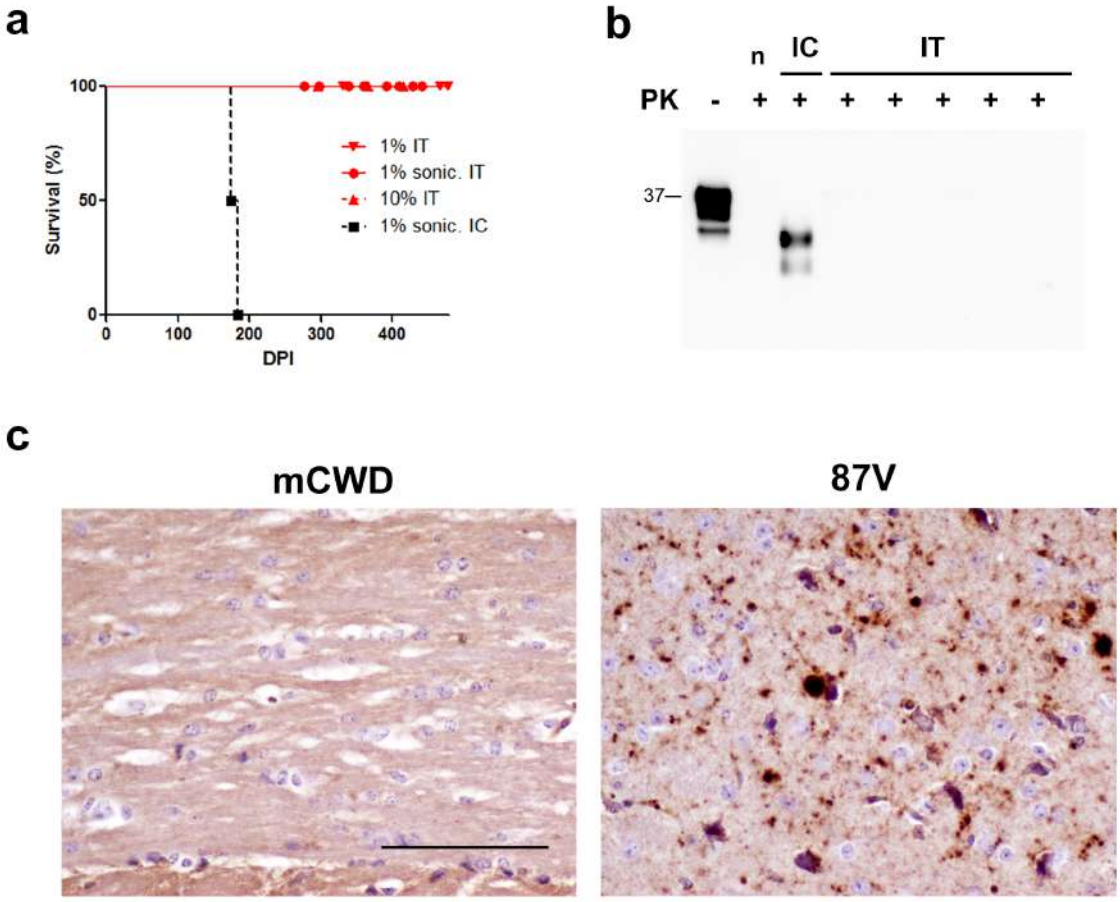

Figure 2.8: mCWD fibrillar prions did not neuroinvade from the IT route following exposure to higher concentration of PrP^{Sc}. (a) Survival curves show that no mice died with detectable mCWD prion plaques. (b) Western blots show no PK-resistant PrP^{Sc} in mice inoculated by the IT route. (c) PrP immunohistochemical stains of brain sections from mice exposed IT to 10% mCWD or 10% 87V. n: mock-inoculated brain control. For mCWD mouse groups: n = 10 (1% sonic.), 5 (10% IT), 5 (1% IT), 4 (1% IC). The mice inoculated with 1% mCWD prions IT and IC are the same as those shown in Fig. 1C. Scale bar = 100 μm.

Chapter 3

Neuronal ESCRT-0 depletion accelerates synapse loss in prion disease

Early synaptic dysfunction and endolysosomal trafficking defects are central to neurodegenerative diseases, including prion disease. Intracellular prions traffic through the multivesicular body (MVB) for degradation or release in exosomes, yet how prion transport through the endolysosomal pathway is linked to prion spread and neuronal toxicity is unclear. To determine how blocking a key prion intracellular transport pathway impacts conversion and toxicity in vivo, here we depleted hepatocyte growth factor receptor (Hrs), an evolutionarily conserved component of ESCRT-0, from astrocytes, microglia, and neurons using a conditional mouse model (*Hgs*$^{f/f}$), and inoculated mice with prions. While Hrs depletion from astrocytes and microglia had no detectable impact on survival, Hrs depletion from neurons markedly reduced survival time despite

mice having unaltered prion levels. Neuronal Hrs depletion accelerated the synaptic structural alterations and biochemical profile typical for terminal prion disease, including longer and deeper post-synaptic densities and increases in phosphorylated synapsin-1 and GluA1 AMPA receptor levels in the pre- and post-synapse, respectively. Moreover, prion-infected wild type mice show a massive post-translational loss of Hrs and Stam1 (ESCRT-0), but not ESCRT-I, -II, or –III components, indicating a specific reduction in ESCRT-0. This work therefore indicates that severely diminished Hrs in prion disease accelerates synaptic pathology/phenotype and reduces survival time and may contribute to the reported synaptic dysfunction in prion disease.

3.1 Introduction

Prion diseases are rapidly progressive neurodegenerative disorders with a typical clinical course of six months and are characterized pathologically by deposits of aggregated prion protein (PrP^{Sc}), gliosis, neuronal spongiform degeneration, and synaptic loss in the central nervous system (CNS). PrP^{Sc} accumulates in the CNS following the misfolding and aggregation of the cellular prion protein, PrP^{C}, which is highly expressed in neurons, particularly at the synapse. Clinical disease is coincident with synaptic dysfunction and the formation of large intracellular vacuoles in neuronal dendrites.

Pioneering efforts using in vitro cellular models have identified prion conversion sites at the plasma membrane (Goold et al., 2013; Veith et al., 2009) and along the endocytic pathway, namely in early recycling endosomes (Marijanovic et al., 2009), multivesicular bodies (MVBs) (Yim et al., 2015), and lysosomes (Caughey et al., 1991). Moreover, additional studies show immunogold-labelled PrP^{Sc} in neuronal MVBs (Jeffrey et al., 1992) and in exosomes emerging from cultured cells (Fevrier et al., 2004), further supporting prion transit and conversion within

the endolysosomal pathway. Yet how intracellular prions impact endolysosomal protein trafficking in neurons and glial cells remains poorly understood, and the relationship between neuronal prion replication, vacuolation, and synaptic loss is not known.

Multiple lines of evidence indicate that endolysosomal trafficking defects are central to prion disease progression. For example, SORCS1 (VPS10), an endosomal trafficking and sorting protein, and syntaxin6 have been identified in two GWAS studies of risk factors for human prion disease (Mead et al., 2012). Moreover, the distribution of endolysosomal pathology correlates with PrP^{Sc} aggregates and lesion localization in CJD (Liberski et al., 2010). The endosomal sorting complexes required for transport (ESCRT) is a highly conserved pathway in eukaryotes that bind and sorts K63 ubiquitinated transmembrane proteins sorts ubiquitinated proteins into multivesicular bodies for degradation in lysosomes or extracellular release in exosomes (Bache et al., 2003). Four complexes function sequentially to sort and guide endosomal proteins into MVBs. ESCRT-0, the first complex in the pathway, is a heterotetramer comprised of two proteins, Hrs and Stam1 (Bache et al., 2003). Interestingly, depleting Hrs disrupts PrP^{C} trafficking into MVBs and sharply reduces prion conversion in prion-infected neuroblastoma cells (Vilette et al., 2015; Yim et al., 2015), suggesting a key role for ESCRT proteins in PrP^{C} internalization and prion propagation.

Despite compelling evidence for intracellular prion conversion in vitro, the subcellular sites and functional impact of intracellular prion conversion in vivo have been challenging to investigate. We reasoned that a cell-targeted approach to disrupt the ESCRT pathway provides an opportunity to identify mechanistically how the ESCRT pathway is impacted by prion conversion within neural cells. We first discovered that prion-infected mice show a massive and specific post-translational reduction in Hrs, but not other ESCRT proteins. We then utilized

the *Hgs*$^{f/f}$ mouse, a model highly relevant to intracellular prion conversion, to investigate in a cell-specific manner how Hrs depletion affects prion replication, endolysosomal trafficking, autophagy, and synaptic degeneration. *Hgs*$^{f/f}$ mice were crossed to Syn-Cre, GFAP-Cre, and LysM-Cre mice to deplete Hrs from neurons, astrocytes, and microglia, respectively, and Cre+ and Cre- littermates were inoculated with prions. Prion-infected mice show a highly predictable disease progression and mimic most aspects of human and animal prion disease. Interestingly, mice with Hrs depleted from astrocytes or microglia showed no alteration in disease course or pathology. In stark contrast, mice with Hrs depleted from neurons showed a markedly accelerated disease progression with concurrent development of severe pre- and post-synaptic defects together with morphologic and biochemical features consistent with excitotoxicity, similar to the Cre- mice but at an earlier timepoint. Collectively, these findings provide evidence that reduced Hrs exacerbates excitotoxicity and synaptic loss and contributes to the rapid clinical progression characteristic of prion disease.

3.2 Results and discussion

Hrs levels are markedly reduced in mice infected with diverse prion strains

The ESCRT pathway delivers ubiquitin-tagged membrane proteins into MVBs for clearance by autolysosomal degradation or by release in exosomes, and critically regulates cell membrane receptor levels (Schmidt and Teis, 2012). To determine how ESCRT proteins are impacted by prion disease, we analyzed brain from terminal prion-infected (22L strain) and age-matched, uninfected mice. Surprisingly, Hrs and Stam1 levels in prion-infected brain were reduced by approximately 80% compared to uninfected control brain (Fig. 3-1a-c). In contrast, Tsg101

(ESCRT-I) and endosomal Rab5 and Rab7 protein levels were unchanged (Fig. 3-1c), suggesting that the reduction in the ESCRT-0 complex was not simply due to neuron loss or a down-regulated ESCRT pathway Remarkably, mice infected with six additional prion strains, including GPI-anchored, GPI-anchorless, oligomeric, or fibril-forming prions, also showed markedly reduced Hrs levels (Fig. 3-1a,b, Fig. 3-9), indicating that Hrs reduction is not strain-specific but a widespread occurrence in prion infection. The Hgs transcript levels in prion-infected and control mice were similar (Fig. 3-1d), indicating Hrs loss is post-translational.

To determine how Hrs levels impact prion disease, we used an *Hgs*$^{f/f}$ mouse model, which has exons 2-4 floxed and generates a truncated non-functional Hrs protein when floxed (Tamai et al., 2008). We depleted Hrs in astrocytes, microglia, and neurons by crossing *Hgs*$^{f/f}$ mice with GFAP-Cre (*Hrs*$^{f/f}$ *GFAP-Cre*+), LysM-Cre (*Hrs*$^{f/f}$ *LysM-Cre*+), and synapsin1-cre (*Hrs*$^{f/f}$ *Syn1-Cre*+) mice, respectively, and inoculating *Cre*+ and *Cre*- littermate control mice with 22L prions. Although 22L prions replicate in astrocytes (Hannaoui et al., 2013; Makarava et al., 2019; Makarava et al., 2020; Sarasa et al., 2012; Tahir et al., 2020), interestingly, we found no differences in survival times when Hrs was depleted from astrocytes [prion-infected *Hrs*$^{f/f}$ *GFAP-Cre*+: 153 $\pm$ 2 versus Cre-: 151 $\pm$ 2 days post-inoculation (dpi)] (Fig. 3-2b). Additionally, there were no differences in survival times when Hrs was depleted from microglia (*Hrs*$^{f/f}$ *LysM-Cre*+: 143 $\pm$ 2 versus Cre-: 146 $\pm$ 1 dpi) (Fig. 3-2c). PrP^{Sc} levels and neuropathologic lesions were also indistinguishable in Cre+ and Cre- mice (Fig. 3-2d-g). Thus, there were no detectable differences in the terminal disease state due to Hrs depletion. To further confirm, we assessed the mice by repeating the experiment in *Hrs*$^{f/f}$ *GFAP-Cre* and *Hrs*$^{f/f}$ *LysM-Cre* mice and evaluating brains at the 75% timepoint (114 dpi), but yet again found no differences in PrP^{Sc} levels or brain lesions (Fig. 3-11a,b), indicating that Hrs depletion in astrocytes or

microglia had no detectable effect on prion pathogenesis.

Neuronal Hrs depletion in mice profoundly accelerates prion disease

While depleting Hrs in astrocytes and microglia had no detectable effect, Hrs depletion in neurons substantially accelerated prion disease progression by nearly 25% [Cre+: 106 $\pm$ 2 versus Cre-: 139 $\pm$ 2 dpi] (Fig. 3-2j), with Cre+ mice showing typical terminal signs of prion disease, including kyphosis, ataxia, and inactivity. The short survival time was surprising considering that Hrs depletion in cultured immortalized cells reduces prion conversion (Vilette et al., 2015; Yim et al., 2015), a finding that we reproduced using Hrs-depleted primary neurons infected with prions (Fig 3-10a).

To determine whether the disease acceleration was due to more rapid prion conversion, we measured the proteinase-K (PK) resistant PrP^{Sc} levels at terminal disease. Interestingly, the PrP^{Sc} levels in the*Hrs*$^{f/f}$*SynCre*+ mice were nearly half that of the *Cre*- mice (45 $\pm$ 2% reduction) (Fig. 32k,l). To directly compare the PrP^{Sc} levels between*Hrs*$^{f/f}$*SynCre*+ and *Cre*- mice at the same timepoint, we repeated the experiment and assessed the PrP^{Sc} levels and histologic features in prion-infected mice at 106 dpi, when only the*Hrs*$^{f/f}$*SynCre*+ mice showed clinical signs. Here we observed no differences in the PrP^{Sc} levels or glycoform profile between the*Hrs*$^{f/f}$*SynCre*+ and *Cre*- mice (Fig. 3-2m,n), suggesting that the kinetics of neuronal prion conversion were unaffected by Hrs depletion, although subtle differences in neuronal PrP^{C} conversion may have been masked by abundant astrocytic prion replication. In cultured neurons, Hrs depletion did not alter total PrP^{C}, but increased surface PrP^{C} levels by approximately 30% (Fig. 3-10c), and we considered the possibility that Hrs depletion increased ADAM10-cleavage of PrP^{C} and extracellular PrP^{Sc} conversion. To test this possibility, we used an antibody rec-

ognizing an ADAM10-cleaved PrP neoepitope (Linsenmeier et al., 2018), however found no differences in ADAM10-cleaved PrP^{Sc} levels at 106 dpi (Fig. 3-2p,q). Furthermore, there were no differences in PrP^{Sc} morphology or distribution in any brain region (Fig. 3-2o). Therefore, neuronal Hrs depletion specifically and markedly accelerated disease progression in the context of unaltered PrP conversion kinetics.

We next assessed the possibility that neuroinflammation or spongiform degeneration was driving the early disease onset, yet we observed significantly less spongiform change and microglial activation in the terminal prion-infected *Hrs*$^{f/f}$ *SynCre*+ mice than in the Cre- mice (Fig. 3-3a-c). Notably, the microglial activation in the prion-infected *Hrs*$^{f/f}$ *SynCre*+ was surprisingly low, similar to the uninfected control brain (Fig. 3-3b,c). In stark contrast, astrocyte activation was profoundly and consistently increased in all prion-infected *Hrs*$^{f/f}$ *SynCre*+ as compared to the terminal *Cre*- brain (Fig. 3-3d,e), despite the lower PrP^{Sc} levels. Thus, in the *Cre*+ mice, PrP^{Sc} levels, spongiosis, and microglial activation were low yet astrocytic activation was exceedingly high, revealing an unusual uncoupling of the microglial and astrocytic response.

Proteostasis: Autophagy is unaltered, while ubiquitinated proteins accumulate excessively

Depleting ESCRT proteins reportedly disrupts autophagic flux (Filimonenko et al., 2007; Lee et al., 2007; Tamai et al., 2007), which may accelerate neurodegeneration. We depleted Hrs in cultured neurons and also found that autophagic flux was impaired following autophagic induction with rapamycin (Fig. 3-12).

Since prion disease is associated with impaired autophagy (Boellaard et al., 1991; Liberski et al., 2008; Lopez-Perez et al., 2019a; Lopez-Perez et al., 2019b; Lopez-Perez

et al., 2020; Xu et al., 2012), we next tested the autophagic protein levels in prion-infected brain. Prion-infected*Hrs*$^{f/f}$ *SynCre*+ showed significantly lower p62 and LC3-II/I than the terminal*Hrs*$^{f/f}$ *SynCre*- brain, with levels comparable to uninfected brains (Fig. 3-4a-c), suggesting that autophagy does not underlie the accelerated disease. Histologically, LAMP1 immunostaining in the brain was also low in the terminal prion-infected*Hrs*$^{f/f}$ *SynCre*+ mice, indicating a lack of accumulated lysosomes (Fig. 3-4d).

Since ESCRT-0 sorts K63-tagged ubiquitinated membrane proteins, we reasoned that ubiquitinated proteins may accumulate at earlier disease stages in the prion-infected*Hrs*$^{f/f}$ *SynCre*+ mice. We observed a similar increase in ubiquitinated protein accumulation in the *Cre*- and *Cre*+ mice at terminal disease (Fig. 3-4 e-f), indicating that the clearance of ubiquitinated proteins was severely disrupted. To then assess whether ubiquitinated protein clearance was retarded more in the *Cre*+ mice, we compared *Cre*+ and *Cre*- mice at the same timepoint. Consistent with the loss of Hrs function, ubiquitinated proteins accumulated to two-fold higher levels in the prion-infected*Hrs*$^{f/f}$ *SynCre*+ brain as compared to the *Cre*- brain at 106 days, indicating that the clearance of ubiquitinated proteins was significantly disrupted (Fig. 3-13) .

Select other endosomal proteins were altered, but only in the prion-infected, Hrs-depleted mice. Whereas the recycling endosomal protein, Rab11a, and late endosomal protein, Rab7, levels were unaltered (Fig. 3-5a,c, d), the early endosomal protein, Rab5, and retromer protein, Vps35, were reduced by 84 days or by terminal disease, respectively (Fig. 3-5a,b, e). Both Rab5 and Vps35 are localized to the pre-synaptic terminal in neurons and are important in synaptic vesicle (SV) recycling (Inoshita et al., 2017; Shimizu et al., 2003; Star et al., 2005; Vazquez-Sanchez et al., 2018; Wucherpfennig et al., 2003). Collectively, these results indicate

that neuronal Hrs depletion in prion-infected mice leads to more severe and early astroglial activation, ubiquitinated protein accumulation, and a reduction in specific endosomal proteins involved in SV recycling, Rab5 and Vps35 (Inoshita et al., 2017; Shimizu et al., 2003).

Accelerated development of severe synaptic structural defects in *Hrs$^{f/f}$ SynCre+* prion-infected mice

The altered Rab5 and ubiquitinated protein levels may indicate dysregulated SV and glutamate receptor recycling in the Hrs-depleted mice, particularly during prion-infection. To investigate how Hrs depletion impacts synapses in prion disease, we first characterized the synaptic ultrastructure in the*Hrs$^{f/f}$ SynCre*+ and *Cre*- mice. We serially imaged 20 synaptic fields (hippocampal CA1 molecular layer at 15,000X) from 12 mice at 84, 106, and 139 dpi, and measured the curvature and post-synaptic density (PSD) depth, post-synaptic length, and the presence of docked SVs in terminal prion-infected and uninfected*Hrs$^{f/f}$ SynCre*+ and *Cre*- mice (8 infected and 4 uninfected). By 84 dpi, the synapses of the prion-infected*Hrs$^{f/f}$ SynCre*+ mice were highly curved (primarily concave). However, by 145 dpi, the terminal*Hrs$^{f/f}$ SynCre*- mice also showed highly curved synapses (Fig. 3-6a,b), indicating that the *Cre*+ mice had developed a markedly accelerated post-synapse curvature phenotype.

By terminal disease,*Hrs$^{f/f}$ SynCre*+ mice (106 dpi) and*Hrs$^{f/f}$ SynCre*- mice (139 dpi) also showed a thickened and irregular PSD, with increased length and depth (Fig. 3-6d,e). Notably, an increase in PSD length and depth has been reported with excitotoxicity and lack of post-synaptic receptor recycling (Fischer et al., 2000; Marrone and Petit, 2002; Matus, 2000; Tao-Cheng, 2019). Remarkably, the*Hrs$^{f/f}$ SynCre*+ mice had a significant increase in the PSD area as early as 84 dpi, whereas the*Hrs$^{f/f}$ SynCre*- mice exhibited no increase in the PSD area

at 84 or 106 dpi.

Since the ESCRT pathway is particularly important for the recycling of SV proteins (Sheehan et al., 2016), we evaluated synapses for the presence of docked SVs. At 84 dpi, nearly all synapses showed docked SVs (Fig. 3-6f). However, by terminal disease, there were more synapses that lacked docked SVs in the prion-infected *Cre*- and *Cre*+ mice than in the control mice (Fig. 3-6f), which may occur with synaptic expansion. Together, the numerous highly curved synapses, longer and deeper PSDs, and frequent lack of docked SVs in the terminal prion-infected mice may be due to the synapses becoming larger , with the *Cre*+ mice developing this synaptic phenotype more than 30 days earlier.

Neuronal Hrs depletion accelerates synaptic protein loss in prion disease

We reasoned that diminished Hrs at the synapse may reduce the endocytosis of ubiquitinated post-synaptic receptors, potentially causing glutamate dysregulation, therefore we next analyzed a panel of pre- and post-synaptic proteins at 84 days, 106 days (terminal *Cre*+ mice), and 139 days (terminal *Cre*- mice). Hrs binds Snap25 on SVs (Sheehan et al., 2016), yet neither Hrs depletion nor prion-infection altered the levels of three SV proteins, Snap25, VAMP2, or synaptophysin, at any timepoint (Fig. 3-7a-d). Interestingly, by 84 dpi, prion-infected $Hrs^{f/f}$ *SynCre*+ mice showed a significantly higher level of the phosphorylated SV protein, synapsin-1 (p-syn1) and GluN1 than *Cre*- mice, yet there were no significant differences between *Cre*+ and *Cre*- mice for most other synaptic proteins assessed (synapsin-1, mGluR5, GluA1, PSD95, synaptophysin, Vamp2, Snap25) (Fig. 3-14). By 106 days, prion-infected *Cre*+ mice (terminal) showed a marked reduction in total syn-1 (*Cre*+: 0.91 ± 0.09, *Cre*-: 1.35 ± 0.05) (Fig. 3-15). Finally, by 139 days, prion-infected *Cre*- mice (terminal) also showed an increase

in p-syn1 and a reduction in syn-1 mice (*Cre*+: 0.66 $\pm$ 0.05 and *Cre*-: 0.55 $\pm$ 0.05 relative to uninfected brain)(Fig. 3-7a,e), indicating that the syn1 dysregulation was similar yet accelerated in the Hrs-deficient, prion-infected mice.

Post-synaptic proteins, including ionotropic and metabotropic receptors, were also altered in prion-infected mice. The level of post-synaptic scaffolding protein, PSD95, was unaltered at the 106 day timepoint (Fig. 3-7a,g, Fig. 3-15). Total GluA1 receptor levels were unchanged at all timepoints (Fig. 3-7a, h, Fig. 3-15). However, the phosphorylated GluA1 receptors, GluA1 p831 and p845, were increased in terminal prion-infected $Hrs^{f/f}$ *SynCre*+ mice (106 days) and *Cre*- mice (139 days) (Fig. 3-7k-m), suggesting that GluA1 may route to the post-synaptic membrane with prion infection. Similarly, mGluR5 was significantly reduced in the terminal prion-infected *Cre*+ mice (106 days) and *Cre*- mice (139 days) (*Cre*+: 0.75 $\pm$ 0.05, *Cre*-: 0.73 $\pm$ 0.05 relative to uninfected) (Fig. 3-6a,f). Arc levels were increased in all terminally affected mice (Fig. 3-6i), consistent with synaptic remodeling. We considered that a heightened loss of neurons in the $Hrs^{f/f}$ *SynCre*+ prion-infected mice may underlie differences in protein levels, yet Neu1 immmunolabeled cortical sections revealed similar numbers of total neurons (Fig. 3-16). Taken together, our data show a significantly accelerated increase in syn1 and GluA1 receptor phosphorylation and loss of select pre- and post-synaptic proteins, particularly syn-1 and mGluR5, in the $Hrs^{f/f}$ *SynCre*+ prion-infected mice, suggesting that the massive, widely observed loss of Hrs may be a driver of the severe synaptic degeneration that is a well-established pathological hallmark of prion disease.

Discussion

In this study, we define a role for Hrs in prion disease progression. Hrs is one of two proteins in the ESCRT-0 complex that specifically sorts ubiquitinated endosomal proteins into MVBs to be degraded in lysosomes or released in exosomes. Here we observed significant synaptic protein loss in the brains of prion-infected *Hrs*$^{f/f}$ *Syn1-Cre*+ and *Hrs*$^{f/f}$ *Syn1-Cre*- mice compared to uninfected *Hrs*$^{f/f}$ *Syn1-Cre*+ mice and littermate controls. This finding is in line with the growing evidence suggesting that synapse loss is a cause of death in prion disease. (Belichenko et al., 2000b; Brown et al., 2001; Chiti et al., 2006; Ferrer, 2002b; Jeffrey et al., 2000; Johnston et al., 1997; Mallucci et al., 2007; Sisková et al., 2009). Studies have seen a loss of either pre-synaptic (Gray et al., 2009b) or post-synaptic (Ferrer and Puig, 2003) proteins in prion disease. While we saw more of an effect on both pre- and post-synaptic proteins (synapsin-I and mGluR5), other differences may be more subtle and region-specific. Furthermore, the role of Hrs in the regulation of synapse is supported by recent studies, implicating the importance of Hrs in synaptic vesicle recycling (Sheehan et al., 2016) and ubiquitination of receptors at neuromuscular junctions (Watson et al., 2015). However, the exact mechanism of synapse loss in prion disease, accentuated by loss of Hrs, remains to be elucidated. The ultrastructure of neurons at terminal prion disease reveals dramatic alterations to synapse morphology that are in line with previous observations of prion infected brains. Studies show an increase in area of post-synapses and a decrease in the degree of curvature of the synapses during prion disease; the post-synapses appear to engulf the pre-synapses (Siskova et al., 2009). In the *Hrs*$^{f/f}$ *Syn1-Cre*+ mice, ultrastructure showed similar changes: not only was there a decrease in the number of synapses, but the degree curvature of the synapses was decreased.

PrP^{C} interacts with synaptic proteins, which has been implicated as a mechanism of

neurotoxicity in prion disease (Beraldo et al., 2011; Um et al., 2013). One such receptor, mGluR5, has been identified to interact with PrP^C. We interestingly discovered that mGluR5 levels are decreased in all prion-infected mice. Increased excitotoxicity exhibited through PrP binding mGluR5 would lead to increased endocytosis of the synaptic receptors. These findings are corroborated by reports that that Amyloid-β exhibits toxicity through PrP^C and mGluR5 (Um et al., 2013). In addition, a recent study illustrates that Amyloid-β oligomers impair glutamate re-uptake in neurons and astrocytes, causing excitotoxicity (Corbett et al., 2019), which would lead to synapse loss. If prion excitotoxicity is exhibited through mGluR5, this could be one such cause of synapse loss in prion disease. We suspect that depletion of Hrs could accelerate excitotoxicity effects through dysregulation of endocytic pathways.

Additionally, our findings may also provide insight into the role of other endosomal proteins in neurodegeneration. In the prion infected *Hrs*$^{f/f}$ *Syn1-Cre*+ mice, we observed a decrease specifically in Rab5 and Vps35 proteins, both of which are important for synaptic vesicle recycling. Hrs works in conjunction with Rab5 to sort endosomes into the ESCRT pathway. Rab5 is essential for the endo- and exo-cytosis of synaptic proteins and vesicles within the synapses (Shimizu et al., 2003; Wucherpfennig et al., 2003) and is localized to the pre-synaptic terminal (Pavlos et al., 2010). Interestingly, Rab5 loss only occurs with Hrs-depletion and prion disease combined, suggesting a compounding effect of prion disease and ESCRT pathway dysregulation on Rab5 endosomes. Vps35, an essential protein in the retromer complex, has also been localized to the presynaptic terminal and important, but not essential, for synaptic vesicle recycling (Inoshita et al., 2017; Vazquez-Sanchez et al., 2018). Our findings implicate a novel connection between prion disease and early endosomal proteins, as well as link between Hrs and these proteins, contributing to presynaptic terminal dysfunction. Our findings are corrobo-

rated by RNAseq studies that have observed a decrease in Vps35 and other endosomal protein transcripts in both mice and human prion-infected brains (Bartoletti-Stella et al., 2019), reaffirming the need for additional research on early endosomal pathways in neurodegeneration.

Given that previous reports (Vilette et al., 2015; Yim et al., 2015), as well as our own data, concluded that Hrs depletion results in a decrease in PrP^{Sc} conversion in vitro, we were initially surprised that depletion of Hrs in neurons, astrocytes, or microglia did not noticeably affect prion conversion in vivo. The location of prion conversion remains highly controversial, with the field being equally uncertain whether prion conversion occurs intracellularly or extracellularly (Goold et al., 2011) (Borchelt et al., 1992), yet in vivo studies of prion conversion are scarce. One in vivo study reduced levels of muskelin (Heisler et al., 2018), which resulted in increased exosomal and surface PrP^{C} levels, and when inoculated with prion disease, accelerated disease and increased PrP^{Sc} load, implicating the cell surface as the major site of prion conversion. When depleting Hrs in neurons, we also observed altered subcellular trafficking, resulting in an increase in surface PrP^{C}. Yet, contrary to this study, we did not see accelerated disease due to increased PrP^{Sc} load or increased ADAM-10 cleaved PrP^{Sc}. Taken together, these findings support the need to investigate prion conversion sites further in vivo. Additionally, glial cells are large contributors to prion propagation, and could overshadow any decrease in neuron conversion.

It is conceivable that depletion of Hrs could contribute to autophagosome accumulation in prion disease and accelerate neuron death due to the role of the ESCRT pathway in autophagy (Filimonenko et al., 2007; Lee et al., 2007; Tamai et al., 2007). We demonstrate that loss of Hrs results in a block of autophagosome maturation, as evident from the LC3-GFP-mCherry assay in the primary neurons which is in agreement with previously reported data from

MEF cells (Tamai et al., 2007) and yeast (Hatakeyama and De Virgilio, 2019; Schafer et al., 2020), but had yet to be seen in neurons. In prion disease, autophagy is impaired at terminal disease, leading to accumulation of autophagosomes (Lopez-Perez et al., 2019a; Lopez-Perez et al., 2020; Sikorska et al., 2007; Xu et al., 2012). Additionally, prion infection impairs lysosomal degradation (Shim et al., 2016). We initially hypothesized that acceleration of death in *Hrs*$^{f/f}$ *Syn1-Cre*+ prion-infected mice was due to the combination of induced autophagy from prion disease and impaired degradative pathways from Hrs depletion, but we observed no accumulation of autophagosome proteins LC3 and p62 in *Hrs*$^{f/f}$ *Syn1-Cre*+ prion-infected mice, whereas*Hrs*$^{f/f}$ *Syn1-Cre*- prion-infected mice have high levels of p62 and LC3-II/I, as previously reported. We concluded that autophagosome accumulation occurs much later in disease and is likely a secondary effect of prion disease, which is in line with the most recent studies on autophagy and prion disease (Lopez-Perez et al., 2020).

Our findings are the first report of an uncoupling of astrogliosis and microgliosis in prion disease. Gliosis is a signature characteristic of prion disease. Both microglia and astrocytes are activated in prion disease, but the exact role of glia in prion disease remains controversial. Microglial activation occurs early on in prion disease (Vincenti et al., 2015), and has been proposed as protective by several studies (Aguzzi and Zhu, 2017; Gomez-Nicola et al., 2013; Muth et al., 2017; Zhu et al., 2016). In lieu of the *Hrs*$^{f/f}$ *Syn1-Cre*+ mice lacking microgliosis and disease is accelerated, our data is in line with the model that microglia are protective and do not contribute to “synaptic stripping” (Sisková et al., 2009). One possible explanation for the uncoupling of astrogliosis and microgliosis is that astrocytes were a secondary reaction to excitotoxicity during prion disease. Astrocytes are necessary for synapse health; they regulate synapse signaling, recycle neurotransmitters, and function as metabolic support (Allen

and Eroglu, 2017). But astrocytes can also contribute to disease pathogenesis, for example, by phagocytosing synapses. Astrocytes are activated by excess glutamate at the synapses, which could be occurring through excitotoxicity in prion disease. A recent study highlights the involvement of astrocytes in synapse loss during prion disease (Smith et al., 2020), suggesting that reactive astrocytes are neurotoxic in prion disease. Collectively, this data suggests that astrogliosis may negatively impact synapses during prion disease, as we see higher levels of astrocytes with an earlier onset of disease in the *Hrs*$^{f/f}$*Syn1-Cre*+ mice, whereas lack of microgliosis suggest a more protective effect of microglia in prion disease.

3.3 Concluding remarks

Our findings highlighting the importance of the endolysosomal pathway in neuronal health and neurodegeneration provide new insights into mechanisms of neurotoxicity. Our data supports targeting preservation of synapse health as a therapy in neurodegeneration, rather than prion conversion. Future investigations are necessary to further dissect the mechanisms of protein aggregation causing synapse loss and ways to prevent it.

3.4 Materials and Methods

Mouse lines and animal care

Hrs$^{f/f}$ mice, which express Hrs with flox sites surrounding exons 2-4 (Tamai et al., 2008) were bred to *Syn1-Cre*, *GFAP-cre*, or *LysM-cre* (The Jackson Laboratory) – genotyped for both the floxed Hgs gene and Cre. Mice were maintained under specific pathogen-free conditions on a 12:12 light/dark cycle. Mice had access to standard laboratory chow and water ad libitum.

Primary neuron culture

Primary Neuron Culture: Primary cortical neurons from P0 *Hrs*$^{f/f}$ mouse pups were cultured in neurobasal media (Gibco) containing 2% B27 plus Supplement (Gibco) and 1X GlutaMAX^{TM} (Gibco). In brief, the cerebral cortices were dissected, dissociated with 0.25% trypsin at 37°C for 20 min, treated with DNase, and triturated. Debris was removed by passing the cells through a 70 μm cell strainer. Cells were then centrifuged for 10 min and resuspended in neurobasal media with 2% B27plus and 1X GlutaMAX^{TM}.

Prion inoculations

Groups of 10-15 male and female *Hrs*$^{f/f}$*-Cre+* and *Cre-* littermate control mice (6-8 weeks old) were anesthetized with ketamine and xylazine and inoculated into the left parietal cortex with 30 μl of 1% 22L prion-infected brain homogenate prepared from terminally ill mice. Strain 22L is a mouse-adapted prion originally derived from sheep scrapie that have different cellular targets in the brain and plaque morphologies and was a kind gift from Dr. Michael Oldstone.

Mice had access to standard laboratory chow and water ad libitum. Prion-inoculated mice were monitored three times weekly for the development of terminal prion disease, including ataxia, kyphosis, stiff tail, hind leg clasp, and hind leg paresis, and were euthanized at the onset of terminal disease. The brain was halved, and one hemisphere was immediately fixed in formalin. Fixed brains were treated for 1 hour in 96% formic acid, post-fixed in formalin for 2-4 days, cut into 2 mm transverse sections, and paraffin-embedded for histological analysis. The remaining brain half was frozen for biochemical studies. Survival time was calculated from the day of inoculation to the day of terminal clinical disease. No mice were excluded from the

analysis.

Immunoblot analysis of mouse brains

Brain tissue was homogenized in PBS using a Beadbeater^{TM} tissue homogenizer. For PrP^{Sc} levels, protein levels were quantified using a BCA, and equal amounts homogenates were lysed in 2% sarcosyl buffer with benzonase and digested with 50 μg/ml proteinase K at 37 °C for 30 min and the reaction stopped by boiling samples for 5 min in LDS loading buffer (Invitrogen). Samples were electrophoresed in 10% Bis-Tris gel (Invitrogen) and transferred to a nitrocellulose membrane by wet blotting. Membranes were incubated overnight with monoclonal antibody POM19 at 1:10,000 in blocking buffer (discontinuous epitope at C-terminal domain, amino acids 201–225 (Polymenidou et al., 2008), a kind gift from Dr. Adriano Aguzzi) followed by a 1 hr incubation with an HRP-conjugated anti-mouse IgG secondary antibody (Jackson Immunolabs). To analyze shed PrP^{Sc} levels, a NaPTA (previously described) was performed to precipitate the PrP^{Sc}, which was analyzed by western blotting. Membranes were incubated with A228 antibody (1:1000, in blocking buffer), and developed. After developing, the same membranes were then stripped with RestoreTM western blot stripping buffer (Thermo Fisher), and then incubated with Pom19 antibody (1:10,000) For synaptic and endolysosomal protein level analysis, homogenates were lysed in 2% sarcosyl buffer with benzonase, PhosStop, and Complete MiniTM protease inhibitor for 30 min, and then centrifuged for 5 min at 2000xg to remove debris. Protein levels in the lysates were quantified by BCA so that equal amounts of brain homogenate were compared, and then analyzed by western blot. Actin or GAPDH was used as a loading control.

Antibodies for western blots

The following antibodies were used for western blotting. Mouse anti-PrP (1:10,000, POM19, amino acids 201–225 (Polymenidou et al., 2008), a kind gift from Dr. Adriano Aguzzi); mouse anti-PrP Pom1 (1:10,000); anti-Hrs (1:5000, Cell Signaling Technology); anti-β actin (1:5000, Genetex); anti-Gapdh (1:5000, ***); anti-Stam1 (1:1000, Cell Signaling Technology); anti-Rab7 (1:1000, Cell Signaling Technology); anti-Tsg101 (1:1000, Genetex); anti-Rab5 (1:1000, Cell Signaling Technology); Ubiquitin (1:7000, Dako); Rab11a (1:1000, Cell Signaling Technology); anti-Vps35 (1:10,000, Genetex); anti-Chmp2B (1:1000, Cell Signaling Technology); anti-LC3-I/II (1:1000, Cell Signaling Technology); anti-p62 (1:4000, Abnova); anti-Synapsin-I (1:10,000, ***); anti-Synaptophysin (1:10,000, Invitrogen); anti-PSD95 (1:5000, Calbiochem); anti-Vamp2 (1:10,000, Cell Signaling Technology); anti-Snap25 (1:10,000, Cell Signaling Technology); anti-mGluR5 (1:2000, Cell Signaling Technology); anti-GluA1 (1:1000, Cell Signaling Technology); anti-phosphorylated GluA1 S831 (1:1000, Cell Signaling Technology); anti-phosphorylated GluA1 S845 (1:1000, Cell Signaling Technology); anti-phosphorylated Synapsin-I (1:1000, Cell Signaling Technology); anti-Arc (1:1000, Proteintech)

Histological analysis of mouse brains

Tissue sections were cut from blocks of formalin-fixed paraffin embedded mouse brain. Four-micron tissue sections were stained on a Ventana Discovery Ultra (Ventana Medical Systems, Tucson, AZ, USA). with antibodies to GFAP (Dako; 1:6000), Iba-1 (Wako; 1: 3000), Ubiquitin (Dako, 1:3000), LAMP1 (DSHB; 1:150). Antigen retrieval was independently optimized for each epitope to yield the maximal signal to noise ratio. For PrP, slides were incubated in protease 2 for 20min followed by antigen retrieval in CC1 (tris-based; pH 8.5; Ventana) for 64 min

at 95°C. For GFAP only the protease P2 was used (Ventana) for 16 minutes. For LAMP1, Iba-1, and ubiquitin all retrieval was done using CC1 for either 24 (Lamp1) or 40 min (Iba-1, ubiquitin). Following retrieval, all antibodies were incubated on the tissue for 32 min at 37°C. The secondary antibody (HRP-coupled goat anti-rabbit; OmniMap system; Ventana) was incubated on the sections for 12 min at 37°C. The primary antibody was visualized using DAB as a chromagen followed by hematoxylin as a counterstain. Due to the low level expression of LAMP1, an additional amplification step was included before the DAB reaction using the Ventana HQ-Amp system for 12 min. Slides were rinsed, dehydrated through alcohol and xylene and coverslipped.

Transmission electron microscopy of mouse brains

Immersion fixation: Mouse brains were halved, a 2 mm thick coronal section at the level of the hippocampus was immersed in modified Karnovsky's fixative (2.5% glutaraldehyde and 2% paraformaldehyde in 0.15 M sodium cacodylate buffer, pH 7.4) for 2 days. (4 mice)

Perfusion: One mouse from each group was transcardially perfused with PBS containing 0.5% EDTA (CHK) followed by modified Karnovsky's fixative to obtain high resolution ultrastructure of the synapses. (4 mice)

All brains were treated for 1 hour in 96% formic acid, washed in 0.15 M sodium cacodylate buffer 3 times, and post-fixed in modified Karnovsky's fixative for 3 days.

The CA1 hippocampal sections were then immersed in 1% osmium tetroxide in 0.15 M cacodylate buffer for 1 hour and stained in 2% uranyl acetate for 1 hour. Samples were dehydrated in ethanol, embedded in Durcupan epoxy resin (Sigma-Aldrich), sectioned at 50 to 60 nm on a Leica UCT ultramicrotome, and picked up on Formvar and carbon-coated copper grids. Sections were stained with 2% uranyl acetate for 5 min and Sato's lead stain for 1 minute. Grids

were viewed using a JEOL 1200EX II (JEOL, Peabody, MA) transmission electron microscope and photographed using a Gatan digital camera (Gatan, Pleasanton, CA).

qRT-PCR

Brain samples were collected and rapidly frozen on dry ice. To isolate RNA from brain, brains were thawed in RNAice Later, (Thermo Fisher AM7030), lysed with the PureLink RNA isolation lysis buffer, decontaminated in 5.3 M guanidine isothiocyanate for 24 hours, and RNA isolated using the PureLink RNA isolation kit. (Thermo fisher 12183025). cDNA synthesis was performed using Promega cDNA synthesis kit. Random hexamers, M-MLV RT buffer 5X, dNTP mix (10mM), and M-MLT RT. qRT-PCR was performed using FAM labeled primers for Hgs (Thermo fisher 4331182; Mm00468632m1), and control murine GAPDH (Thermo fisher, 4448892, Mm99999915g1). cDNA was mixed with TaqMan Gene Expression Master MixII with UNG (Life technologies 4423710) and run in the StepOnePlus (Applied Biosystems) in MicroAmp Fast 96-well reaction plates (Applied Biosciences, 4346907). We analyzed 3 mice from each group in triplicate.

Lentivirus generation

Hek293T cells were plated in 10cm plates.The next day, to generate the recombinant lentivirus, cells at 80% confluency were cotransfected with the shuttle vector (Cre-FUWG2, empty-FUWG2, or LC3-mCherry-GFP) and the two helper plasmids, delta8.9, and VSV-G envelope vector using a CalPhosTM transfection kit (Takara, 631312), the media was changed after 14 hours and then collected after 24 hours and 36 hours. The media was centrifuged at 2000 x g for 10 min and filtered through a 0.22 μM filter. The media was then incubated with

PEG-it (System Bioscience, LV810A-1) overnight in 4°C. The next day, media was spun down at 1500xg for 30 min at 4 °C. The media was removed, virus was pelleted and centrifuged again at 1500xg for 5 min to remove excess media. Media was completely removed and virus was resuspended in cold sterile PBS and immediately frozen at -80°C.

Partial purification of prions

22L prion-infected and uninfected 10% brain homogenates (200μL) were lysed in 2% sarcosyl in PBS (200μL) with add 16 μL of benzonase + MgCl2 (8μl MgCL2 and 8μl benzonase). Lysates were incubated for 30 min at 37 °C, shaking at 1000rpm. Samples were then centrifuged at 4 °C at 18,000xg for 30 min. The supernatant was removed, and pellets, containing the partially purified prions, were resuspended in 100μL of PBS. Partially purified samples were then heated to 65 °C sterilize samples for cell culture.

PrP^{Sc} in neurons assay

Primary neurons plated in 12-well plates were transduced with either Cre-lentivirus or Control-lentivirus after 6 DIV. 5 days after transduction, cells were then infected with 10 μL of partially purified 22L prions or mock brain for 3 days. Neurons were then washed with PBS twice, and collected in 2% N-lauryl sarcosine with benzonase™ and lysed on ice for 30 min. A BCA was run to quantify protein levels. 100 μg of protein was aliquoted and digested with Proteinase K (10ug/mL final concentration) for 30 min at 37 °C. The PrP^{Sc} levels in the cell lysates were measured by western blot using Pom1 and Pom19 antibodies. The PrP^{Sc} signals were captured and quantified using the Fuji LAS 4000 imager and Multigauge V3.0 software. For other protein levels (Hrs, PrP, Actin), both prion-infected and uninfected neuron lysates were

run on a gel at equal concentrations and volumes of lysate and quantified by western blot. n=4 experiments were ran in duplicate.

Biotinylation assay

Primary neurons plated in 6-well plates were transduced with either Cre-lentivirus or Control-lentivirus (as described above) after 6 DIV. After one week, cells were washed with ice cold PBS. Biotin at 1mg/mL (21335 – life technologies) in 0.1M HEPES was added (or 0.1M HEPES as a control) to neurons, and neurons were incubated for 30 min rocking on ice at 4C. Reaction was quenched with 100mM of ice cold glycine in 0.1M HEPES buffer twice, at 15 min each. Cells were then washed with PBS. IP buffer (10 mM Tris-HCl, 150 mM NaCl, 10 mM EDTA, 0.5% NP40, 0.5% DOC; pH 7.4 with CompleteMiniTM Protease inhibitors) was added to cells. Cells were scraped into microfuge tubes, solubilized, and left on ice for 30 min. Lysates were then spun down at 10,000xg for 5 min and supernatant was collected, and PierceTM BCA protein assay (Thermo Scientific, 23225) to quantify protein concentration. 150μg of protein was incubated with the beads and 10ug of protein was saved for input. 30μL of streptavidin-conjugated magnetic beads were added to each tube and incubated at 4°C overnight on a rocker.

Elucidation: A magnetic holder was used to collect magnetic beads and remove supernatant. Magnetic beads were washed with lysis buffer 3 times, rotating for 5 min each and removing as much liquid as possible. 30μL of elution buffer with 0.2M DTT was added to beads, samples were boiled at 50°C for 5 min, then 95°C for 5 min before being loaded in a gel.

LC3-mCherry-GFP assay

Hippocampal neurons cultured in a 24 well dish on 12mm round coverslips were transduced with the LC3-mCherry-GFP lentivirus along with the Cre-lentivirus or Control-Lentivirus. One week after transduction, neurons were incubated with Bafilomycin (50nM) or Rapamycin (.25μM) for 4 hours. Cells were then fixed 4%PFA and stained with Cre-antibody (CST) using Alexa-647 secondary, as per the immunofluorescence protocol.

Neuron Immunofluorescence

Cells were fixed with 4% paraformaldehyde (PFA) (Fisher Scientific, J19943K2) For the fixation, PFA was added directly to the cells in media, diluted 1:1 in media and incubated in PFA for 20 min at 37C. Fixative was removed and 4% paraformaldehyde was added for an additional 10 min at room temperature. Cells were washed 3 times in PBS and permeabilized in 0.5% Triton X-100 in PBS buffer for 5 min. Cells were washed 3x with PBS and blocked in 3% BSA in 0.1% Triton X-100 in PBS for 1 hour. Cells were incubated with primary antibody overnight at 4°C in blocking buffer (3% BSA in 0.1% Triton X-100 in PBS). Cells were washed 4 times for 5 min in wash buffer (0.1% Triton X-100 in PBS) and incubated with secondary (1:250, Jackson laboratories) for 1 hour in wash buffer. Cells were washed 4x5 min, with a 5-minute DAPI (Sigma-Aldrich, D9542) incubation during the second wash. Coverslips were mounted onto ProLongTM Gold Mountant (Invitrogen, P36941) and sealed with nail polish.

Western blot analysis

To quantify the relative immunoblot signal intensities, images were acquired using a chemiluminescent substrate (Supersignal West Dura ECL, ThermoFisher Scientific) and visual-

ized on a Fuji LAS 4000 imager. The chemiluminescent signals were captured and quantified using the Fuji LAS 4000 imager and Multigauge V3.0 software.

Experimental analyses

Electron microscopy images from the CA1 region of the hippocampus were analyzed using ImageJ. N represents number of synapses analyzed across 9 mice. Synaptic proteins, endolysosomal proteins, and PrP were analyzed by immunoblotting of brain homogenates. PrP^{Sc} was detected after proteinase K digestion. For neuron imaging analysis of LC3 puncta, n represents the number of cells quantified across 3 experiments. Only cre-positive cells were analyzed to compare with the cre-negative control.

Statistical analyses

Student's t-tests were applied to all data sets with two tails. ANOVA testing was performed using one-way analysis with Tukey's post-hoc test for group effects. Statistical tests were performed using GraphPad/Prism. All data in bar charts represents mean $\pm$SEM.

3.5 Acknowledgements

The authors would like to thank members of the members of the Sigurdson lab, particularly Patricia Aguilar-Calvo and Julia Callendar for their thorough reading of this manuscript. Thanks to Don Pizzo for his histology and discussion of analysis methods used in this manuscript. Thanks to Xu Chen for her Cre and LC3-mCherry-GFP plasmids and lentivirus, as well as her scientific discussion. J.A.L. is supported by a Ruth L. Kirschstein Institutional National Research Award from the National Institutes of Health, NINDS F31NS103588.

Chapter 3, in full, is a reprint of material submitted to be published in: **Lawrence, JA.**, Sigurdson C. Neuronal ESCRT-0 depletion accelerates synapse loss in prion disease. *in preparation*. The dissertation author was first author of this paper.

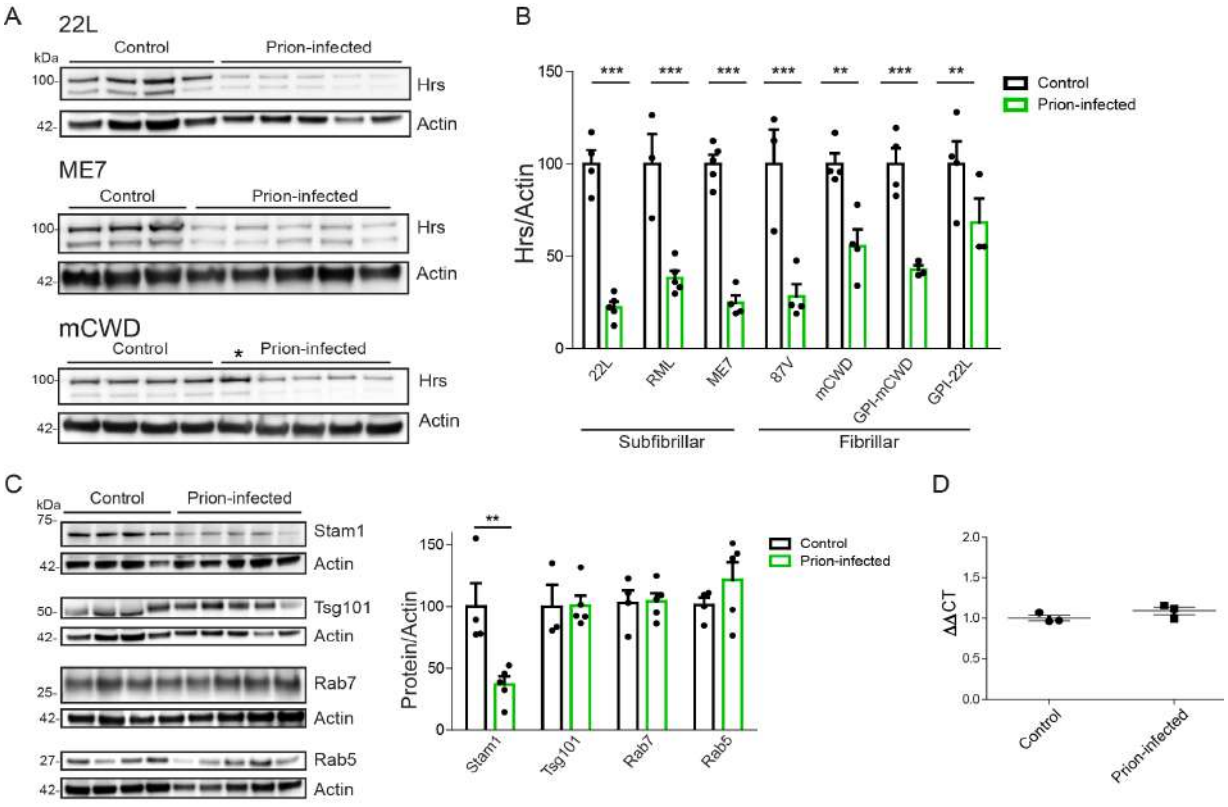

Figure 3.1: Decreased ESCRT-0 protein levels at terminal prion disease but not additional endosomal proteins. (A-B) Hrs levels in the brains of mice at terminal prion disease alongside uninfected age-matched controls for strains 22L, ME7 and mCWD reveal a significant decrease in Hrs levels. Quantification of Hrs levels was normalized to the average of the uninfected controls (B). Control: Actin. Mean and SEM shown. student t test, $^{**}p<0.01$, $^{***}p<0.001$. n=3-5 mice. (C) Levels of additional endosomal Stam1, Tsg101, Rab7, and Rab5 proteins at terminal disease of 22L-infected mice and age-matched uninfected controls reveal a loss of Stam1 protein at terminal prion disease, but not Tsg101, Rab7, or Rab5 proteins. n=4-5 mice. (D) Hgs transcript levels in 22L prion-infected mouse brains compared to uninfected age matched controls measured by qRT-PCR. n=3 mice. No significant differences, student t test.

Figure 3.2: Hrs depletion accelerates prion disease when depleted in neurons, but not astrocytes or microglia. (A, E, I) *Hrs$^{f/f}$-GFAP-Cre* (A), *Hrs$^{f/f}$-LysM-Cre* (E), or *Hrs$^{f/f}$-Synapsin1-cre* (I) positive and negative age-matched mice were infected intracerebrally with 1% of 22L-infected brain homogenate. Incubation times until onset of terminal prion disease are shown. Uninfected *Cre+* mice survival was not impacted by Hrs depletion. No differences in survival times were seen in *Hrs$^{f/f}$-GFAP-Cre* (A) or *Hrs$^{f/f}$-LysM-Cre* (E) prion-infected mice. In contrast, *Hrs$^{f/f}$*-Synapsin-*Cre+* mice accelerated prion disease by 27%. (B and F) Representative western blots of PrP^{Sc} amounts in brain homogenates of terminally diseased *GFAP-Cre* (B) and *LysM-Cre* positive and negative mice upon proteinase K digestion reveal no differences in PrP^{Sc} levels, (J) Representative western blots of PrP^{Sc} amounts in brain homogenates of terminally diseased Synapsin-Cre positive and negative mice upon proteinase K digestion reveal less PrP^{Sc} in *Synapsin-Cre+* mice at terminal disease. (C and G) Quantifications of PrP^{Sc} levels normalized to the average of the *Cre-* mice for *GFAP-Cre* (C) and *LysM-Cre* (G) reveal no significant differences in PrP^{Sc} between *Cre+* and *Cre-* mice. (K) Quantifications of PrP^{Sc} levels reveal 50% less PrP^{Sc} at terminal disease in *Synapsin-Cre+* mice compared to *Synapsin1-Cre-* mice, by 50%. (D, H, L) Immunostaining for PrP^{Sc} (Saf84) in the CA1 region of the hippocampus at 40X magnification of both *Cre+* and *Cre-* mice from *GFAP-Cre* (D), *LysM-Cre* (H), and Synapsin-Cre (L) groups. (M and N) Western blots of PK-digested brain homogenates of Synapsin-Cre positive and negative mice sacrificed at 106 days post inoculation (M) and quantification reveal no significant differences in PrP^{Sc} levels at the same time point. (N), n=5 Cre-negative and n=4 positive. (O) Immunostaining for PrP^{Sc} (Saf84) in the cortex of Synapsin-Cre positive and negative mice at 106 days post inoculation. (P and Q) NaPTA precipitation and proteinase K digest of brain homogenates from Synapsin-Cre positive and negative mice at 106 days post inoculation with an antibody specific for shed ADAM-10 cleaved PrP (A228) and total PrP^{Sc} (POM1) levels. (Q) Quantification of Shed PrP^{Sc}/total PrP^{Sc} reveal no statistical differences between *Cre-* (n=5) and *Cre+* (n=4) groups. ***p$<$0.001 Log-rank (Mantel-Cox) test (Panels A, E, I). ***p$<$0.001 Student t test (Panels C, G, K, N, Q).

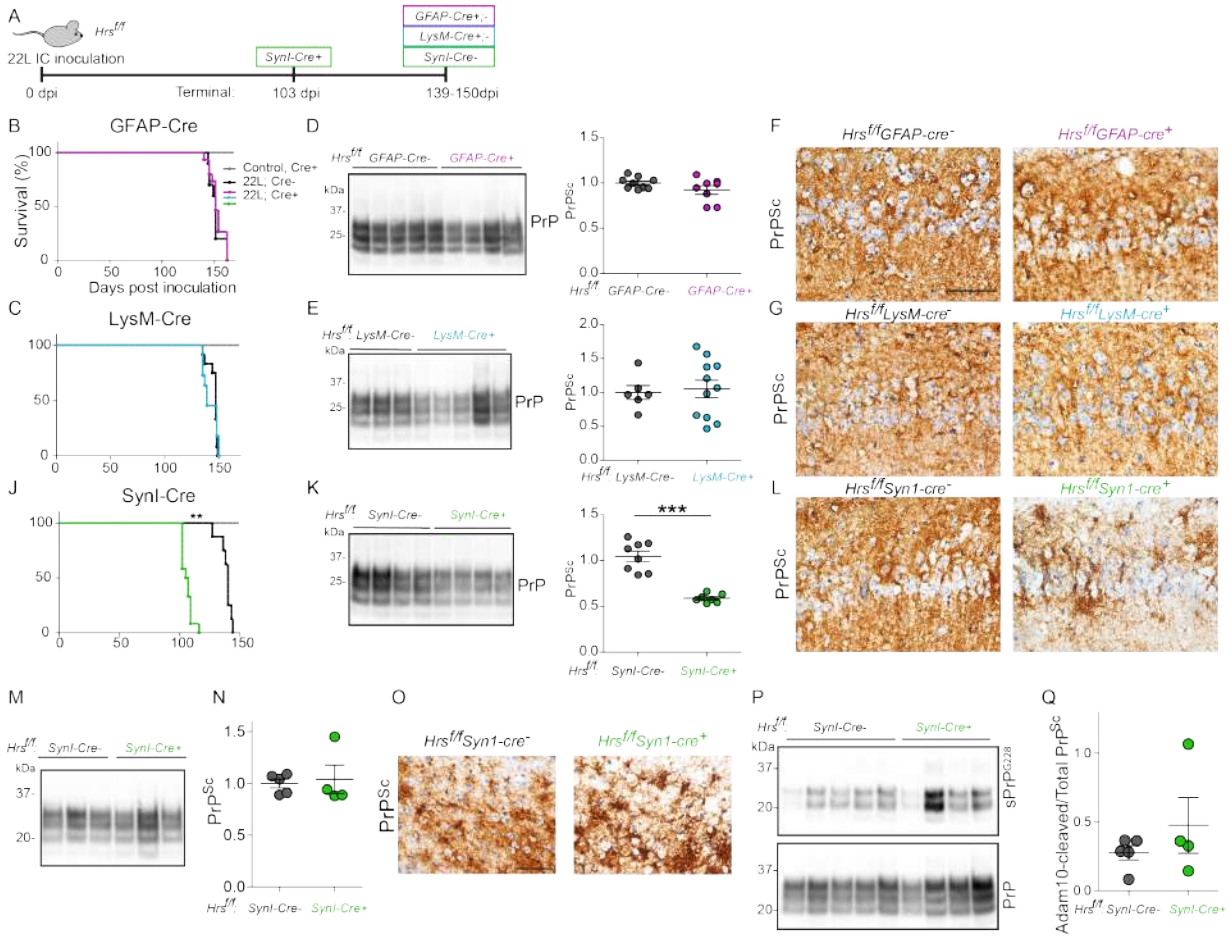
A
Hrsf/f
22L IC inoculation
Synl-Cre+
GFAP-Cre+,-
LysM-Cre+,-
Synl-Cre-
0 dpi
Terminal:
103 dpi
139-150dpi
B
GFAP-Cre
Survival (%)
Control, Cre+
22L, Cre-
22L; Cre+
Days post inoculation
C
LysM-Cre
J
Synl-Cre
D
E
K
PrP
PrPSc
F
G
L
Hrsf/fGFAP-cre-
Hrsf/fGFAP-cre+
Hrsf/fLysM-cre-
Hrsf/fLysM-cre+
Hrsf/fSyn1-cre-
Hrsf/fSyn1-cre+
M
N
O
P
Q
sPrPC228
PrP
Adam10-cleaved/Total PrPSc

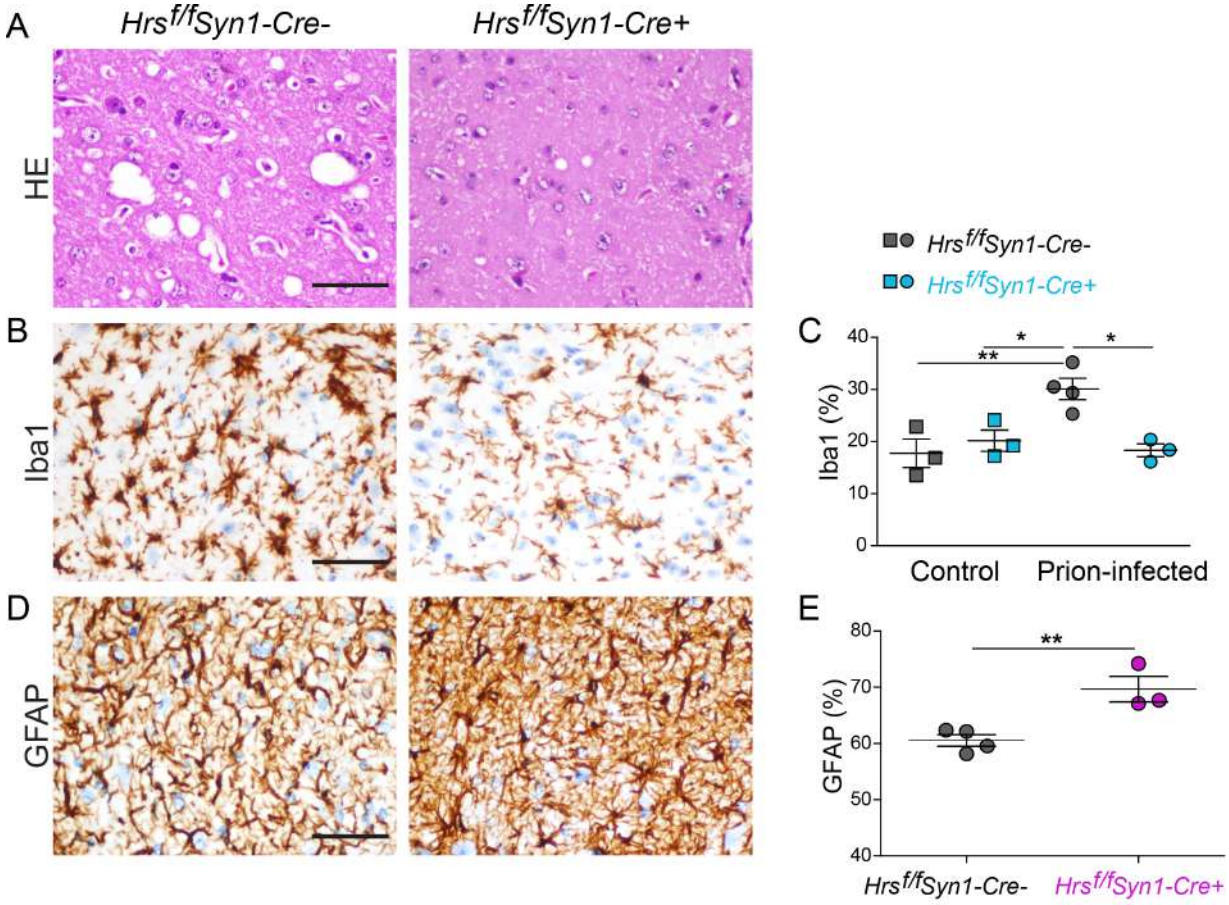

Figure 3.3: Astrogliosis is significantly higher during prion disease when Hrs is depleted in neurons. (A) HrsSynCre prion-infected brains stained with haemotoxylin and eosin (HE) at terminal disease shows higher spongiform change in *Cre-* than *Cre+* mice in the thalamus. (B) Immunostaining for microglia (Iba1) in the brains of $Hrs^{f/f}$ *Syn1-Cre-* and *Cre+* mice reveal much less microgliosis in the brains of *Cre+* mice at terminal disease. (C) Quantification of %Iba1 staining over total area in the brains of prion-infected and uninfected *Cre+* and *Cre-* mice show a significant difference. (D) Immunostaining for astrocytes (GFAP) in the brains of $Hrs^{f/f}$ *Syn1-Cre-* and *Cre+* mice at terminal disease reveal high levels of astrogliosis in the brains of *Cre+* mice at terminal disease. (E) Quantification of %GFAP staining over total area in the brains of prion-infected and uninfected *Cre+* and Cre- mice show significantly higher levels of astrogliosis in *Cre+* mice at terminal disease. Mean and SEM shown. Scale bar = 100 microns for all images. (n=3 *Cre+*, 4 *Cre-* mice), One-way ANOVA, **$p<0.01$.

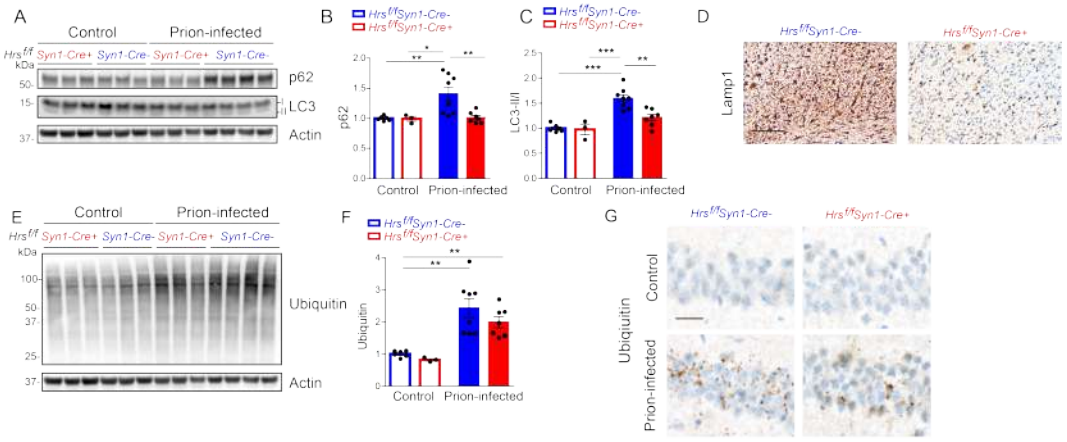

Figure 4

Figure 3.4: Autophagosome accumulation is not the cause of death in *Hrs*$^{f/f}$ *Syn1-Cre*+ prion-infected mice. (A) Western blots of p62 and LC3 II/I protein levels and (E) ubiquitinated protein levels in the brain homogenates of both age-matched uninfected and prion-infected *Hrs*$^{f/f}$ *Syn1-Cre*+ and *Cre*- mice reveal significant differences between prion-infected and uninfected mouse brains. Control: Actin. Levels were quantified and normalized to the average of uninfected*Hrs*$^{f/f}$ *Syn1-Cre*- for p62 (B), LC3-II/I (C) and ubiquitinated proteins (D). (n=3 uninfected, 6 prion-infected *Hrs*$^{f/f}$ *Syn1-Cre*+, 8 prion-infected*Hrs*$^{f/f}$ *Syn1-Cre*- mice). Mean and SEM shown. (D) Immunohistochemistry of Lamp1 in the brains of terminal prion infected HrsSynCre positive and negative mice reveal more Lamp1 staining in the brains of*Hrs*$^{f/f}$ *Syn1-Cre*- mice. Scale bar = 200 microns. (G) Immunohistochemistry of Ubiquitin in the brains of terminal prion-infected and uninfected mice reveal ubiquitin inclusions at terminal prion disease. Scale bar = 20 microns. 2way-ANOVA, *p$<$0.05, **p$<$0.01

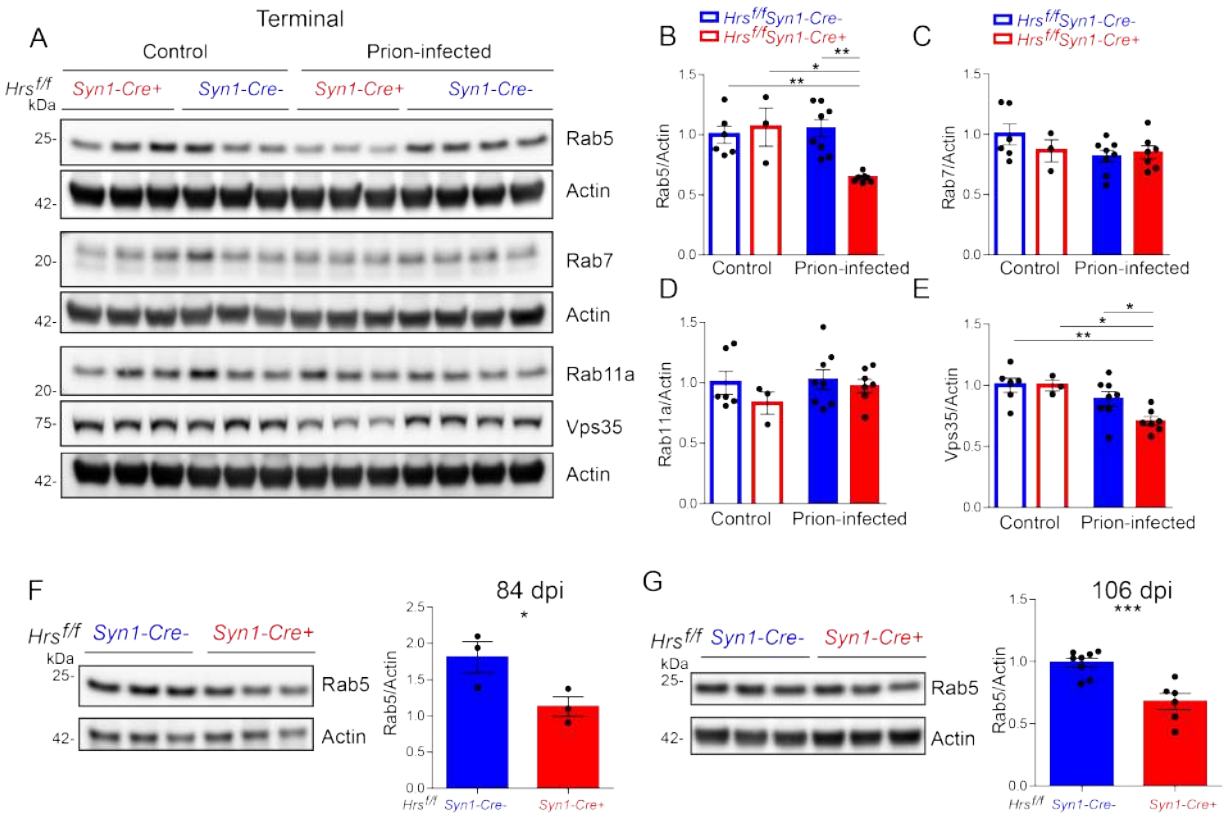

Figure 3.5: Loss of early endosomal proteins during prion infection when Hrs is depleted. (A) Western blots of endosomal proteins in the brains of both age-matched uninfected and prion-infected *Hrs*$^{f/f}$ *Syn1-Cre+* and *Cre-* mice and quantification normalized to uninfected *Cre-* control reveal significantly less Rab5 (B) and Vps35 (D) protein levels in only prion-infected *Cre+* mice. No changes were seen in Rab7 (C) or Rab11a (D) protein levels. Control: Actin. Mean and SEM shown. (n=3 uninfected, 6 prion-infected *Hrs*$^{f/f}$ *Syn1-Cre+*, 8 prion-infected*Hrs*$^{f/f}$ *Syn1-Cre-* mice). 2way-ANOVA, *p$<$0.05, **p$<$0.01.

Figure 3.6: Synapse morphology is impaired in prion-infected mice. (A) Representative timeline of *Hrs*$^{f/f}$ *Syn1-Cre*+ and *Cre*- mice clinical signs and terminal disease. (B) Transmission electron microscopy images of uninfected *Hrs*$^{f/f}$ *Syn1-Cre*+ and *Cre*- mice and prion-infected *Hrs*$^{f/f}$ *Syn1-Cre*+ and *Cre*- mice at 84, 106, and 139 dpi reveal vast ultrastructural differences. Terminal disease for *Hrs*$^{f/f}$ *Syn1-Cre*+ was 106 dpi, and 139 dpi for *Cre*- mice. (C) Quantification of the degree of curvature reveals a significant decrease to the degree of curvature of the post-synapse around the pre-synapse prion-infected mice, even earlier on in *Cre+* prion-infected mice. Mean and SEM shown. (D) Quantification of postsynaptic density area reveals a significant increase in all groups compared to uninfected *Cre*- control. Mean and SEM shown. (E) Quantification of synapse length (nm) reveals a significant increase in all groups compared to uninfected *Cre*- control. Mean and SEM shown. (F) Percent of synapses with docked synaptic vesicles per image were quantified, and prion-infected mouse brains at terminal disease had significantly fewer synaptic vesicles docked to synapses. Mean and SEM shown. 30 images per mouse, n=2 uninfected *Cre*-, 1 uninfected *Cre+*, 3 prion-infected *Cre*-, and 2 prion-infected *Cre+* mice.

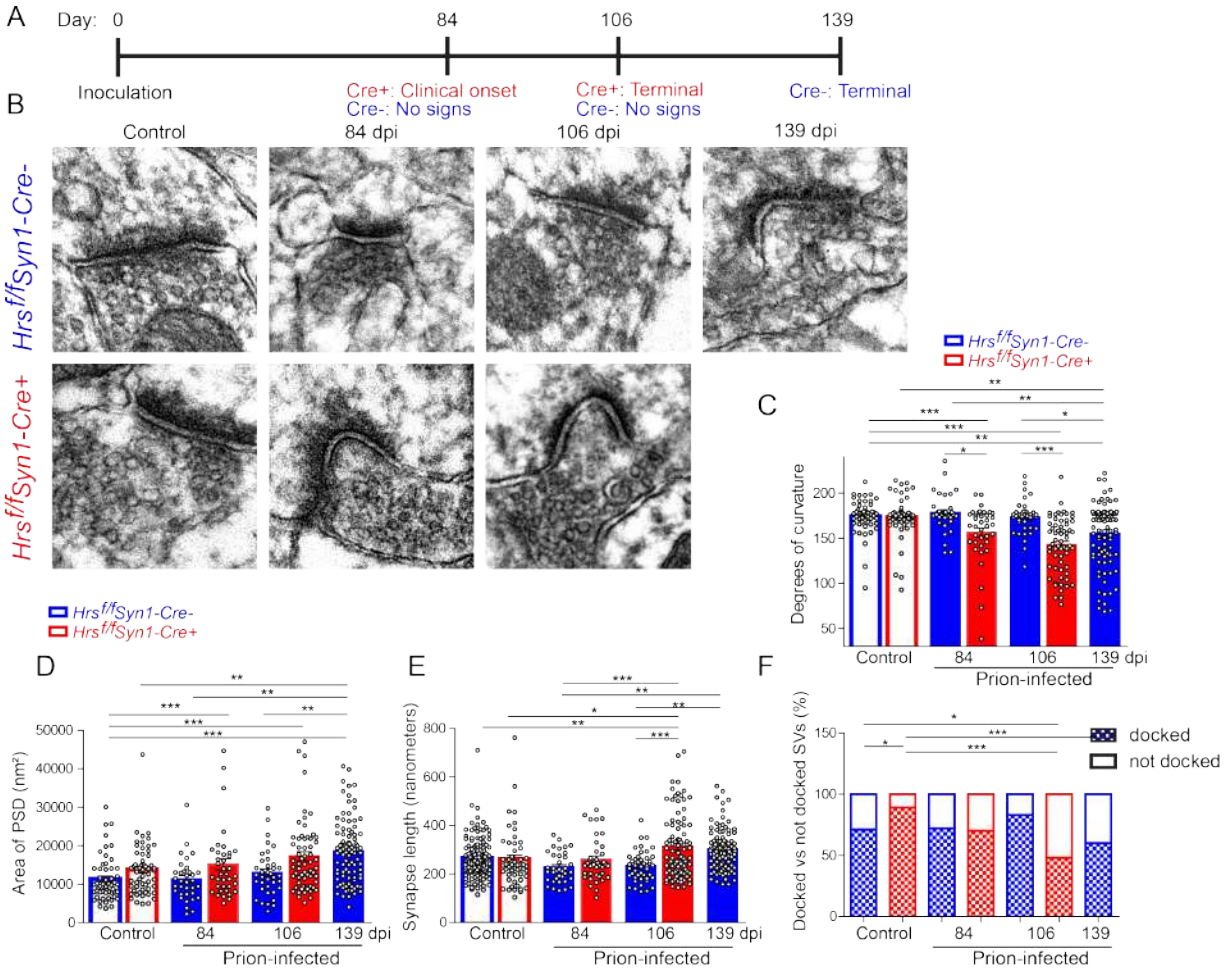
A
Day: 0
84
106
139
Inoculation
Cre+: Clinical onset
Cre-: No signs
Cre+: Terminal
Cre-: No signs
Cre-: Terminal
B
Control
84 dpi
106 dpi
139 dpi
Hrsf/fSyn1-Cre-
Hrsf/fSyn1-Cre+
C
Degrees of curvature
Control
84
106
139 dpi
Prion-infected
D
Area of PSD (nm²)
E
Synapse length (nanometers)
F
Docked vs not docked SVs (%)
docked
not docked

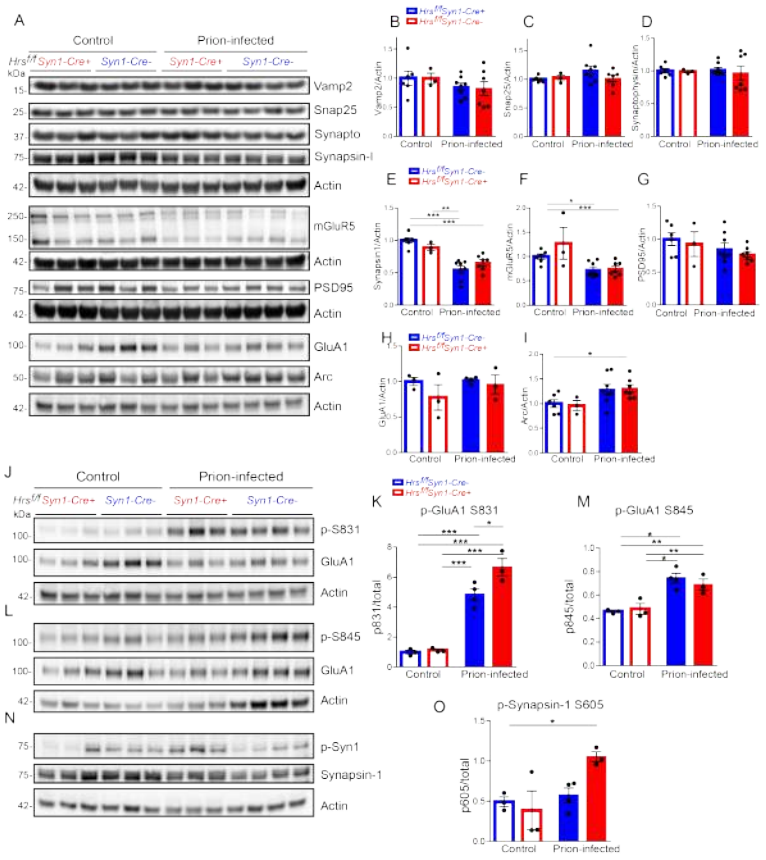

Figure 3.7: Loss of synaptic proteins Synapsin-I and mGluR5 in prion disease coincide with increased phosphorylation of AMPA receptors. (A-I) Western blots of synaptic proteins (A) in the brains of both age-matched uninfected and prion-infected *Hrs*$^{f/f}$ *Syn1-Cre+* and *Cre-* mice and quantification normalized to uninfected *Cre-* control. A significant loss at terminal prion-disease was quantified in synapsin-I (C) and mGluR5 (F). No significant differences were seen in Vamp2 (B), Snap25 (C), synaptophysin (D), PSD95 (I), or GluA1 (G). A significant increase in Arc protein was observed in terminal prion disease (H). (J-O) Western blots of the amount of phosphorylation compared to total protein. Each phosphorylation blot was stripped and reprobed for the total protein levels. GluA1 at S831 (K) and S845 (M) revealed a significant increase in phosphorylation at terminal prion disease when normalized against total protein. Synapins-1 phosphorylation (O) was significantly increased in *Hrs*$^{f/f}$ *Syn1-Cre+* mice at terminal prion disease. Mean and SEM shown. (n=3 uninfected, 6 prion-infected *Hrs*$^{f/f}$ *Syn1-Cre+*, 8 prion-infected*Hrs*$^{f/f}$ *Syn1-Cre-* mice). 2way-ANOVA, *p$<$0.05, **p$<$0.01, ***p$<$0.001.

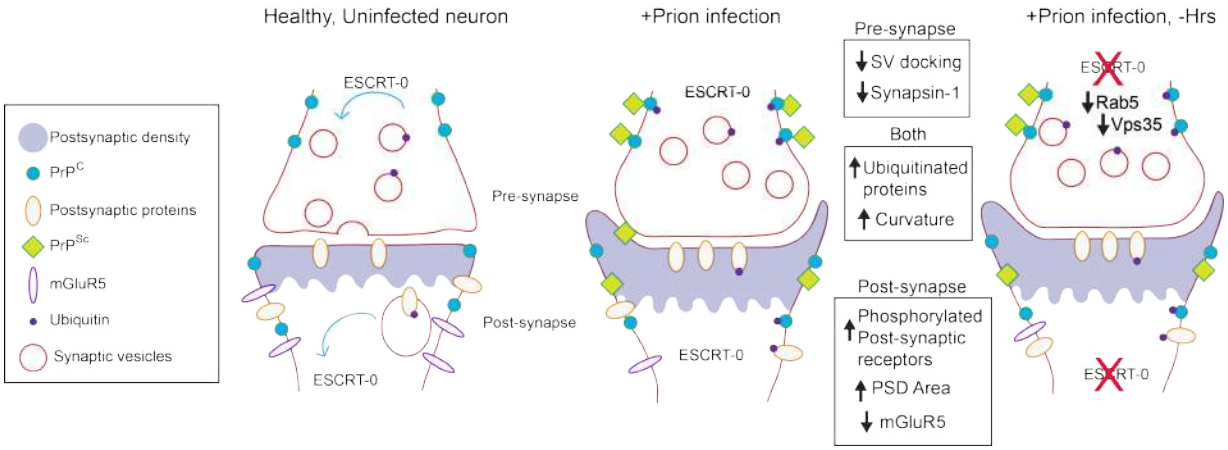

Figure 3.8: Hrs depletion in neurons accelerates prion-induced synaptic toxicity. Summary figure representing what we see at the synapse in prion disease, and how those changes are accelerated with Hrs depletion.

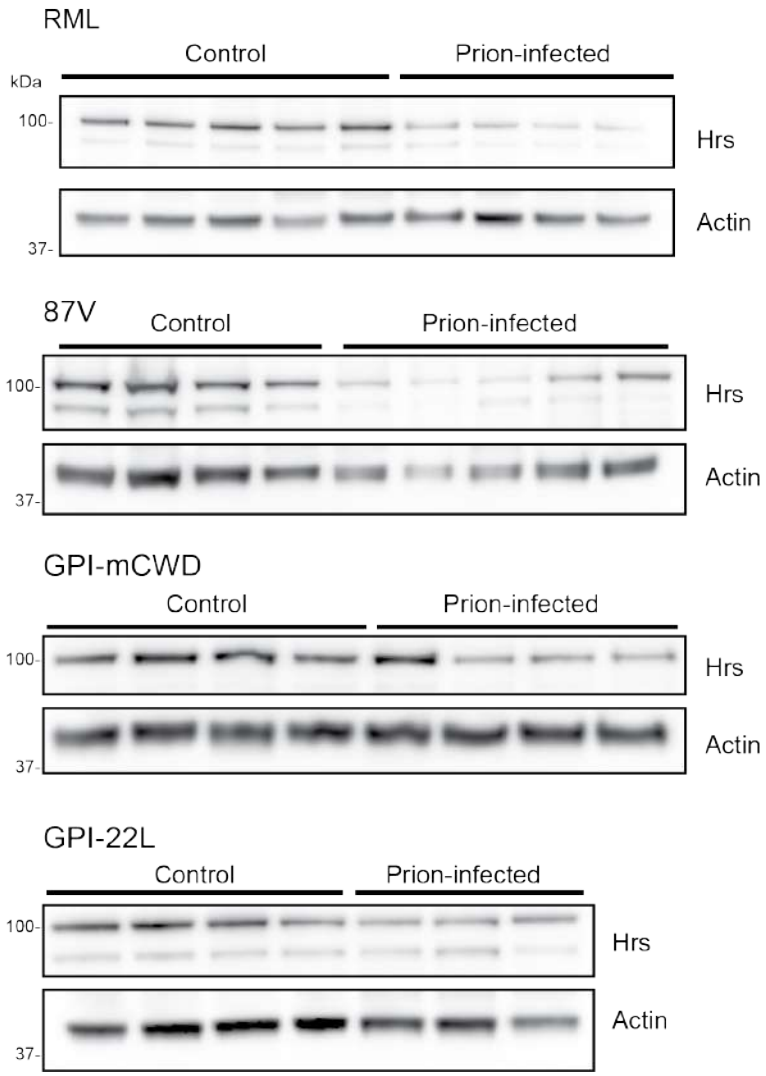

Figure 3.9: Hrs levels are down in all prion strains at terminal disease. Immunoblots of Hrs levels in the brains of prion-infected mice at terminal disease compared with age-matched controls that were quantified in Figure 8b for prion strains RML, 87V, GPI-mCWD, and GPI-22L.

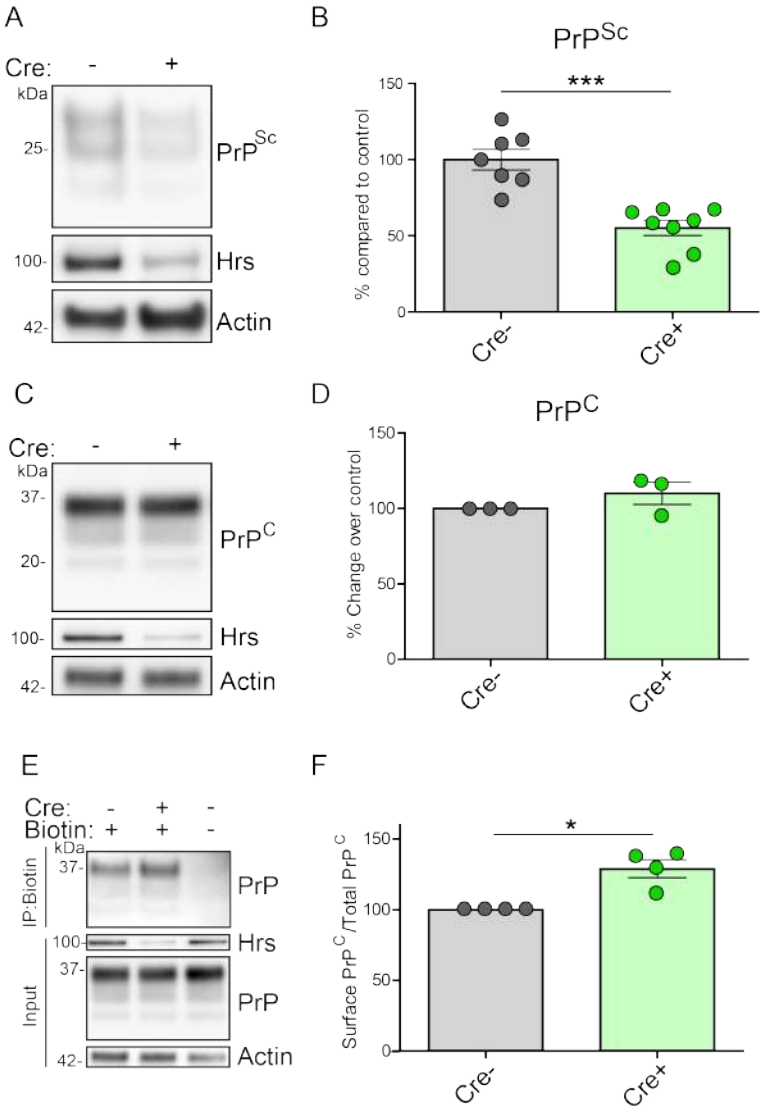

Figure 3.10: Hrs depletion in primary neurons decreases prion conversion. (A) Representative western blot of proteinase K digested *Hrs*$^{f/f}$ primary neuron lysates transduced with either *Cre-* or *Cre+* lentivirus to deplete Hrs reveals a decrease in PrP^{Sc} with Hrs depletion, also shown. (B) Quantification of PrP^{Sc} levels normalized to Cre lysate. (n=4 in technical duplicate, mean and SEM shown). Control: Actin. Student's t test, ***p$<$.0001 (C) Western blot of primary neuron lysates with *Cre-* or *Cre+* lentivirus reveal no differences to PrP^{C} protein levels with Hrs depletion. Levels of Hrs depletion shown. Control: Actin. (D) Plotted are the levels of PrP^{C} normalized to actin, fold change compared *Cre-* control lysates. (E) PrP^{C} cell surface levels upon biotinylation of *Cre-* and *Cre+ Hrs*$^{f/f}$ neurons reveal an increase in surface PrP^{C} upon depletion of Hrs. Control with no biotin labeling also shown. (F) Quantification of biotinylated surface PrP^{C} over total PrP^{C} levels (n=4, mean and SEM shown) show significant difference. Control: Actin. Student t test, *p $<$0.05.

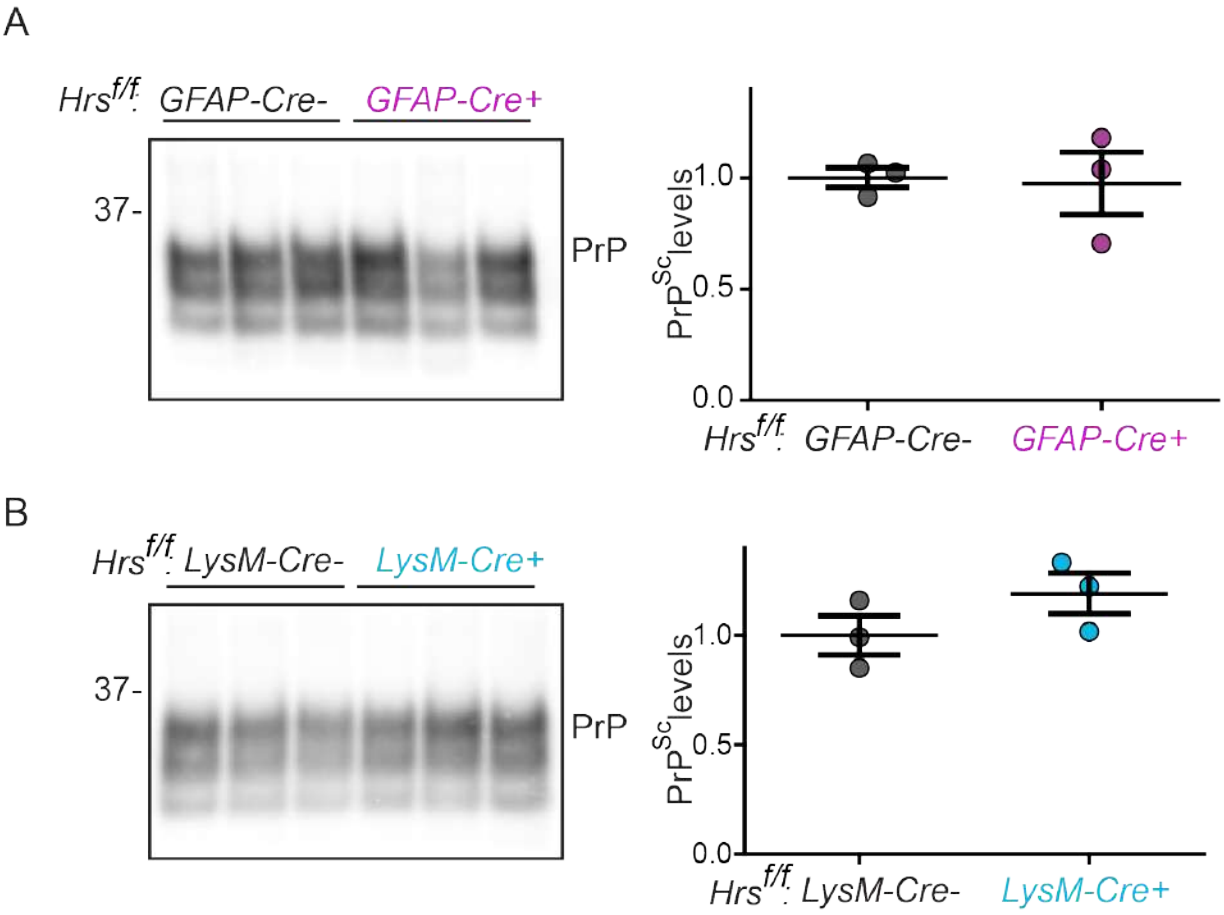

Figure 3.11: PrP^{Sc} levels are unchanged in GFAPCre and LysCre mice at 75% of disease course. (A and B) Immunoblots and quantification of PrP^{Sc} levels in proteinase K digested-brains of *Cre+* and *Cre-* HrsGFAPCre (A) and HrsLysCre (B) mice at 114 days post inoculation, 75% of disease, reveal no differences in PrP^{Sc} levels. n=3 for each group.

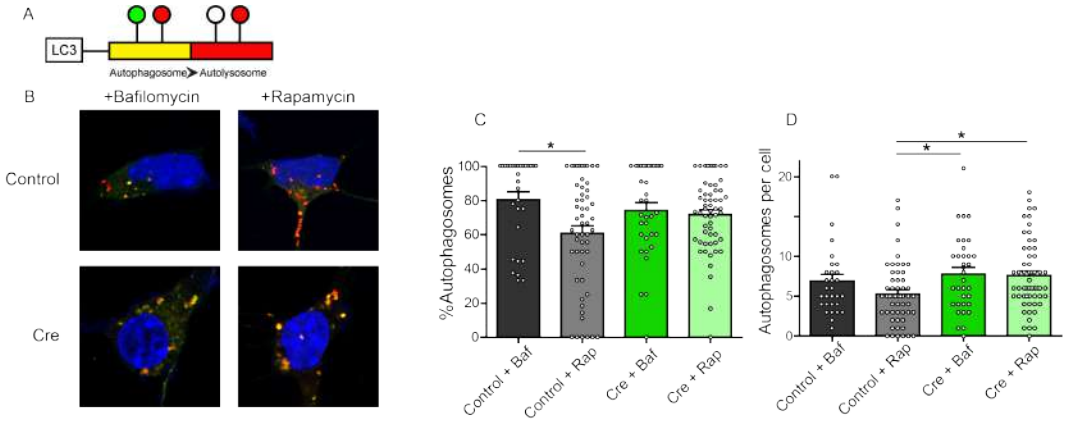

Figure 3.12: Hrs depletion impairs autophagic flux in vitro. (A) Schematic of LC3-mCherry-GFP plasmid. When bound to autophagosomes, both GFP and mCherry fluoresce, appearing yellow. When the autophagosome matures to a lysosome, GFP no longer fluoresces, resulting in red puncta. (B) Images of autophagic flux in primary $Hrs^{f/f}$ neurons transduced with LC3-mCherry-GFP plasmid and Cre+ or Cre- plasmid for one week and incubated with an autophagy inducer (Bafilomycin – baf) or autophagy inhibitor (rapamycin - rapa) for 4 hours. Yellow puncta (autophagosomes) and red puncta (autolysosomes) were quantified in each cell. (C and D) With adding rapamycin (rapa) to control neurons compared to adding bafilomycin (baf), quantifications reveal a decrease in (C) percent autophagosomes compared to total LC3 puncta (80.7% baf vs 60.9% rapa) and (D) total autophagosome number per cell (6.9 baf vs 5.3 rapa autophagosomes/cell), but when rapamycin is added to the Hrs depleted neurons, compared to adding bafilomycin to the Hrs depleted neurons, no significant decrease in (C) % autophagosomes (74.4% baf vs 71.98% rapa) or (D) total autophagosome number per cell (7.8 baf vs 7.6 rapa autophagosomes/cell) are seen. Mean and SEM shown. (C) and (D) were calculated for n=3 experiments and a total of 120 cells per condition. 1way-ANOVA, *$p<0.05$

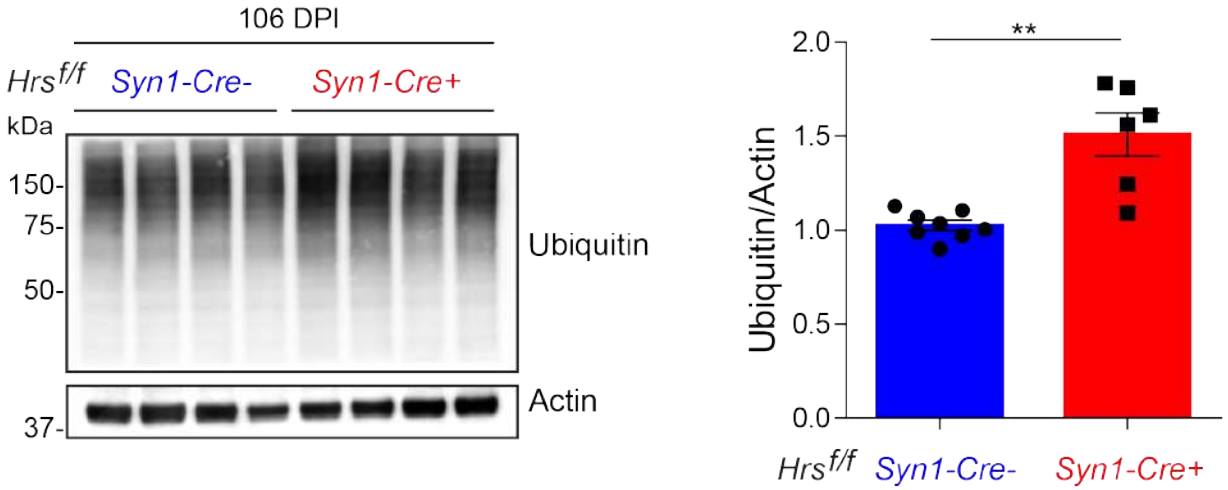

Figure 3.13: Hrs depletion accelerates ubiquitinated protein accumulation in prion disease. (A-C) Westerns blots (A) of the brains of *Hrs*$^{f/f}$ *Syn1-Cre+* and *Cre-* mice at 106 days post inoculation and quantification reveal an increase in ubiquitinated proteins in *Cre+* mice at 106 DPI (B) and a significant decrease in Synapsin-I (C). Control: Actin. n=4 *Cre+* and *Cre-* mice. Student t test **$p<0.01$, ***$p<0.001$

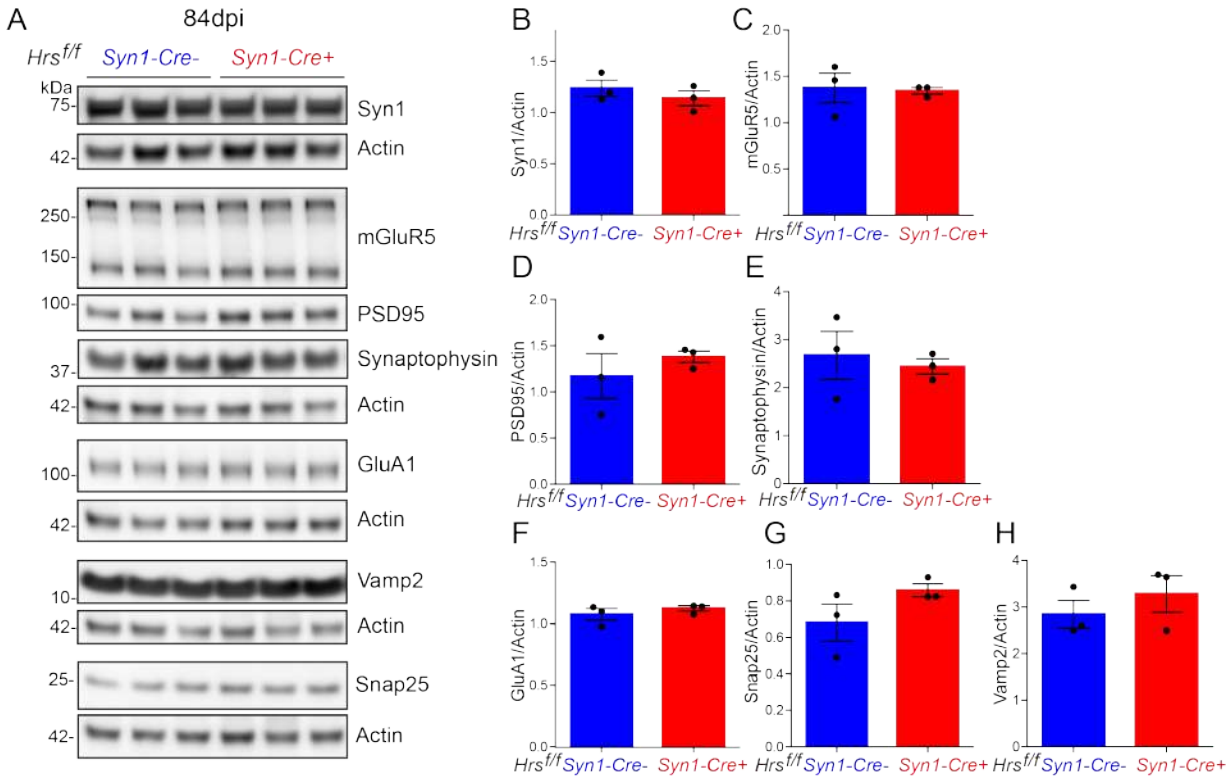

Figure 3.14: Loss of synaptic proteins is a characteristic of terminal disease. (A) Westerns blots of the brains of *Hrs*$^{f/f}$ *Syn1-Cre+* and *Cre-* mice at 84 days post inoculation and quantification reveal no differences in synaptic protein levels before terminal disease. Quantification of synapsin-I (B), mGluR5 (C), PSD95 (D), synaptophysin (E), GluA1 (F), Snap25 (G), and Vamp2 (H). Control: Actin. n=3 *Cre+* and *Cre-* mice. Student t test, no significant differences.

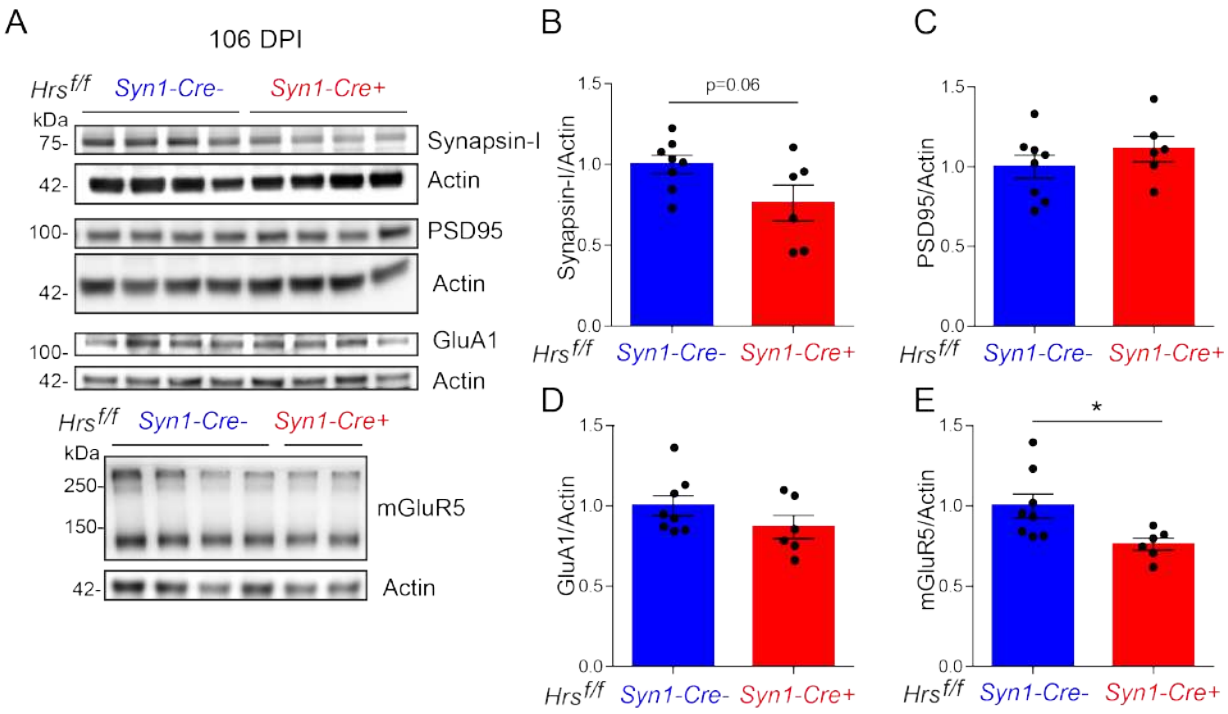

Figure 3.15: Loss of mGluR5 and synapsin-I is a characteristic of terminal disease. (A) Westerns blots of the brains of *Hrs*$^{f/f}$ *Syn1-Cre+* and *Cre-* mice at 106 days post inoculation and quantification reveal differences in synaptic protein levels are a characteristic of terminal disease. Quantification shows differences in (B) Synapsin-I and mGluR5 (E), but not PSD95 (C) or GluA1 (D). Control: Actin. n=6 *Cre+* and 8 *Cre-* mice. Student t test *$p<0.05$.

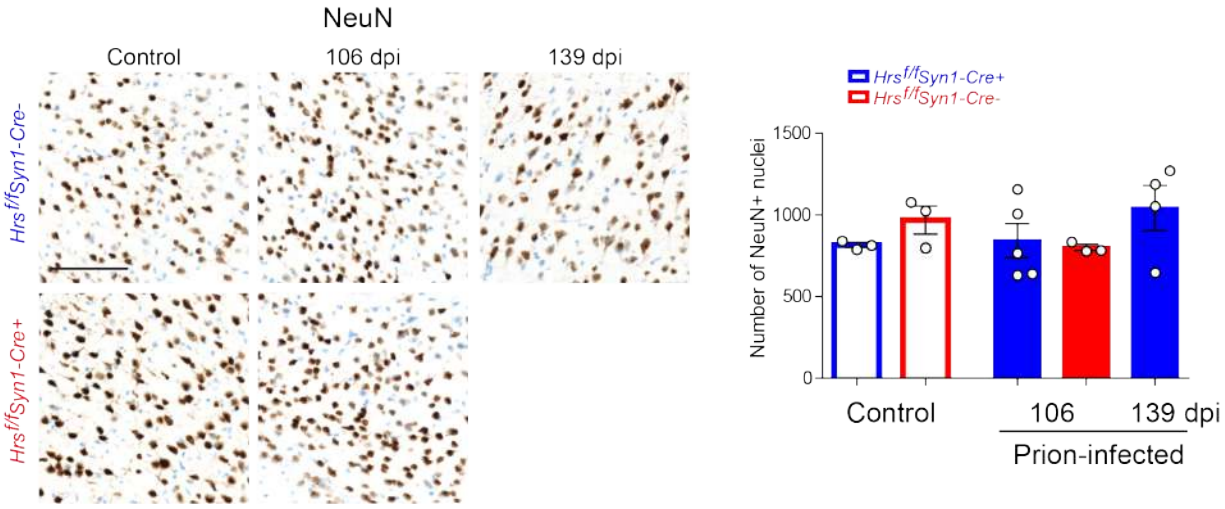

Figure 3.16: No differences in NeuN+ nuclei in cortex between all mouse groups. Quantification of the NeuN+ nuclei in the frontal cortex region over identical sized areas (427,193 microns2). NeuN immunohistochemistry shown for each group. One-way ANOVA performed followed by multiple Tukey's comparison. Scale bar = 100 microns.

Chapter 4

Arc and an impaired endolysosomal pathway contribute to synapse damage in early prion disease.

Prion diseases are infectious neurodegenerative disorders caused by PrP^{Sc}, a misfolded and aggregated isoform of the cellular prion protein, PrP^{C}. PrP^{Sc} accumulates exponentially and spreads through the CNS, causing neurodegeneration, gliosis, and ultimately death. However, the mechanisms underlying the early events in the brain that lead to prion spread and neuron death remain poorly defined. Here, we have investigated the role of the endolysosomal pathway in prion-induced changes within the brain through genetic, biochemical, and histological approaches to uncover mechanisms that propagate prion spread and toxicity. We performed RNAseq analysis at 40% of disease course (60 days post inoculation) in the hippocampus of 22L prion-infected mice and found an upregulation of synaptic remodeling genes to be among

the first changes during prion infection. We discovered an increase in Arc coinciding with loss of synaptic proteins mGluR5 and synapsin-I in the hippocampus as early as 40% of the disease course. We also observed alterations to endolysosomal and ESCRT pathways and an accumulation of ubiquitin inclusions in the hippocampus. Our studies suggest that prion infection initially disrupts the endolysosomal pathway at the synapse and causes a cascade of synaptic remodeling that suggest targets for early therapy.

4.1 Introduction

Both synapse and endolysosomal pathway dysfunction occur early in many neurodegenerative diseases, yet how these pathways contribute to disease pathogenesis remains elusive (Cataldo et al., 2000; Ginsberg et al., 2010b; Xu et al., 2016). Endolysosomal processes including endocytosis, trafficking and degradation of proteins, protein recycling to the cell surface, and remodeling of cellular domains are critical for neuron homeostasis and synaptic transmission and are implicated in driving many neurodegenerative diseases, including AD, PD, prion diseases.

Prion diseases are rapidly progressing neurodegenerative diseases affecting humans as well as other mammals caused by the misfolding and aggregation of the cellular prion protein (PrP^{C}) into PrP^{Sc}. PrP^{C} is a GPI-anchored protein expressed on the outer leaflet of the cell membrane and trafficked from the cell membrane through the endolysosomal pathway for recycling or degradation (Sunyach et al., 2003). Prion diseases are excellent models for understanding the sequence of events in neurodegenerative disease, as they share many pathological hallmarks, including inflammation, protein aggregation, synapse dysfunction, and neuron death. Using prion-infected mice, we studied biochemical, histological, and genetic changes at seven

different time points throughout prion disease to further understand the sequence of events in prion disease.

We have previously found that depleting the initiating component of the ESCRT (endosomal sorting complexes ready for transport) pathway, Hrs, in neurons rapidly accelerates prion disease in mice specifically by advancing the damage in synapses (Chapter 3). Hrs is part of the first complex in the ESCRT pathway that recognizes ubiquitinated endosomal proteins to sort them into multivesicular bodies (MVBs)(Bache et al., 2003). Additionally, we discovered a substantial (80%) decrease of Hrs protein levels at terminal prion disease in eight different prion strains in wildtype mice, further emphasizing the potential contributions of the ESCRT pathway to prion disease and neurotoxicity. From these studies, we concluded that loss of Hrs in prion disease may be one major driver of prion-induced synapse loss.

The role of the ESCRT pathway in synapse maintenance remains widely unknown. The loss of synapses early in prion disease is well established (Cunningham et al., 2003a; Ferrer, 2002a; Gray et al., 2009a), but mechanisms of synapse loss remain controversial (Belichenko et al., 2000a; Brown et al., 2001; Jeffrey et al., 2000). Furthermore, whether prions dysregulate the pre- or post-synapse, or both, continues to be debated. Endosomal proteins have proven to be essential in maintaining synaptic transmission and synaptic vesicle recycling. Rab GTPases are localized to synaptic terminals and are involved in endocytosis and exocytosis of synaptic vesicles (Shimizu et al., 2003; Star et al., 2005; Wucherpfennig et al., 2003). Retromer component Vps35 also has a role in synaptic vesicle recycling and has been identified as a contributor to neurodegeneration in both Alzheimer's and Parkinson's disease (Eleuteri and Albanese, 2019; Miura et al., 2014; Young et al., 2018). Several studies have implicated an important role for the ESCRT pathway in synaptic vesicle protein degradation (Sheehan et al., 2016; Uytterhoeven et

al., 2011; Watson et al., 2015), but the ESCRT pathway in neurodegenerative disease has yet to be thoroughly examined.

We investigated the earliest changes in the brain following prion infection and discovered ubiquitin inclusions together with PrP^{Sc} aggregates in the hippocampus at the 40% time-point (pre-clinical), coinciding with an increase in Arc and reduction in synapsin-I and mGluR5. We also observed an increase in ESCRT proteins, Rab5 and Rab11a, but not Rab7, p62, or Lamp1, suggesting a block in the endolysosomal system in early, preclinical prion disease. To better understand how the endolysosomal system contributes to prion disease, we performed a longitudinal study, inoculating mice with the prion strain 22L or normal brain, and collected brain samples at seven time points through terminal disease (0, 20, 40, 60, 80, 90, 100% of disease course terminating after approximately 150 days). Interestingly, we observed a loss of Hrs occurring in the clinical phase (90% time point) of prion disease. This study reveals the importance of the ESCRT pathway in not only synapse health, but also prion disease pathogenesis, and the synaptic pathways affected by these changes. This study indicates the need to further understand the mechanism underlying endolysosomal pathway dysfunction at synapse in prion-induced neurodegeneration.

4.2 Results and discussion

RNAseq analysis of prion-infected hippocampus reveals upregulated synaptic remodeling genes among earliest changes

To determine the early transcriptional changes in the prion-infected brain, we conducted RNAseq on the hippocampus from prion (22L)-infected and age-matched mock-inoculated mice

(n=3 each) at the 40% timepoint (60 days post-inoculation). 22L is a prion strain derived from sheep scrapie, characterized by diffusely distributed fine aggregates (Kim et al., 1990a; Kim et al., 1990b). We focused on the hippocampus as it often severely affected in prion disease (Cunningham et al., 2003b). We identified 270 differentially expressed genes (Fig. 4-1a, Fig. 4-2). Interestingly, immediate early genes (*Arc, Homer1, Fos, Fosb, Fosl2, Egr1, Egr2 Egr3, Egr4*) showed the highest increase in expression in the prion-infected hippocampus compared to mock-infected mice (Fig. 4-1b), and are indicative of neuronal activity and synaptic plasticity (Korb and Finkbeiner, 2011; Peebles et al., 2010). Additional synaptic remodeling genes were also increased in response to prion disease (*Crh, Adrb1, Vgf1, Tshz3, Htr2a*). Notably, there were no significant changes in the transcription of genes associated with activated microglia or astrocytes during prion disease (GFAP, Tgfb1, Ptges2, CD14, CD68, C1qb), consistent with reports indicating upregulation occurs in the clinical phase of disease (Fig. 4-1b) (Hwang et al., 2009; Vincenti et al., 2015). Thus, changes to synapses were among the earliest responses to prion disease.

Loss of synaptic proteins correlate with changes to synaptic remodeling pathways

To assess the state of the synapse, we quantified a diverse panel of synaptic proteins in the hippocampus of the same mice. We found a 1.5-fold increase in the Arc protein in prion-infected hippocampi (Fig. 4-3a,b), consistent with the RNAseq data. Arc mediates the insertion or endocytosis of synaptic receptors to facilitate either long-term potentiation or depression (Waung et al., 2008; Wilkerson et al., 2018), respectively, in response to stimuli at the synapse. Additionally, there was a significant decrease in the pre-synaptic vesicle protein, synapsin-I and

phosphorylated synapsin-I (Fig. 4-3a,b) and the post-synaptic metabotropic glutamate receptor protein, mGluR5 (Fig. 4-3a,b). However, no changes were seen in synaptic vesicle proteins Vamp2 or synaptophysin, or postsynaptic proteins PSD95 and AMPA receptor subunit GluA1 (Fig. 4-3c). Our data suggests that prions induce a reduction in synapsin-I and mGluR5, potentially through an Arc-mediated response (Wilkerson et al., 2018).

To next determine whether the synaptic alterations were an immediate response to prion infection, we cultured primary neurons and exposed cells to partially purified prions for 24 hours. It has been previously reported that spine loss in neurons occurs in as little as 24 hours post-prion exposure (Fang et al., 2016), and we considered that this spine loss could be mediated through Arc. Interestingly, we observed significantly increased Arc protein levels in neurons 24 hours post-prion (22L) exposure (Fig. 4-4a,b), however, we observed no changes to mGluR5, p-Syn1, or total Syn1 levels (Fig. 4-4a,c,d,e). Together, this data suggests that an increase in Arc is an early and rapid response to prion infection and could contribute to the pathogenesis seen in neurons during prion disease.

Increase of ESCRT proteins occurs early in prion disease within the hippocampus

As endocytosis is important in synaptic vesicle recycling and post-synaptic receptor recycling, and both Lrrk2 and Lamp2 transcripts were increase at 40% of disease (data not shown), we next investigated how endolysosomal pathway (ELP) proteins were altered in the hippocampus at 40% of prion disease. We found a significant increase in LRRK2 protein (Fig. 4-5a,b), which is involved in regulation of vesicular trafficking and interacts with a number of RabGTPases (Boon et al., 2014; Kuwahara and Iwatsubo, 2020). Provided that enlarged endosomes occur early in prion disease (Ersdal et al., 2009; Kovács et al., 2007), we next quantified levels

of various Rabs in the ELP. Here we observed an increase in Rab5 and Rab11a (Fig. 4-5a,b), proteins involved in early endosomal sorting, indicating a potential increase in early (Clague and Urbé, 2001; Moya-Alvarado et al., 2018; Numrich and Ungermann, 2014; Simpson and Jones, 2005) and recycling endosomes (Welz et al., 2014; Zulkefli et al., 2019), respectively. However, there were no changes in late endosomal protein Rab7, or autophagosome protein p62 (Fig. 4-5c,d), implicating that endolysosomal or autophagic flux was not increased (Hausser and Schlett, 2019; Kümmel and Ungermann, 2014; Lopez-Perez et al., 2020; Ng et al., 2012; Ng and Tang, 2008; Numrich and Ungermann, 2014). We also observed lower Lamp1 levels histologically in prion-infected brains compared to uninfected brains, suggesting that neither lysosome levels nor endolysosomal flux was increased (Fig. 4-5e).

Endosomes can be sorted to different destinations, and the multivesicular body versus the retromer pathway are two opposing directions (Hu et al., 2015; Norris et al., 2017; Zhang et al., 2018), so we examined levels of ESCRT and retromer proteins to further investigate what subcellular compartments were altered in prion disease. We discovered a significant increase in Hrs, and trending increases of Tsg101 and Chmp2B (Fig. 4-5a,b), suggesting an increase in MVBs (Schmidt and Teis, 2012). Opposingly, we found no changes to the retromer protein Vps35 (Fig. 4-5c,d), indicating the ESCRT pathway and contributing endolysosomal proteins (Rab5, Rab11) were specifically impacted by prion disease.

The ESCRT pathway sorts ubiquitinated proteins, which we found significantly increased in prion-infected hippocampi (Fig. 4-5a,b), further substantiating damaged proteostasis. Increased early endosomal and ubiquitinated proteins coinciding with no changes to late ELP proteins and lower levels of Lamp1 suggests a potential block in endolysosomal flux, which has also been observed in CJD brains (Kovács et al., 2007). As we see a lack of Lamp1 and p62

in the hippocampus at 40%, lysosome formation and function could be impaired, as previously reported in prion disease (Shim et al., 2016). Together, our data implicates an impairment to the endolysosomal pathway at the first signs of disease, correlating with a loss of synaptic proteins potentially mediated by an increase in Arc.

Histology reveals ubiquitin inclusions appear early in prion disease

To determine the timeline of the changes to synapses and the ELS relative to the PrP^{Sc} levels and spongiform degeneration in prion disease, we collected brains of 22L prion or mock-infected mice at seven different time points between inoculation (0 dpi) and terminal disease [150 (dpi)] (0, 20, 40, 60, 80, 90, 100% of disease course) and analyzed brains by immunohistochemistry. We observed ubiquitin inclusions in the prion-infected brain as early as 40% within the hippocampus and increased through terminal disease (Fig. 4-6b), coinciding with the early detection of PrP^{Sc} aggregates (Fig 4-6a). This finding supports that the ELP and degradative processes are impaired early in prion disease. Spongiform change and inflammation appeared at 80% of disease and increased in severity through terminal disease (Fig 4-6c-e). Taken together, these findings suggest a loss of degradative pathway function early in disease, followed by inflammation and neuronal death.

ESCRT-0 in the brain decreases at symptomatic stage of disease

To determine the magnitude of the altered synaptic and ELP proteins globally over time, we next quantified protein levels in whole brain from 22L prion- or mock-infected mice at the 7 different time points. We detected PrP^{Sc} in the brain at 40% of disease by sodium phosphotungstic acid (NaPTA) precipitation (Fig. 4-7a,b), similar to what we observed histologically.

Globally, ubiquitinated protein levels in whole brain were significantly increased after 80% of disease (Fig 4-7c). Coincidentally, at 90% of disease, Hrs and Stam1, proteins that sort ubiquitinated endosomal proteins, were significantly decreased (130 DPI)(Fig. 4-7d, Fig. 4-9a). Tsg101, part of the ESCRT-I complex, increased starting from 80% of disease (Fig. 4-7c), but we observed no significant changes to Chmp2B, part of the ESCRT-III complex, at any timepoint (Fig. 4-9b). Despite the alterations at the protein level, there were no changes in transcript levels of Hgs, Stam1, or Tsg101 by qRT-PCR at any time point (Fig. 4-8), consistent with the lack of changes to these pathways in the RNAseq analysis. The accumulation of ubiquitinated proteins coinciding with loss of ESCRT-0 proteins during the clinical prion disease implicates the ESCRT pathway contributing to dysregulation of degradative pathways.

There were no changes to the early endosomal protein Rab5 or late endosomal protein Rab7 at any timepoint in whole brain (Fig. 4-7e). Additionally, there were no changes to the retromer component Vps35 at any stage of disease (Fig. 4-9c), despite that decreased Vps35 transcript levels have been previously reported in CJD (Creutzfeld-Jakob disease) (Bartoletti-Stella et al., 2019). We observed increases in autophagic protein p62 (Fig. 4-9d) at late stages of disease (90-100% of disease course), similar to what has previously been published (Lopez-Perez et al., 2020) where autophagosome accumulation occurs late in disease, also contributing to proteostasis disruption. Together, our results indicate that severe changes to endolysosomal protein levels occurred during clinical disease, emphasizing the important role of the ESCRT pathway not only in the early stages of disease in the initial response to prion infection, but also the clinical stages of disease where spongiform change and symptoms become apparent.

Discussion

In this study, we utilized an unbiased approach to detect the earliest changes in the brain in response to prion infection and found an upregulation of the immediate early genes pathway (*Arc, Homer, Fos*) by RNAseq analysis. By analyzing protein levels in the hippocampus, we also detected a loss of mGluR5 protein correlated with an increase in Arc protein levels. Arc has been of recent interest in neurodegeneration, as it may contribute to synaptic depression in Alzheimer's disease (Bi et al., 2018; Kerrigan and Randall, 2013; Morin et al., 2016; Wu et al., 2011). To our knowledge, we are the first to report changes to Arc in prion disease. However, previous studies have shown changes to synaptic remodeling pathways as some of the first transcriptional changes in prion disease, similar to our results (Majer et al., 2012; Sorce et al., 2020). Arc is known to be involved in synaptic plasticity, regulated via mGluRs, and can result in long term depression and weakened synapse connectivity (Wilkerson et al., 2018). Moreover, activation of mGluR5 leads to structural synapse elimination through the Arc (Wilkerson et al., 2014), and we observed a loss of mGluR5 coinciding with an increase in Arc. Additionally, A-β induced synapse loss by binding to PrP^{C} and activating mGluR5 (Um et al., 2013). Here, we show that early changes to the post synapse affect specifically Arc and mGluR5, and it is warranted that PrP^{Sc} could be mediating neuronal toxicity through mGluR5 in prion disease via the Arc response. Furthermore, these mechanisms may not be specific to prion disease, but parallel changes seen in other neurodegenerative diseases.

At the 40% time point, we observed a loss of synapsin-I, suggesting that dysregulation of synaptic vesicle recycling in the pre-synapse could be one of the first changes in response to prion disease. Synapsin-I functions to maintain a reserve pool of synaptic vesicles in the pre-synapse (Hilfiker et al., 1999), and synaptic vesicle loss occurs in many models of neurodegen-

erative diseases, often preceding other changes to synapse (Esposito et al., 2012; McInnes et al., 2018; Scott et al., 2010). Our previous study observed damages to synaptic vesicle recycling as a result of prion disease, as well as a decrease in synaptic vesicle docking at the synapse. In line with our work, a study examining the effects of another prion strain, ME7, observed a loss of synaptophysin early on in disease, again suggesting that the presynaptic compartment is significantly disrupted early in prion disease (Gray et al., 2009b). Loss of synaptic vesicle proteins could result in an accumulation of damaged or misfolded synaptic vesicle proteins, and that alone can lead to neurodegeneration (Burgoyne and Morgan, 2015; Peng et al., 2013; Rozas et al., 2012; Sharma et al., 2012a; Sharma et al., 2012b; Shimojo et al., 2019; Williamson and Neale, 1998). Our work implicates loss of synapsin-I can contribute to the early synapse loss and synaptic vesicle dysregulation seen in prion disease (Peggion et al., 2019; Robinson et al., 2014).

We have observed what appears to be a block in the ESCRT pathway at 40% of prion disease in the hippocampus, as there is an increase in early endosomal and ESCRT proteins, but not late endosomal or lysosomal proteins, which we believe could contribute to the dysfunctional synapses observed early in prion disease. Interestingly, the importance of the ESCRT pathway in synaptic vesicle recycling has become of relevance in the last decade. ESCRT proteins are recruited to synaptic vesicle pools in order to degrade synaptic vesicle proteins (Sheehan et al., 2016). While we know that the teetering mutation in Hrs leads to accumulation of ubiquitinated proteins at neuromuscular junctions (Watson et al., 2015) and depletion of Hrs in neurons results in an increase of ubiquitinated synaptic proteins (Tamai et al., 2008), much remains to be discovered regarding the role of the ESCRT pathway at synapses.. These studies all implicate the importance of ESCRT proteins at both the pre- and post-synapse, and impairment of this

pathway could very well contribute to synapse loss.

In our study, we analyzed protein and gene expression levels of autophagic components, observing no significant increases until clinical stages of prion disease. The connection between autophagy and prion disease pathogenesis remains controversial. In many models of prion disease, autophagic vacuole accumulation is associated with PrP^{Sc} aggregation, visualized ultrastructurally, biochemically, and histologically (Boellaard et al., 1991; Lopez-Perez et al., 2019a; Sikorska et al., 2007; Xu et al., 2012). Drug stimulation of autophagy flux reduces prion levels in vitro, yet does not significantly delay prion disease in vivo (Abdelaziz et al., 2019; Abdulrahman et al., 2017; Abdulrahman et al., 2019; Aguib et al., 2009; Goold et al., 2015; Heiseke et al., 2009). A recent study found that at terminal prion disease, a negative regulation of autophagy-related genes, accumulation of p62, and a loss of LC3B proteins implicated damaged autophagic machinery (Lopez-Perez et al., 2020). However, there was an absence of changes to autophagy gene regulation and proteins at pre-clinical stages of disease, suggesting that impairments to autophagy were a consequence of disease. Our work further supports these recent findings, as we saw no changes to levels of the autophagosome marker p62 early in prion disease but observed p62 increases during clinical prion disease. Furthermore, autophagy genes were unaffected at the 40% timepoint. While additional experiments are needed to elucidate the role of autophagy during prion disease, taken together, our data supports previous findings that autophagy is not impaired until late disease.

We see an increase in early endosomal proteins, but not late endosome (Rab7), lysosome (Lamp1), or autophagosome (p62) proteins, suggesting impairment in endosomal maturation or lysosomal formation. (Shim et al., 2016) have shown that prion infection interferes with Rab7, resulting in a block of lysosomal maturation and degradation. Consistent with our

observations, they reported no changes in total levels of Rab7 during prion infection but did however observe a decrease in membrane associated Rab7 upon prion infection. Furthermore, additional reports indicate a decrease in rab protein activity as a consequence of prion infection (Ermolayev et al., 2009; Massignan et al., 2010). Rab7 is necessary for lysosome maturation (Girard et al., 2014), and others report decrease in lysosomes (Shim et al., 2016) with prion infection, providing a possible explanation for the observed low levels of Lamp1 early in prion disease. This suggests that prion infection impairs the ELP through altering subcellular localization of Rab7, thereby preventing lysosome maturation. PrP^{Sc} can therefore evade degradation in lysosomes and diverge to multivesicular bodies and the retromer pathway, both of which have been identified as major sites of prion conversion (Marijanovic et al., 2009; Yim et al., 2015). The idea that endosome maturation is damaged in prion infection is further supported by the finding that the brains of CJD patients harbor enlarged Rab5 and Rab7 vesicles that are associated with PrP^{Sc} aggregates (Kovács et al., 2007). Additionally, ultrastructural analysis of BSE in cattle brains highlights an increase in multivesicular bodies within the brain at terminal disease, further supporting a block in the ELS pathway (Ersdal et al., 2009). Thus, we conclude that an impairment to endosomal maturation early in prion disease contributes to pathogenesis.

Our studies suggest that glial activation follows prion aggregation and synapse loss, implicating that gliosis is potentially a secondary reaction to prion disease. Activation of glial cells, the complement system, and inflammation is a defining characteristic of prion disease. Many studies have suggested that activation of microglia and astrocytes occurs early on in prion disease (Hwang et al., 2009; Vincenti et al., 2015), yet it remains unclear whether aggregating PrP^{Sc} or signaling by PrP^{Sc} causes the inflammatory response. The lack of glial transcription profiles and Iba1 immunohistochemistry at 40% in the hippocampus when prions are detected

suggests that activation of microglia occurs after initial effects of prion disease. Yet whether microglia contribute to neurotoxicity (Giese et al., 1998; Rezaie and Lantos, 2001) or aid in the clearance of PrP^{Sc} remains controversial. Some studies suggest that without activated microglia, prion disease progression is accelerated (Kranich et al., 2010; Nuvolone et al., 2017; Zhu et al., 2016), yet depletion of microglia in clinical stages improves prion disease progression (Gomez-Nicola et al., 2013). While the role of glial cells in prion disease remains controversial, more investigation into the subtypes is necessary for understanding their contribution to neurotoxicity and what causes their activation.

4.3 Concluding remarks

In conclusion, the earliest changes that we observe in prion disease are within synaptic, early endosomal and ESCRT pathways. Increase in Arc protein at first signs of prion aggregates correlates with a decrease in synapsin-I and mGluR5. At the same time, we observed an increase in early endosomal proteins, but not late endosome or lysosomal proteins, implicating a block in the endosomal pathways, additionally contributing to the synaptic pathology. While these changes are observed in prion disease, they parallel many changes seen in other neurodegenerative diseases. Further studies on the basic biology of the ESCRT pathway in neurons are necessary for understanding the contributions of ESCRT complexes at the synapse. Additionally, a thorough understanding of Rab activity and a functional analysis of synaptic changes are important for understanding how these changes contribute to synapse loss. We propose that preservation of the synapse is an important therapeutic target for neurodegeneration, potentially through the endolysosomal pathways.

4.4 Materials and Methods

Mouse generation

C57BL6J mice were purchased from Jackson laboratories. Mice were maintained under specific pathogen-free conditions on a 12:12 light/dark cycle. Mice had access to standard laboratory chow and water ad libitum.

Mouse inoculations

Mice (6-8 weeks old) were anesthetized with ketamine and xylazine and inoculated into the left parietal cortex with 30 μl of 1% 22L prion-infected brain homogenate prepared from terminally ill mice. Strain 22L is a mouse-adapted prion originally derived from sheep scrapie that have different cellular targets in the brain and plaque morphologies and was a kind gift from Dr. Michael Oldstone. Strain 22L is a mouse-adapted prion originally derived from sheep scrapie that have different cellular targets in the brain and plaque morphologies and was a kind gift from Dr. Michael Oldstone. 3-5 mice were sacrificed every month after inoculation until clinical disease, and once additionally two weeks after initial clinical symptoms, resulting in sacrifices at 20, 40, 60, 80, 90, and 100% of disease course. TSE (Transmission Spongiform Encephalopathy) was diagnosed according to clinical criteria including ataxia, kyphosis, stiff tail, hind leg clasp, and hind leg paresis. The brain was halved, and one hemi-brain was formalin-fixed for 2-3 days, then immersed in 96% formic acid for 1 hour, washed in water, and post-fixed in formalin for 2-4 days. Brains were then cut into 2 mm transverse sections and paraffin-embedded for histological analysis. The remaining hemi-brain was immediately frozen on dry ice. The remaining brain sections were frozen for biochemical analyses. No mice were excluded

from the analysis. For hippocampal analysis, brains were halved, and the hippocampus was isolated and immediately stored in RNALaterTM.

Western blots

Brain tissue was homogenized in PBS using a Beadbeater^{TM} tissue homogenizer in PBS, to reach a final concentration of 10% brain homogenate. boiling samples for 5 minutes in LDS loading buffer (Invitrogen). Samples were electrophoresed in 10% Bis-Tris gel (Invitrogen) and transferred to a nitrocellulose membrane by wet blotting. Membranes were incubated with monoclonal antibody POM19 (discontinuous epitope at C-terminal domain, amino acids 201–225 (Polymenidou et al., 2008), a kind gift from Dr. Adriano Aguzzi) followed by incubation with an HRP-conjugated anti-mouse IgG secondary antibody (Jackson Immunolabs). The blots were developed using a chemiluminescent substrate (ECL detection kit, ThermoScientific) and visualized on a Fuji LAS 4000 imager.

NaPTA

PrP^{Sc} was concentrated from mouse brains by sodium phosphotungstic acid (NaPTA) precipitation prior to western-blotting (Wadsworth, 2001). Briefly, 100 μl aliquots of 10% brain homogenate in an equal volume of 4% sarkosyl in PBS were incubated for 30 minutes, then digested with an endonuclease [Benzonase^{TM} (Sigma)] followed by treatment with 100 μg/ml proteinase K at 37 °C for 30 minutes. After addition of NaPTA, MgCl2, and protease inhibitors (Complete TM, Roche), extracts were incubated at 37 °C for 30 minutes, and centrifuged at 18,000 g for 30 minutes at 37 °C. Pellets were resuspended in 0.1% sarkosyl prior to electrophoresis and blotting. Samples were electrophoresed in 10% Bis-Tris gel (Invitrogen) and

transferred to a nitrocellulose membrane by wet blotting. Membranes were incubated with monoclonal antibody POM19 (discontinuous epitope at C-terminal domain, amino acids 201–225 (Polymenidou et al., 2008), a kind gift from Dr. Adriano Aguzzi) followed by incubation with an HRP-conjugated anti-mouse IgG secondary antibody (Jackson Immunolabs). The blots were developed using a chemiluminescent substrate (ECL detection kit, ThermoScientific) and visualized on a Fuji LAS 4000 imager.

Histology

Tissue sections were cut from blocks of formalin-fixed paraffin embedded mouse brain. Four-micron tissue sections were stained on a Ventana Discovery Ultra (Ventana Medical Systems, Tucson, AZ, USA). with antibodies to GFAP (Dako; 1:6000), Iba-1 (Wako; 1: 3000), Ubiquitin (Dako, 1:3000), LAMP1 (source; 1:150). Antigen retrieval was independently optimized for each epitope to yield the maximal signal to noise ratio. For PrP, slides were incubated in protease 2 for 20 min followed by antigen retrieval in CC1 (tris-based; pH 8.5; Ventana) for 64 min at 95°C. For GFAP only the protease P2 was used (Ventana) for 16 minutes. For LAMP1, Iba-1, and ubiquitin all retrieval was done using CC1 for either 24 (Lamp1) or 40 min (Iba-1, ubiquitin). Following retrieval, all antibodies were incubated on the tissue for 32 min at 37°C. The secondary antibody (HRP-coupled goat anti-rabbit; OmniMap system; Ventana) was incubated on the sections for 12 min at 37°C. The primary antibody was visualized using DAB as a chromagen followed by hematoxylin as a counterstain. Due to the low level expression of LAMP1, an additional amplification step was included before the DAB reaction using the Ventana HQ-Amp system for 12 min. Slides were rinsed, dehydrated through alcohol and xylene and coverslipped.

qRT-PCR

RNA isolation from prion-infected brains using the PureLink RNA isolation kit (Thermo fisher 12183025). Brain samples were collected and frozen on dry ice. Brains were thawed in RNAice Later. After lysing the brains with the PureLink RNA isolation lysis buffer, brain lysates were decontaminted in 5.3M Guanidine Isothiocynate for 24 hours. Following decontamination, RNA was isolated using the PureLink RNA isolation kit. cDNA synthesis was performed using Promega cDNA synthesis kit. Random hexamers, M-MLV RT buffer 5X, dNTP mix (10mM), and M-MLT RT. qRT-PCR was performed using FAM labeled primers Hgs, Tsg101, Stam1 and control murine GAPDH. cDNA was mixed with TaqMan Gene Expression Master MixII with UNG (Life technologies 4423710) and run in the StepOnePlus (Applied Biosystems) in MicroAmp Fast 96-well reaction plates (Applied Biosciences, 4346907).

RNA-seq

For RNAseq, RNA was isolated and homogenized TRIzol reagent (1mL per 100mg of tissue) and incubated for 24 hours to eliminate infectivity titer. 0.2mL of chloroform per 1mL of TRIzol was added to each brain and vortex briefly and incubated for 5 min at room temperature. Sample was centrifuged at 12,000 g for 15 min at 4°C. 500μL of the aqueous colorless upper phase containing RNA was transferred to a tube containing equal volume of 70% ethanol and vortexed to mix. RNA was then isolated using the PureLink RNA isolation kit (Thermo fisher 12183025). DNase treatment was applied to the RNA alongside the first wash in the spin cartridge. QC and RNAseq was conducted at the IGM Genomics center, University of California, San Diego, La Jolla, CA.

RNA-seq data processing

RNA-sequencing reads were trimmed using cutadapt (v1.4.0) of adaptor sequences and mapped to repetitive elements (RepBase v18.04) using the STAR (v2.4.0i). Reads that did not map to repetitive elements were then mapped to the mouse genome (mm9). GENCODE (v19) gene annotations and featureCounts (v.1.5.0) were used to create read count matrices.

Primary neuron culture

Primary cortical neurons from P0 Hrs f/f mouse pups were cultured in neurobasal media (Gibco) containing 2% B27 plus Supplement (Gibco) and 1X GlutaMAX^{TM} (Gibco). In brief, the cerebral cortices were dissected, dissociated with 0.25% trypsin at 37°C for 20 minutes, treated with DNase, and triturated. Debris was removed by passing the cells through a 70 μm cell strainer. Cells were then centrifuged for 10 minutes and resuspended in neurobasal media with 2% B27plus and 1X GlutaMAX^{TM}. Neurons were cultured on plates treated with Poly-L-Lysine. Neurons were then washed with PBS twice, and collected in 2% N-lauryl sarcosine with benzonase^{TM} and lysed on ice for 30 min. A BCA was run to quantify protein levels. Neuron lysates were run on a gel at equal concentrations and volumes of lysate and quantified by western blot.

Partial purification of prions

22L prion-infected and uninfected 10% brain homogenates (200μL) were lysed in 2% sarcosyl in PBS (200μL) with add 16 μL of benzonase + MgCl2 (8μl MgCL2 and 8μl benzonase). Lysates were incubated for 30 min at 37 °C, shaking at 1000rpm. Samples were then centrifuged at 4 °C at 18,000 g for 30 min. The supernatant was removed, and pellets, containing the

partially purified prions, were resuspended in 100μL of PBS. Partially purified samples were then heated to 65 °C sterilize samples for cell culture.

Antibodies for western blots

The following antibodies were used for western blotting. Mouse anti-PrP (1:10,000, POM19, amino acids 201–225 (Polymenidou et al., 2008), a kind gift from Dr. Adriano Aguzzi); mouse anti-PrP Pom1 (1:10,000); anti-Hrs (1:5000, Cell Signaling Technology); anti-β actin (1:5000, Genetex); anti-Gapdh (1:5000, Novus); anti-Stam1 (1:1000, Cell Signaling Technology); anti-Rab7 (1:1000, Cell Signaling Technology); anti-Tsg101 (1:1000, Genetex); anti-Rab5 (1:1000, Cell Signaling Technology); Ubiquitin (1:7000, Dako); Rab11a (1:1000, Cell Signaling Technology); anti-Vps35 (1:10,000, Genetex); anti-Chmp2B (1:1000, Cell Signaling Technology); anti-LC3-I/II (1:1000, Cell Signaling Technology); anti-p62 (1:4000, Abnova); anti-Synapsin-I (1:10,000, Fisher Scientific); anti-Synaptophysin (1:10,000, Invitrogen); anti-PSD95 (1:5000, Calbiochem); anti-Vamp2 (1:10,000, Cell Signaling Technology); anti-Snap25 (1:10,000, Cell Signaling Technology); anti-mGluR5 (1:2000, Cell Signaling Technology); anti-GluA1 (1:1000, Cell Signaling Technology); anti-phosphorylated Synapsin-I (1:1000, Cell Signaling Technology); anti-Arc (1:1000, Proteintech).

4.5 Acknowledgements

The authors would like to thank members of the members of the Sigurdson lab, particularly Patricia Aguilar-Calvo and Julia Callendar for their thorough reading of this manuscript. Thanks to Don Pizzo for his histology and discussion of analysis methods used in this manuscript. Thanks to Emily Wheeler for her guidance on the methods of RNAseq analysis.

J.A.L. is supported by a Ruth L. Kirschstein Institutional National Research Award from the National Institutes of Health, NINDS F31NS103588.

Chapter 4, in full, is a reprint of material submitted to be published in: **Lawrence, JA**, Sigurdson C. Arc and an impaired endolysosomal pathway contribute to synapse damage in early prion disease. The dissertation author was first author of this paper.

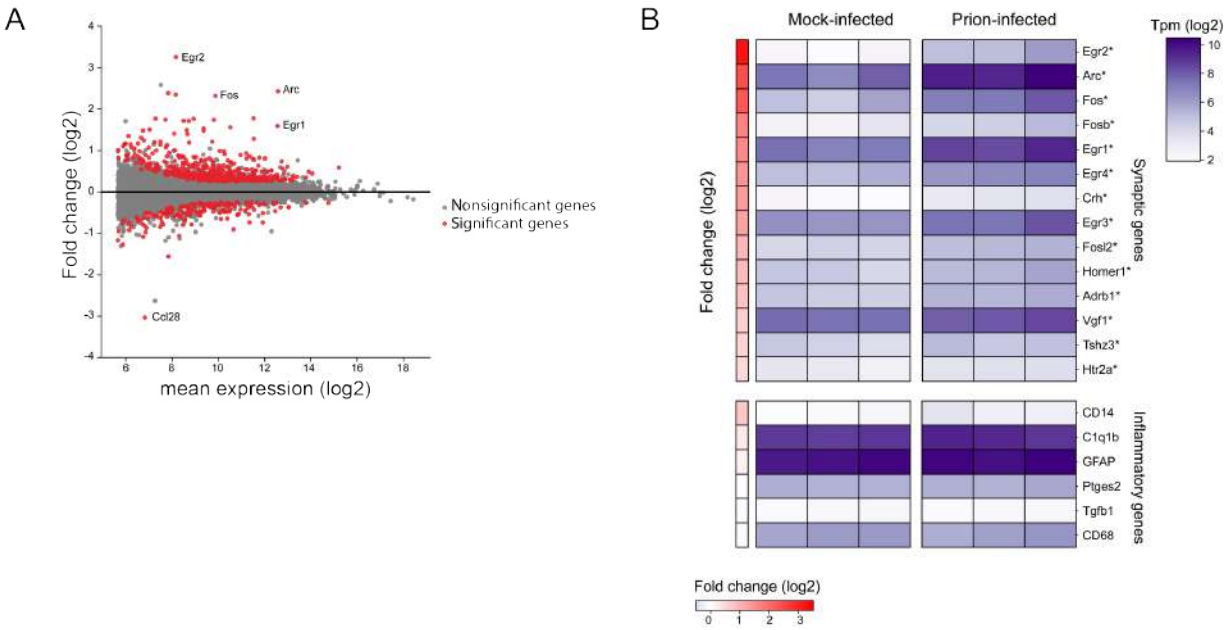

Figure 4.1: RNAseq analysis reveals synaptic remodeling in the hippocampus is among earliest changes during prion disease. RNAseq was performed on isolated hippocampi from 3 mock-infected and 3 prion-infected mice at 40% of disease, revealing 300 differentially regulated genes. (A) Genes significantly different from mock-infected (B) Heat map representation of transcripts per million (tpm, purple) and fold change over mock-infected controls (red). Genes that are significantly different from mock-infected shown by asterisk.

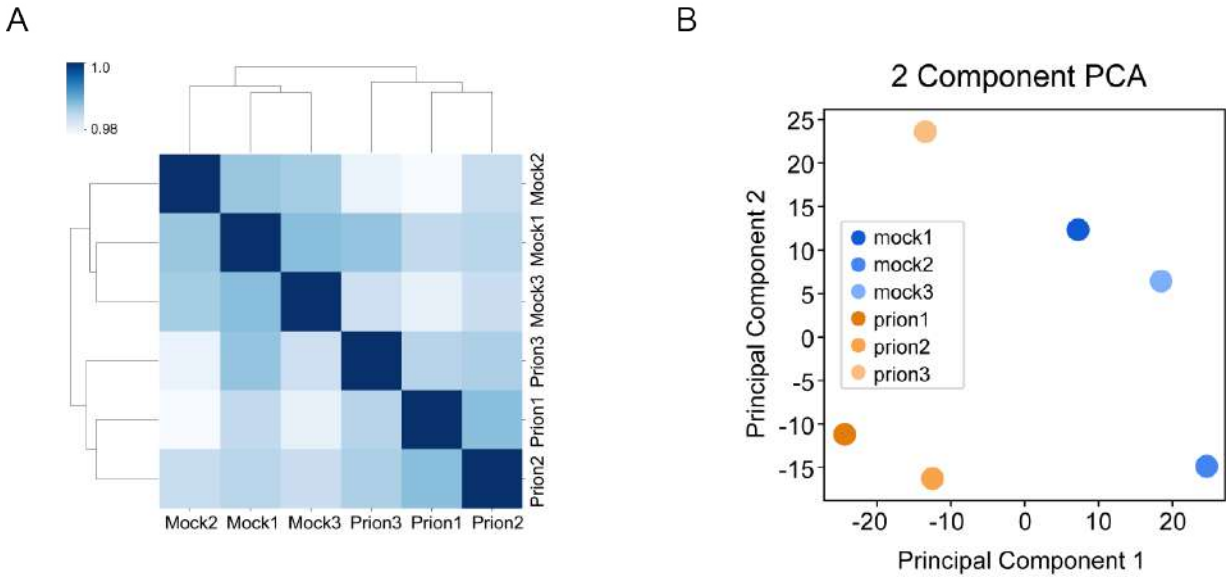

Figure 4.2: Correlation and PCA for RNAseq analysis groups mock and prion mice together. (A) Correlation plot for the RNAseq analysis of mock and prion-infected hippocampus shows that prion-infected transcript profile is most similar to prion-infected mice. (B) PCA shows the differences in mock and prion mice are greater than those within groups.

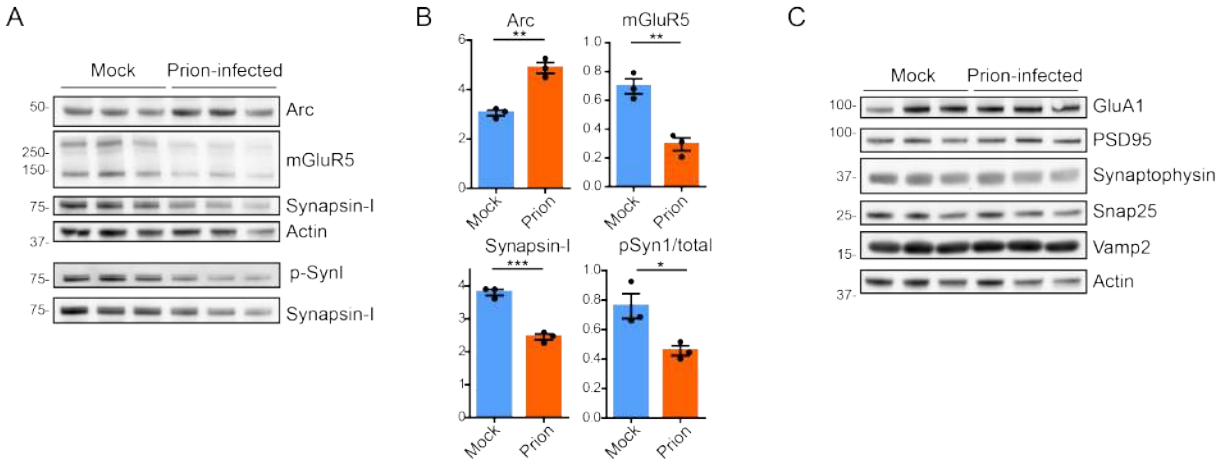

Figure 4.3: Increased Arc protein levels in the hippocampus correlate with a decrease in mGluR5 and synapsin1. Immunoblots of homogenized hippocampi show an increase to Arc proteins in prion infected mice but a decrease to phospho-synapsin1, total synapsin-1, and mGluR5 (A), quantified in the graphs showing mean with SEM, phospho-synapsin1 was compared to total synapsin1 on the same blot (B), where a t-test was performed, *$p<0.05$, **$p<0.01$. (C) Immunoblots show no changes to additional synaptic proteins between mock and 22L-infected brains: GluA1, PSD95, Synaptophysin, Snap25, and Vamp2.

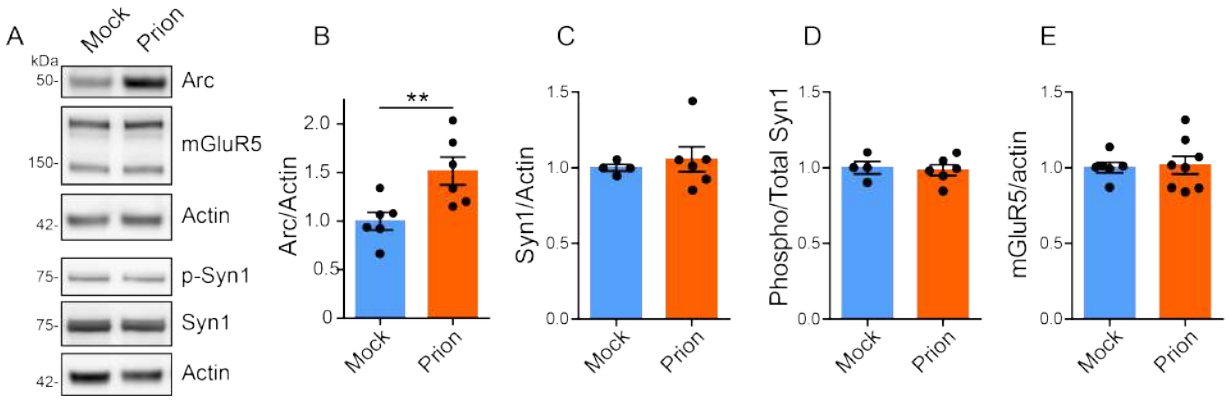

Figure 4.4: Primary neurons infected with prions show an increase in Arc within 24 hours of infection. (A) Immunoblots of wildtype primary neurons, 7 days in vitro (DIV), introduced to partially purified prions or mock-infected brain for 24 hours before collected and lysed, quantified for (B) Arc, (C) total Synapsin1, (D) phosphorylated Synapsin1, and (E) mGluR5. Proteins were normalized to actin, except for phosphorylated synapsin1 was normalized to total synapsin1 on the same blot. T-test performed on the averages, **$p < .01$.

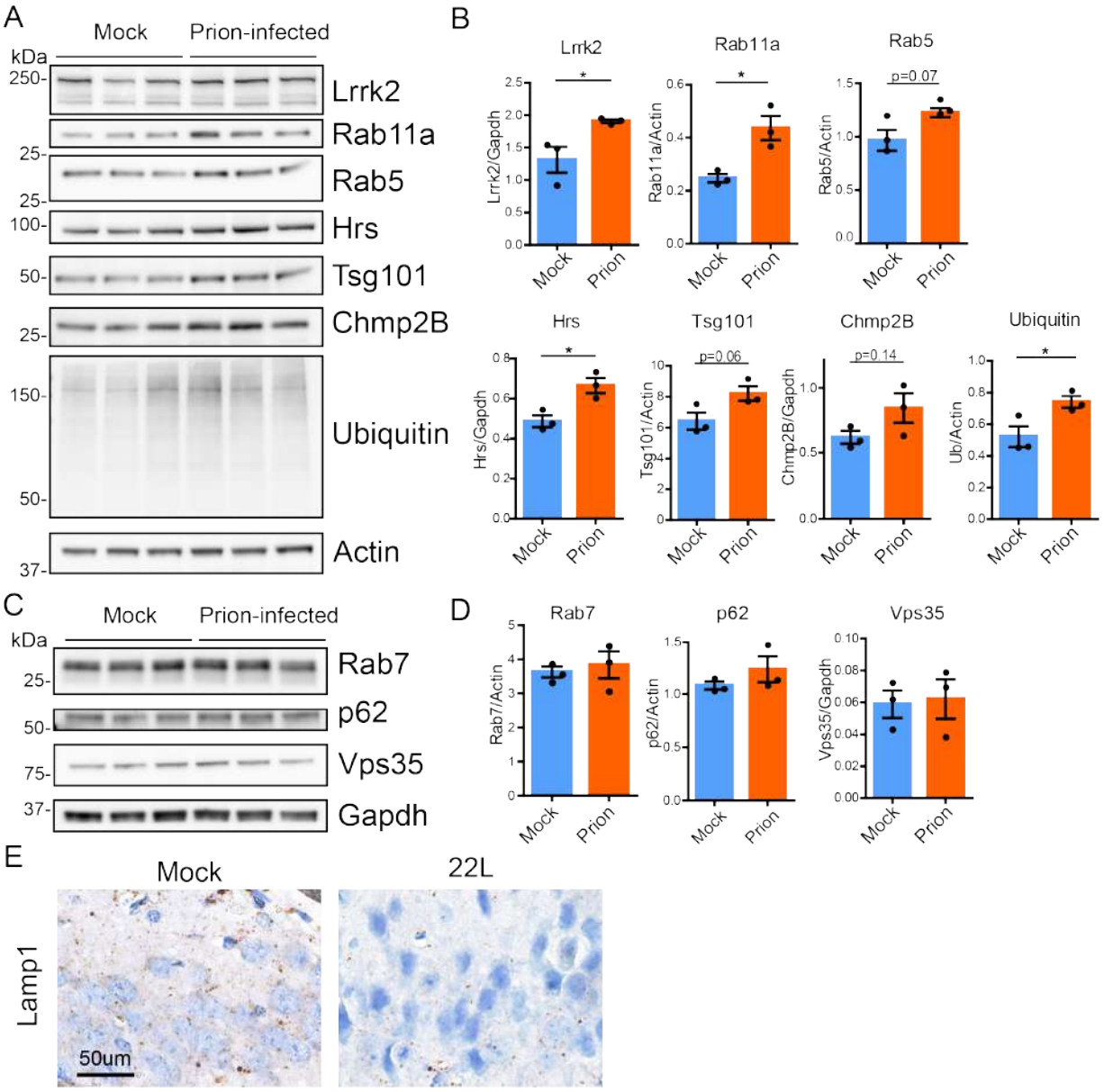

Figure 4.5: Increased early endosomal and ESCRT proteins in the hippocampus at 40%, but not Rab7, p62 or Lamp1 levels. Immunoblots of the hippocampus at 40% of prion disease or mock-infection illustrating increases to Lrrk2, Hrs, Tsg101, Chmp2B, Rab11a, Rab5, and ubiquitin (A), as quantified in the graphs comparing fold-change over mock (B). No changes seen to Vps35, Rab7, or p62 (C), as quantified comparing fold-change over mock-infected (D), n=3. Statistics were performed using a t-test, *p$<$.05. (E) Immunohistochemistry of Lamp1 in the hippocampus at 40% of prion-infection shows lower levels than the mock-infection at 40%. Scale bar, 50 microns.

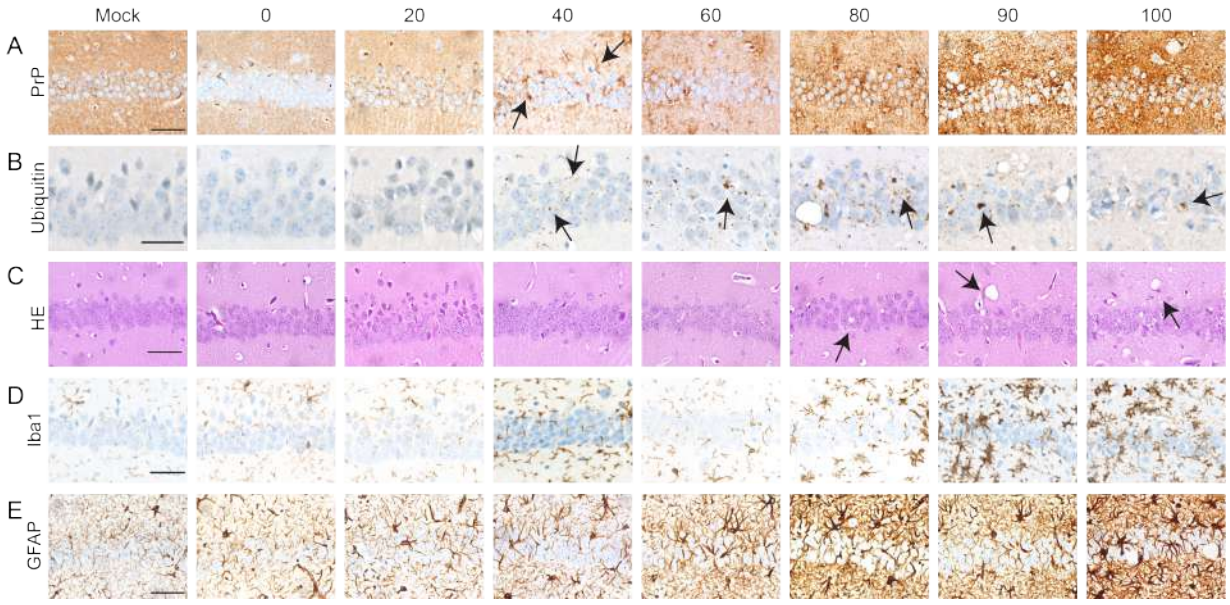

Figure 4.6: Histological analysis of the brain throughout prion disease. Histology of the brain in mock-infected mice and 7 time points throughout prion disease. (A) PrP^{Sc}, showing aggregates starting at 40% (black arrows). (B) Ubiquitinated aggregates in the brain start at 40% (black arrows) and increase through terminal disease. Scale bar is 30 microns. (C) Haemotoxylin Eosin staining (HE), showing spongiform change (black arrows). Iba1 staining for microglia (D) and GFAP staining for astrocytes (E) in the brain. Scale bar is 100 microns for A, C, D and E.

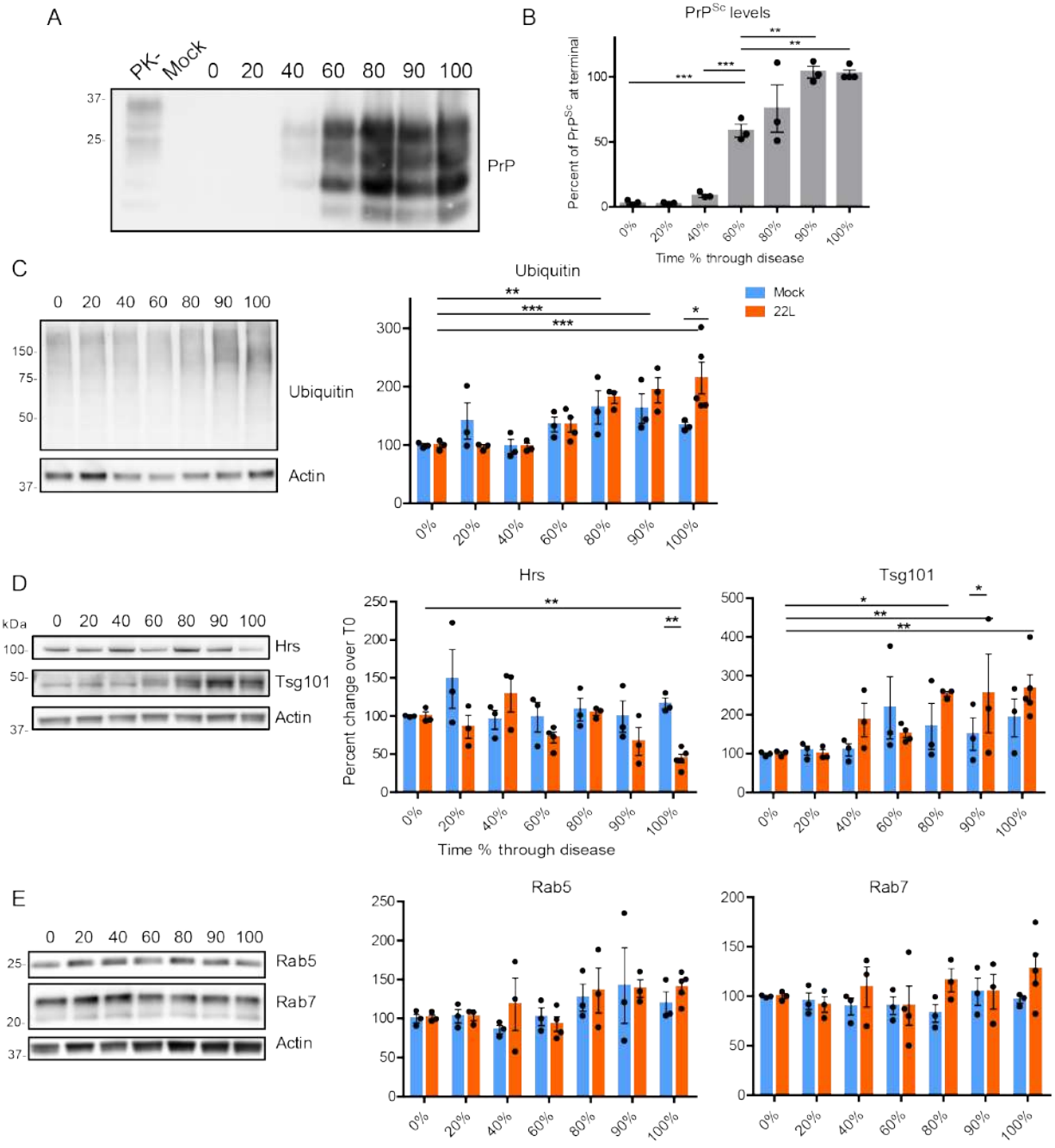

Figure 4.7: Analysis of protein levels at seven different points during prion disease. (A-E) Total brain homogenates from n=3-5 mice at seven different time points, either inoculated with 1% mock- (blue) or 22L prion-infected brain (orange), were analyzed by immunoblot. (A) PrP^{Sc} levels within brain samples, measured by Proteinase K (PK) digestion and immunoblotting for PrP using the POM19 antibody. PK- control and mock + PK controls shown. (B) Graph shows PrP^{Sc} levels normalized to terminal (100%) PrP^{Sc} levels. Data shown as mean and SEM of triplicate mice. Western blots of the total brain homogenate at each time point, and graphs show proteins quantified against actin and normalized to the 0% control of (C) ubiquitin, (D) Hrs and Tsg101, and (E) Rab5 and Rab7. A two-way Anova was performed on each set of data, except PrP^{Sc} levels where a one-way Anova was performed. *$p<0.05$, **$p<.01$.

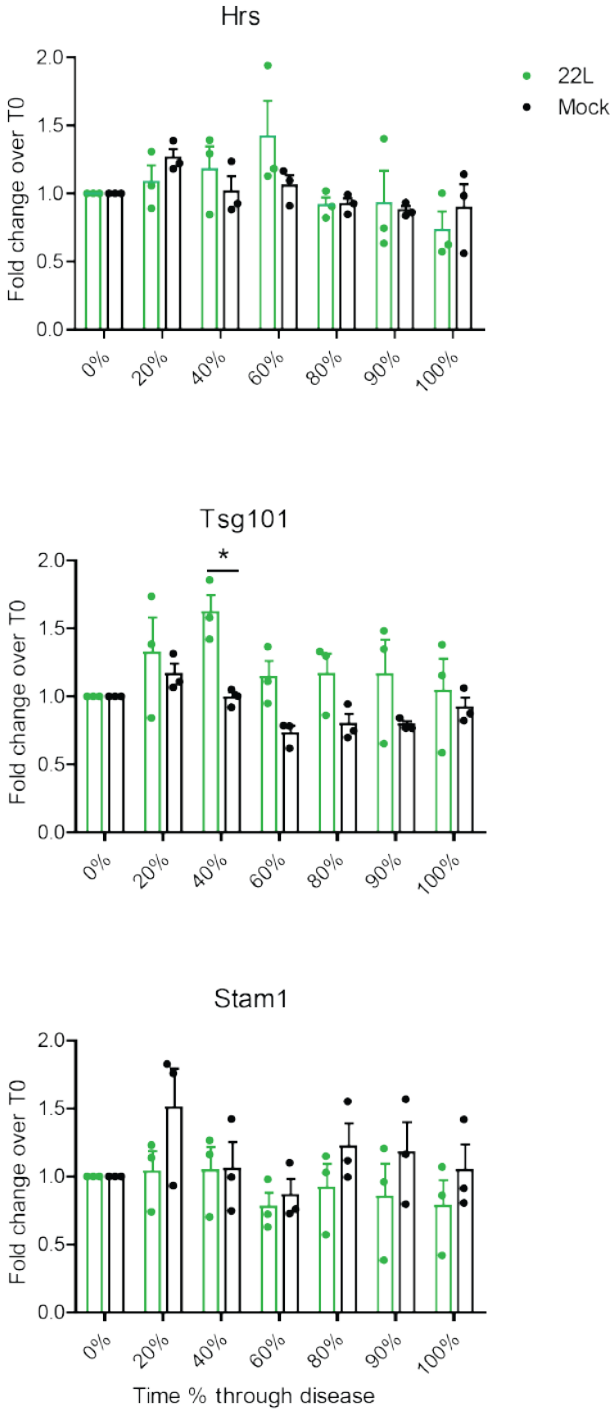

Figure 4.8: No differences in ESCRT transcript levels at any time point. Transcript levels from n=3 mice at seven different time points, either inoculated with 1% mock- (black) or 22L prion-infected brain (green) of *Hgs*, *Tsg101*, or *Stam1*, all part of ESCRT-0 or -I complexes.

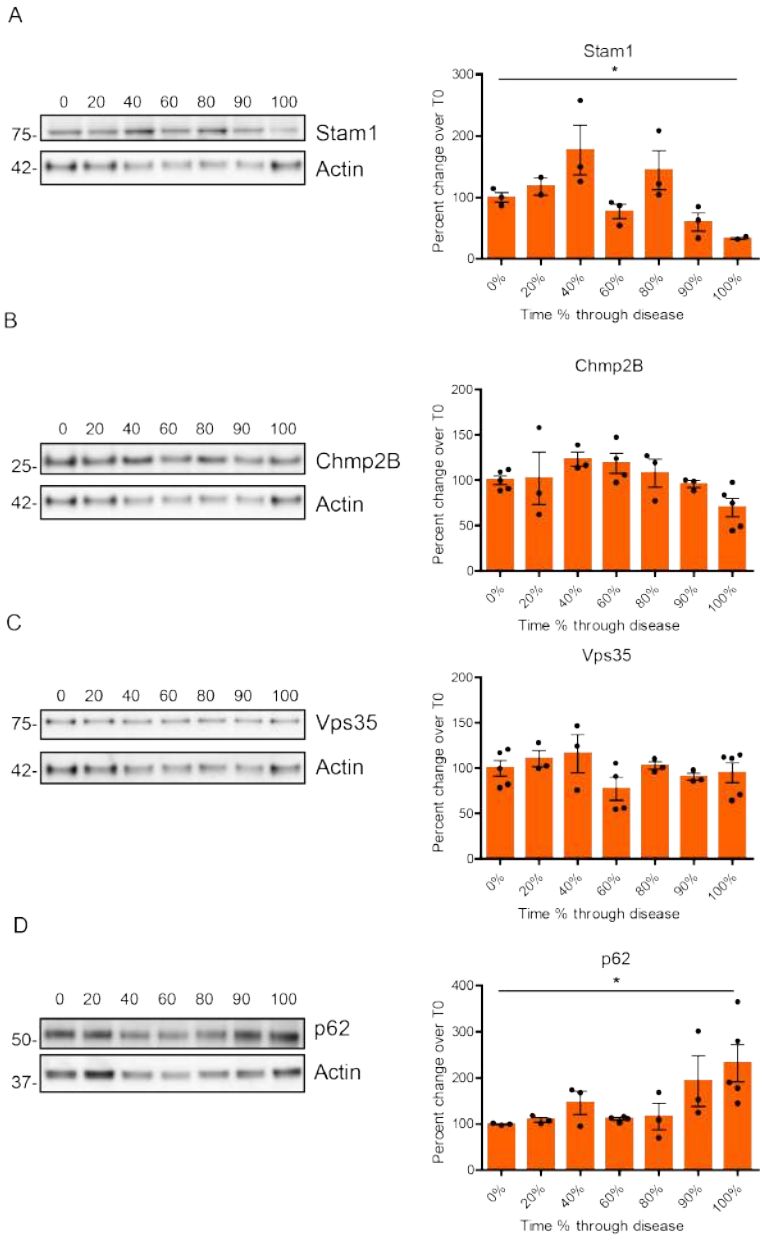

Figure 4.9: Loss of ESCRT-0 at terminal prion disease coincides with an increase in p62. (A-E) Total brain homogenates from n=3-5 mice at seven different time points, inoculated with 22L prion-infected brain, were analyzed by immunoblot. Western blots of the total brain homogenate at each time point, and graphs show proteins quantified against actin and normalized to the 0% control of (A) Stam1, (B) Chmp2B, (C) Vps35 and (D) p62. A one-way Anova was performed on each set of data, followed by Tukey multiple comparison test. *$p<0.05$, **$p<.01$.

Chapter 5

Cellular pathways involved in prion spread

Prion diseases are infectious neurodegenerative diseases caused by the misfolding of the cellular prion protein, PrP^{C}, into PrP^{Sc}. Prions only cause disease upon entering the Central Nervous System and spreading throughout the brain, resulting in neuron loss, spongiform change, and gliosis. Yet, the cellular pathways involved in prion propagation and spread remain unclear. PrP^{C} is GPI-anchored on the extracellular leaflet of the cell membrane and trafficked all throughout the cell, providing a multitude of potential pathways involved in spread and conversion. Here, we further analyzed the role of the endolysosomal pathway in prion conversion, as previous studies suggest certain subcellular compartments are necessary for prion conversion. We depleted specific components involved in endosome trafficking: Hrs, Rab11a, Vps35, and Rab27a, and validated that depletion of Hrs results in a decrease of PrP^{Sc} in prion-infected neuroblastoma cells while depletion of Vps35 causes an increase of PrP^{Sc} conversion. Further-

more, we substantiated the potential for extracellular vesicles as a mechanism of prion spread in the brain, and surprisingly found an increase in extracellular vesicle release from neurons upon depletion of Hrs. These findings have illustrated the importance of the endolysosomal pathway and extracellular vesicles in prion propagation and spread.

5.1 Introduction

Neurodegenerative diseases are characterized by the accumulation of misfolded protein aggregates, such as α-synuclein, amyloid-β, and prions in Parkinson's disease, Alzheimer's disease and prion disease, respectively. Aggregates accumulate in the brain, contributing to synapse loss, gliosis, and neuronal death, but the cellular pathways involved in protein aggregate spread remain unclear. In this study, we interrogate the role of the endolysosomal pathway in prion propagation and conversion.

Prion aggregates are internalized from the extracellular space via macropinocytosis and enter the endolysosomal pathway (ELP) (Goold et al., 2013). Endosomes can be sorted through the retromer pathway to the Golgi apparatus, through the recycling endosome pathway for return to the cell surface, or into multivesicular bodies (MVBs). Vps35 is an important component of the retromer complex, and manipulation of the retromer complex impacts PrP^{Sc} levels (Yamasaki et al., 2018; Yim et al., 2015). Rab11a is a component of recycling endosomes and has also been identified as a key player in autophagy (Grimsey et al., 2016; Kuroki et al., 2018; Li et al., 2019; Puri et al., 2018; Vicinanza et al., 2019). The multivesicular body has been identified as a site of prion conversion (Yim et al., 2015) and is generated by the ESCRT pathway (endosomal sorting complexes required for transport). Manipulating these components of the ELP are necessary for furthering our understanding prion conversion.

The importance of the ESCRT pathway in endosomal sorting has been well-characterized, as it is a pathway highly conserved in eukaryotes, but its role in protein aggregation in the brain remains poorly understood. The ESCRT pathway sorts endosomal proteins into MVBs, the contents of which are then either degraded in lysosomes or released extracellularly in exosomes by Rab27a and Rab27b (Bache et al., 2003; Ostrowski et al., 2010). Four complexes, 0, I, II, and III, function sequentially to sort and package endosomal proteins into MVBs (Katzmann et al., 2001). While there is still controversy as to where cellular PrP conversion occurs, two separate studies conclude that depleting components of ESCRT-0 reduces PrP^{Sc} conversion in prion-infected neuroblastoma cells (Vilette et al., 2015; Yim et al., 2015), suggesting that prion conversion could occur in MVBs. Additionally, when Hrs, a component of ESCRT-0, is knocked down in cells, exosomal production is severely impaired (Vilette et al., 2015), supporting that PrP^{Sc} transits through MVBs.

Prions have been isolated from exosomes derived from infected Mov cells, PrP-expressing RK13 cells, N2a cells, and GT1-7 cells (Fevrier et al., 2004; Guo et al., 2015; Vella et al., 2007; Vilette et al., 2015). Exosomes containing infectious prions have also been isolated from the serum of infected hamsters (Properzi et al., 2015). Additionally, protein aggregates from other neurodegenerative diseases have been isolated from exosomes, such as α-synuclein in Parkinson's disease (Hasegawa et al., 2011), amyloid-β in Alzheimer's disease (Perez-Gonzalez et al., 2012), and tau in many experimental mouse models of tauopathies (Saman et al., 2012). Vilette and colleagues have shown that knocking down Hrs in the Mov neuroglial cell line reduces prion spread between cells (Vilette et al., 2015). These experiments suggest an important role for Hrs in prion spread, but Hrs and additional ELP proteins need to be further examined in additional cell types and in vivo to understand where prion conversion

occurs.

Here, we manipulate ELP components by knocking down Hrs, Rab27a, Vps35, and Rab11a, overexpressing Hrs, and transfecting a dominant-negative mutant form of ESCRT-III component Vps4a in prion-infected neuroblastoma (N2a) cells to identify how different subcellular locations contribute to prion conversion. We found that depletion of Hrs results in a decrease of PrP^{Sc} in these cells, but not due to an increase in autophagic degradation or decreased spread through exosomes, as previously hypothesized. Our findings support the importance of PrP^{Sc} internalization into MVBs for prion conversion to occur and highlight exosomes as a potential mechanism of prion spread.

5.2 Results and Discussion

Depletion of endolysosomal pathway components has opposing effects prion conversion

In order to further determine how the endolysosomal (ELP) pathway contributes to prion propagation, we manipulated ELP components in 22L prion-infected neuroblastoma cells. We used silencing RNA to reduce protein levels of Rab11a, an endosome sorting protein, Vps35, a retromer complex protein, Rab27a, a protein involved in release of exosomes, and Hrs, the first component of the ESCRT pathway. Previously, reducing Hrs protein levels has been shown by two groups to cause a decrease in PrP^{Sc} levels in immortalized cells, as we observed by two different Hrs siRNAs (Fig. 5-1a,b). Conversely, reducing levels of Vps35, a component of the retromer complex, resulted in an increase in PrP^{Sc} levels (Fig. 5-1c,d). Yet reducing Rab11a and Rab27a had no effects on PrP^{Sc} levels (Fig 5-1c,d).

We considered that reducing components of the ELP could alter the levels of total PrP^C, and thereby affect levels of PrP^{Sc}, so we next analyzed PrP^C levels in uninfected N2a cells. Interestingly, we saw no reduction in PrP^C levels when Hrs was reduced in N2a cells (Fig. 5-1e). Yet when either Vps35 or Rab11a was decreased, we observed a significant increase in PrP^C levels (Fig. 5-1e), even though only Vps35 reduction resulted in an increase in PrP^{Sc} levels. Finally, we observed no changes to PrP^C levels when Rab27a was depleted (Fig. 5-1e). Our studies suggest that different areas of the ELP have varying roles in PrP^{Sc} conversion and emphasize the importance of internalizing prions into MVBs for prion conversion.

Hrs depletion blocks autophagosome maturation

We considered that Hrs depletion was resulting in an increase in autophagic flux, as evident by the increase in p62, and therefore an increase in PrP^{Sc} degradation, a hypothesis that Lois Green had also proposed [3]. On the contrary, Tamai and colleagues have proposed that Hrs depletion impairs autophagosome maturation [20]. We found that depletion of Hrs in N2a cells resulted in an increase of p62 protein, a marker for autophagosomes (Fig.5-2a). Interestingly, depletion of Rab27a also caused an increase of p62, but not Rab11a or Vps35 (Fig. 5-2a). However, the increase in p62 levels could be from increased or impaired autophagic flux.

To measure autophagic flux in Hrs-depleted cells, we transfected cells with an LC3-mCherry-GFP plasmid, which expressed both mCherry and pH sensitive GFP on the autophagosome; only mCherry is visible when the autophagosomes mature to lysosomes. We found significantly more autophagosomes than autolysosomes in Hrs-depleted cells, suggesting that Hrs depletion cause a block in autophagosome maturation, not an increase in autophagic flux (Fig.

5-2b). Our results suggest that the decrease in PrP^{Sc} caused by Hrs depletion was not due to an increase in autophagic degradation or to a decrease in PrP^{C}, but to a lack of prion internalization into MVBs.

Hrs overexpression does not affect PrP^{Sc} levels

While decreased Hrs reduces PrP^{Sc} levels in prion-infected cells, therefore we next tested how Hrs overexpression would affect PrP^{Sc} levels. Surprisingly, with a 6-fold increase in Hrs in prion-infected N2a cells over two days (Fig. 5-3b), we saw no impact on PrP^{Sc} levels (Fig. 5-3a).

To next determine how ESCRT-III impacts PrP^{Sc} levels, we transfected cells with the dominant-negative mutant $Vps4a^{E228Q}$, which prevents the MVB formation. We predicted that if MVBs were important for prion conversion, that expression of $Vps4a^{E228Q}$ would negatively impact prion conversion. Transfection efficiency was visualized by GFP fluorescence (Fig. 5-3d). Yet we saw no impact on PrP^{Sc} levels (Fig. 5-3a). We potentially could have seen an impact with higher transfection efficiency after a longer time, but overexpressing Hrs or a dominant negative Vps4a had no obvious effect on PrP^{Sc} levels. Additionally, neither of these transfections had any impact on PrP^{C} levels (Fig. 5-3b).

Given that the ESCRT pathway directly sorts ubiquitinated proteins into MVBs, we were expected that ubiquitinated protein levels would be impacted from altering the ESCRT pathway. We observed a massive accumulation of ubiquitinated proteins with Hrs overexpression (Fig. 5-3c), suggesting that overexpression of Hrs dysregulates ubiquitinated protein clearance. $Vps4a^{E228Q}$ also caused an accumulation of ubiquitinated proteins (Fig. 5-3c), potentially due to lack of MVB formation. Taken together, short term transfection of Hrs or $Vps4a^{E228Q}$ had little

impact on PrP^{Sc} and PrP^{C}, while rapidly increased ubiquitinated protein levels.

Exosomes are a potential mechanism of prion spread in the brain

Hrs is important for exosome generation. We considered that Hrs depletion could prevent the spread of prions through exosomes, decreasing prion propagation. To first determine whether EVs harbor prions, EVs were isolated from media of uninfected and prion-infected N2a (neuroblastoma) cells by differential centrifugation. EVs were enriched for the exosomal proteins CD63, Tsg101, and PrP^{C} (Fig. 4a) and compared to cell lysate. Further, exosomes isolated from prion-infected cells contained infectious prions (Fig. 5-4a), as observed by proteinase K digestion. To visualize and confirm exosomes were present, the exosomal preparation was imaged using electron microscopy (Fig. 5-4b), revealing the characteristic 50-150 nm vesicles.

To validate that PrP^{Sc} was within the EVs and not simply naked PrP^{Sc} aggregates, EVs were purified from cells not expressing PrP^{C} (RK13 cells) by ultracentrifugation over a 20% OptiPrep™ cushion. First, partially purified prions were added to exosomes suspended in PBS overlying the cushion and centrifuged at 100,000g. The PrP^{Sc} was localized to the Optiprep^{TM} fraction or the pellet (Fig. 5-4c). However, pure exosomes, and no PrP^{Sc}, were recovered from the interface of the Optiprep™ and PBS (Fig. 5-4c), indicating that exosomes could be readily separated from naked PrP^{Sc} aggregates. This was compared to a 100,000g spin in PBS in tube 1, where both the exosomes and PrP^{Sc} were pelleted.

Additionally, we have isolated EVs from primary neuron cultures (Fig. 5-4d) and from the brain of mice (Fig. 5-4e). Validating the presence of PrP^{Sc} in exosomes, as well as the abundance of exosomes released by neural cells, has led to our hypothesis that exosomes are a major mechanism of prion spread through the CNS, and we considered that Hrs depletion

could prevent the spread of prions through exosomes and thereby decrease prion propagation.

Hrs depletion in primary neurons increases EVs

The ESCRT pathway is important for exosome generation, and we considered that Hrs depletion could be reducing the spread of prions by reducing exosome generation. We next investigated how Hrs depletion in primary neurons affected extracellular vesicle release. We transduced *Hgs*$^{f/f}$ neurons with Cre-lentivirus to deplete Hrs. We collected the media after a week and precipitated extracellular vesicles using ExoQuickTM. Interestingly, we found an increase in extracellular vesicle (EV) proteins (Tsg101, PrP, and Alix) in Hrs-depleted neuron media (Fig. 5-5a).

To determine whether Hrs depletion could be causing a difference in size of EVs, suggesting that there may be increased vesicles produced from the cell membrane, we performed a more rigorous isolation of EVs using a sucrose gradient to be visualized by transmission electron microscopy (Fig. 5-5b). We quantified the sizes of the EVs by electron microscopy but found no differences between the EVs from Hrs-depleted neurons and control neurons. We found this data to be quite surprising, given the role of Hrs in exosome production. We concluded that the depletion of Hrs could result in a compensatory increase in EV generation, and that the decrease in PrP^{Sc} levels with Hrs depletion was not unlikely to be due to a decrease in spread through EVs, but was instead due to lack of internalization into MVBs to promote conversion.

Discussion

Our studies confirm that internalization of PrP^{Sc} into MVBs is important for prion conversion and show, for the first time, that a decrease in PrP^{Sc} upon Hrs depletion is not due to an

increase in autophagic degradation or a decrease in extracellular vesicle spread, as previous hypothesized.

The location of prion conversion has long been debated, but our studies suggest that prion conversion occurs within the cell, specifically within the MVB. Our data contradicts the idea that upon interaction at the cell membrane with PrP^{C}, PrP^{Sc} conversion occurs (Goold et al., 2011). We found that when recycling proteins Vps35 or Rab11a (Grimsey et al., 2016; Kuroki et al., 2018) were knocked down, which would be expected to increase surface PrP^{C} levels, we observed an increase (Vps35) or no change (Rab11a) in PrP^{Sc} levels, supporting the hypothesis that MVBs are a major site of prion conversion.

Rab27a is necessary for fusion of the MVB with the plasma membrane to release exosomes, and reducing Rab27a prevents exosome release and results in enlarged MVBs (Bobrie et al., 2012; Fukuda, 2013; Iguchi et al., 2016; Ostrowski et al., 2010; Pfeffer, 2010). If prion spread is reduced by a decrease in exosome spread, we would expect to see less PrP^{Sc} propagating in N2a cells with reduction in Rab27a. However, if the MVB was the major site of prion conversion, knock down of Rab27a, causing an enlargement of MVBs, would enhance prion conversion. We observed no differences in PrP^{Sc} levels when Rab27a was depleted, perhaps due to the opposing effects on prion conversion (enlarged MVBs) and spread (reduced exosomes). Our Rab27a data further supports the hypothesis that prions replicate in MVBs, but the role of exosomes in prion spread remains unclear.

Exosomes are a proposed mechanism of protein aggregate spread throughout the brain. Our data supports that prions are found within exosomes isolated from cells (Fevrier et al., 2004; Guo et al., 2015; Vella et al., 2007; Vilette et al., 2015). Additionally, exosomes are a likely to occur as communication between neurons and throughout the brain, based on our data

and previous research (Vella et al., 2017). However, how prions are packaged into exosomes and the major pathways underlying exosomal spread of prions remain unknown. Studies are inconsistent in deciding the exosome generation pathway essential for prion packaging into exosomes, which is further confounded by the lack of basic understanding of the generation of exosomes (Cocucci and Meldolesi, 2015; Coleman et al., 2012; Guo et al., 2015; Guo et al., 2016). We hypothesized that Hrs depletion would lead to a decrease in exosome production, but instead we observed an increase in the amount of extracellular EV proteins, while quantifying no differences in EV size. Perhaps the lack of MVB formation caused overactive alternative exosome generating pathways or stress on the cell by Hrs depletion caused compensatory EV release.

Additionally, understanding the role of autophagy in exosome production has led to conflicting results. We observed that Hrs depletion blocked autophagy, which consequentially led to an increase in EVs. One study recently published that activation of autophagy through mTORC1 inhibition or rapamycin causes an increase in EV release and production (Zou et al., 2019). Conversely, another study published that rapamycin caused a decrease in EV release, and by blocking EV release through Rab27a knockdown, autophagy is activated (Oshima et al., 2019). While these studies used different exosome isolation protocols and cell types, they highlight the vast inconsistencies in the exosome field. Exosomes are an exciting prospect in diagnostics, therapeutics, and understanding of neurodegenerative diseases. While we were unable to determine if exosomes were the primary mechanism of spread, they are likely one mechanism of prion spread. The many components of the endolysosomal pathway provide such unique roles in prion propagation and examining them in disease states provide further understanding of their basic biology. Like exosomes, more research is necessary to understand their contribution to

disease and potentials as therapeutic targets.

5.3 Materials and Methods

N2a culture

Uninfected and 22L-prion infected N2a (neuroblastoma cells) were gifted from Byron Caughey. Cells were maintained in OptiMEM medium supplemented with 10% fetal bovine serum (FBS), 100U/mL penicillin and 100ug/mL streptomycin (all Gibco) and maintained at 37 C in a humidified incubator with 5% CO2.

Western blot analysis

To quantify the relative immunoblot signal intensities, images were acquired using a chemiluminescent substrate (Supersignal West Dura ECL, ThermoFisher Scientific) and visualized on a Fuji LAS 4000 imager. The chemiluminescent signals were captured and quantified using the Fuji LAS 4000 imager and Multigauge V3.0 software.

Antibodies for western blots

The following antibodies were used for western blotting. Mouse anti-PrP (1:10,000, POM19, amino acids 201–225 (Polymenidou et al., 2008), a kind gift from Dr. Adriano Aguzzi); mouse anti-PrP Pom1 (1:10,000); anti-Hrs (1:5000, Cell Signaling Technology); anti-β actin (1:5000, Genetex); anti-Tsg101 (1:1000, Genetex); Ubiquitin (1:7000, Dako); Rab11a (1:1000, Cell Signaling Technology); anti-Vps35 (1:10,000, Genetex); anti-CD63 (1:300, Santa Cruz Biotechnologies); anti-p62 (1:4000, Abnova).

siRNA protocol

N2a cells were plated in a 24-well plate at 150K cells per well and transfected the next day using RNAiMax (ThermoFisher, 13778100) with siRNA (Hrs-1 s67515, Hrs-2 s67516, Vps35 s82381, Rab27a s201063, Rab 11a s79313; Life technologies 4390771) or NS siRNA (Life technologies, 4390843 Neg Control-1) on days 1 and day 4. On day 6, they were expanded to a 12-well plate and collected on day 7 in PBS, pelleted, and resuspended in lysis buffer (50mM Tris-HCl pH 8.0, 150mM NaCl, 0.5% Na Deoxycholate, 1% NP-40, 0.1% SDS). To quantify protein levels in cell lysates, PierceTM BCA protein assay (Thermo Scientific, 23225) was performed.

Hrs/Vps4a transfection

Plasmids were purchased from Addgene (Hrs 39101, Vps4a^{E228Q} 80351). N2a cells were plated at 200K cells per well in a 12-well plate. The next day, cells were transfected using Lipofectamine 3000 kit (Life Technologies). After 24 hours, cells were collected in PBS, pelleted, and resuspended in lysis buffer (50mM Tris-HCl pH 8.0, 150mM NaCl, 0.5% Na Deoxycholate, 1% NP-40, 0.1% SDS). To quantify protein levels in cell lysates, PierceTM BCA protein assay (Thermo Scientific, 23225) was performed.

PrP^{Sc} analysis in N2a cells

To analyze PrP^{Sc}, cell lysates were Proteinase K digested (10ug/mL final concentration) at equal concentrations of protein (50-100μg depending on the experiment) for 30 min at 37°C. We then added 4X LDS and heat inactivated at 95°C for 5 min. To analyze protein levels (Hrs, Rab11a, Vps35, Rab27a, p62, Ubiquitin, and PrP^{C}), 10μg of cell lysate was diluted into 20μL

of lysis buffer, and 8μL of 4X LDS was added before boiling lysates at 95C. Lysates were then loaded onto a gel and subjected to western blot analysis.

LC3-mCherry-GFP assays

N2a cells were cultured in a 24 well dish on 12mm round coverslips (not Carolina biologics) were transduced with the LC3-mCherry-GFP lentivirus along with the Cre-lentivirus or Control-Lentivirus. Cells were fixed with 4% paraformaldehyde (PFA) (Fisher Scientific, J19943K2) and incubated in PFA for 20 min at RT. Cells were washed 4x5 min, with a 5-minute DAPI (Sigma-Aldrich, D9542) incubation during the second wash. Coverslips were mounted onto ProLongTM Gold Mountant (Invitrogen, P36941) and sealed with nail polish.

Exosome isolation by differential centrifugation

N2a cells were cultured for 3 days prior to media collection in 2x75cm2 flask in exosome-free media. 32 mLs of media was centrifuged at 2000 g for 10 min. Supernatant was then centrifuged at 10,000 g for 30 min at 4 °C. Exosomes in the supernatant were ultracentrifuged at 100,000 g for 70 min at 4 °C. Pellets were resuspended in RIPA lysis buffer or PBS for western blot analysis or TEM analysis, respectively. For PrP^{Sc} analysis in isolated exosomes, a BCA was used to quantify protein levels, and 100ug of exosome isolation was subject to proteinase K digestion for 30 min at 37°C, before adding 4X LDS and heating to 95°C to be analyzed by western blot.

Exosome isolation with PrP spike

100 mLs of media from RK13 cells was collected and subject to exosome isolation by differential centrifugation. Pellet was resuspended in 1mL of PBS. In tube 1, 500μL of exosomes was added to the tube and filled to 2mLs with PBS. In tube 2, 500μL of 20% OptiprepTM was added, followed by 500μL of exosomes in PBS, filled to 2mLs with PBS. In both tubes, 50μL of partially purified prions was added before ultracentrifugation occurred at 100,000 g for 2 hours at 4 °C. For tube 1, only the pellet was resuspended. For 2 tube, the interface of OptiprepTM and PBS was collected, as that was where the exosomes were thought to be, the OptiprepTM fraction, and the pellet at the bottom of the tube were saved and resuspended in PBS, then centrifuged at 100,000 g for 1 hour at 4 °C. All pellets were then resuspended in PBS and analyzed by western blots by loading equal volumes of the resuspended pellets.

Brain exosome isolation

Isolation of exosomes from mouse brains was adapted from Perez-Gonzalaz et al., 2012. In brief, Brains were dissected, and the cerebellum and olfactory bulbs were removed. These tissues were gently chopped before being incubated in 2 ml of 20 units/ml papain (LS003119, Worthington) in Neuronal Basal Media for 20 min at 37 °C. The reaction was stopped with 8 ml of ice-cold Hibernate-A containing 1 Complete protease inhibitor mixture (Complete MINI TM). The tissue was gently disrupted by pipetting with a 10-ml pipette, followed by a series of differential 4 °C centrifugations at 300 g for 10 min, take supernatant; 2000 g for 10 min, take supernatant; 10,000 g for 30 min to discard pellets containing cells, membranes, and nanodebris, respectively. The supernatant from the 10,000 g centrifugation step was passed through a 0.22-μm syringe filter (Millex-GP, Millipore) and centrifuged at 100,000 g for 70 min at 4 °C to pellet exosome-

like EVs. The EV pellet was then resuspended in 2 ml of ice-cold PBS (17-516Q, Lonza), and the EV solution was centrifuged at 100,000 g for 70 min at 4 °C. The washed EV pellet was resuspended in 1.3 ml of 0.95 M sucrose in 20 mM HEPES (15630-080, Life Technologies) and then inserted into a sucrose step gradient column (six 1.3-ml steps from bottom 2.0, 1.65, 1.3, 0.95, 0.6, and 0.25 M on top). The sucrose step gradient was centrifuged at 200,000 g for 16 h at 4 °C. The original six 1.3-ml fractions were collected and resuspended in 6 ml of ice-cold PBS, followed by a 100,000 g centrifugation for 70 min at 4°C.

EM of exosomes

10μL of exosomes isolated in PBS were added to 100-window carbon-coated copper grids for 5 min. Grids were washed 3 times water. Grids were then mounted onto uranyl acetate for 1 minute, and then removed to dry. Grids were viewed using a JEOL 1200EX II (JEOL, Peabody, MA) transmission electron microscope and photographed using a Gatan digital camera (Gatan, Pleasanton, CA).

Exoquick EV isolation

After 5 days in culture, neurons Control-lentivirus of Cre-lentivirus was added to Hrsf/f neurons to deplete Hrs. Media was collected after 1 week and centrifuged at 2000 g for 10 min. Supernatant was saved and centrifuged at 10,000 g for 10 min. Exoquick-TC (Life technologies) was added to saved supernatant at 1:5 volume compared to supernatant, and incubated upright overnight at 4°C. The next day, media was centrifuged at 1500 g for 30 min at 4°C. Supernatant was removed and thrown away, pellet was centrifuged again for 5 min at 1500 g and 4°C. All supernatant was removed and pellet was resuspended in 2% sarcosyl before being analyzed

by western blots. Neurons were also collected in 2% sarcosyl, lysed for 30 min on ice, and centrifuged at 2000 g for 5 min to get rid of cellular debris. Equal volumes of cell lysates were loaded in the western blot to compared cell numbers between Hrs-depleted and control.

Iodixanol gradient exosome isolation

Exosomes were isolated as previously described (Zabeo et al., 2017). Conditioned media was harvested and centrifuged at 300 g for 10 min to remove cells. The supernatant was then centrifuged at 16,500 gavg for 20 min to remove apoptotic bodies and larger particles. Lastly, the supernatant was ultracentrifuged at 118,000 gavg (Type 45 Ti) for 3.5 h and the resulting pellet was resuspended in phosphate buffered saline (PBS). To obtain a higher purity of EVs, an isopycnic centrifugation, using an iodixanol (OptiPrep, Sigma Aldrich, Saint Louis, USA) gradient, was conducted. EVs in PBS (1 ml) were mixed with 60% of iodixanol (3 ml) and laid on the bottom of an ultracentrifuge tube. A discontinuous iodixanol gradient (35, 30, 28, 26, 24, 22, 20%; 1 ml each, but 2 ml for 22%) in 0.25 M sucrose, 10 mM Tris, and 1 mM EDTA was overlaid and finally the tubes were filled to completion with approximately 400 μ l of PBS. Samples were ultracentrifuged at 178,000 gavg (SW 41 Ti, k-factor 143.9, Beckman Coulter) for 16 h. Fractions (1 ml) were collected from the top to the bottom and subjected to Western blot analysis to identify EV markers. Mixture of fraction 2 and 3 were diluted with PBS (up to 94 ml) and ultrancetrifuged at 118,000 gavg (Type 45 Ti) for 3.5 h. The pelleted EVs were resuspended in PBS. Protein concentration was measured with the BCA protein assay kit (Thermo Fisher Scientific). EVs isolated by ultracentrifugation with density gradient was used for all the experiments in this study. Importantly, all experiments were done in sequence and EVs were never frozen.

Statistics

Data are presented as mean +/- SEM unless otherwise indicated with group differences tested using standard parametric methods (Student's t test, 2-tailed). P values of less than 0.05 were considered statistically significant.

5.4 Acknowledgements

The authors thank Xu Chen for her LC3-mCherry-GFP and Cre lentivirus constructs. We thank Timo Meerloo and Vanessa Goodwin for help with the electron microscopy of exosomes. We thank Dr. Andrew Hill for his insight into exosome isolation, especially from brain tissue. J.A.L. is supported by a Ruth L. Kirschstein Institutional National Research Award from the National Institutes of Health, NINDS F31NS103588.

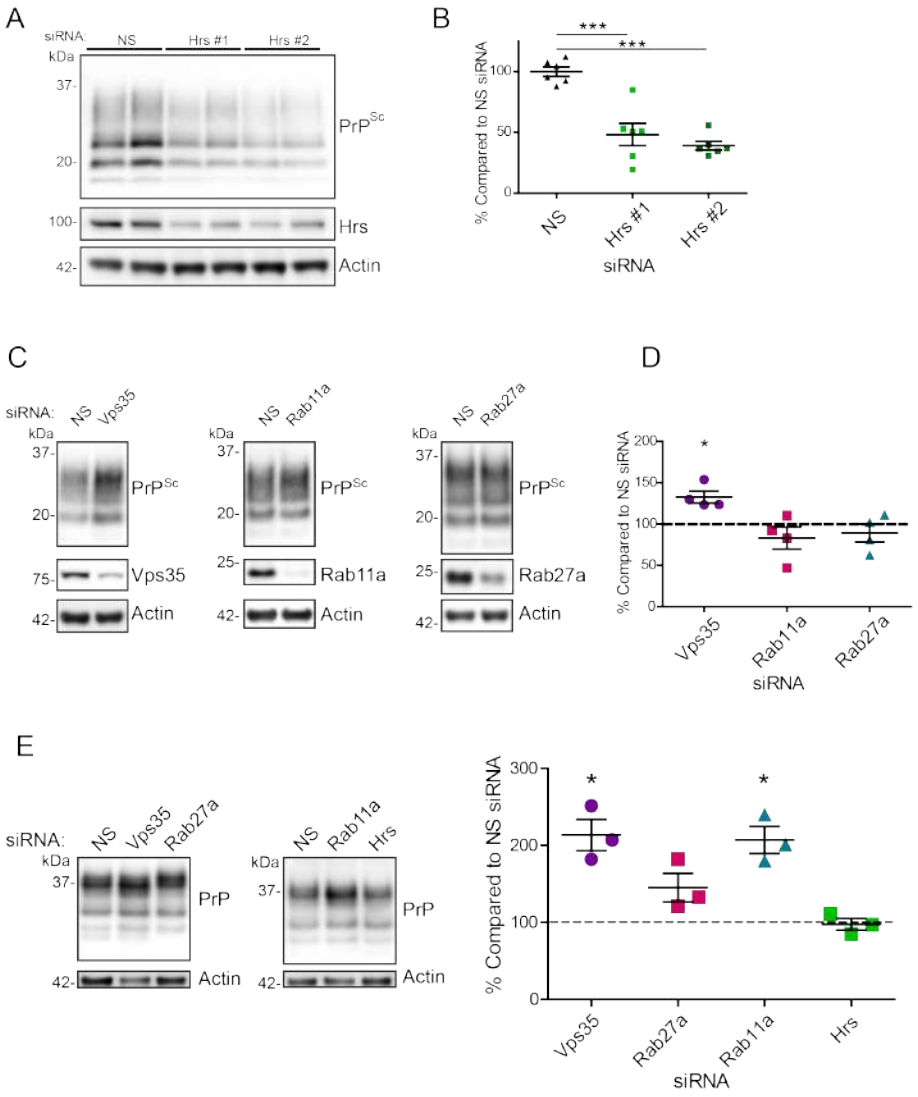

Figure 5.1: Depletion of Hrs reduces prion levels in prion-infected neuroblastoma cells. (A-B) Hrs depletion by siRNA shown by western blot consequentially reduces PrP^{Sc} levels measured in cell lysates by proteinase K digestion (A). Western blots were quantified in (B). Actin was used as a loading control. n=3 experiments in technical duplicate. ***$p<<0.001$, student t test. (C-D) The effect of knocking down Vps35, Rab11a, and Rab27a on PrP^{Sc} levels in prion-infected N2a cells is shown by western blot where cell lysates were digested with Proteinase K (C) and quantified (D). Actin was used as a loading control. n=4 experiments. *$p<0.05$, One sample t test. (E) Western blots of total PrP^{C} in uninfected N2a cells transfected with nonspecific (NS), Vps35, Rab27a, Rab11a, or Hrs siRNA reveal increased PrP^{C} levels with reduction of Vps35 or Rab11a. Actin was used as a loading control. n=3 experiments. *$p<0.05$, One sample t test.

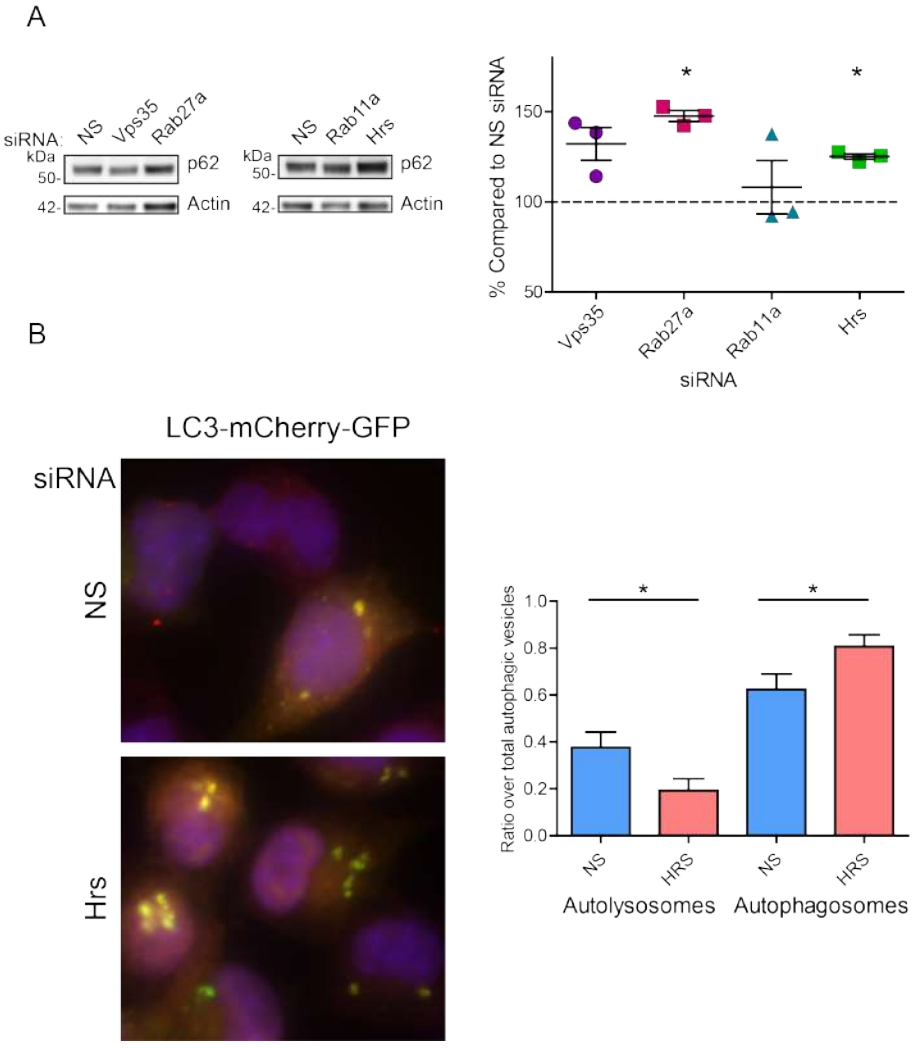

Figure 5.2: Hrs depletion impairs autophagosome maturation. (A) Western blots of p62 levels in uninfected N2a cells transfected with nonspecific (NS), Vps35, Rab27a, Rab11a, or Hrs siRNA reveal increased p62 levels with reduction of Rab27a or Hrs. Actin was used as a loading control. n=3 experiments. *$p<0.05$, One sample t test. (B) Hrs depleted N2a cells were transfected with an LC3-mCherry-GFP plasmind. When bound to autophagosomes, both GFP and mCherry fluoresce, appearing yellow. When the autophagosome matures to a lysosome, GFP no longer fluoresces, resulting in red puncta. Yellow puncta (autophagosomes) and red puncta (autolysosomes) were quantified in each cell. Quantification reveals a significant decrease in the ratio of autolysosomes to autophagosomes when Hrs is depleted in N2a cells. n=50 cells. *$p<0.05$, Student's t test.

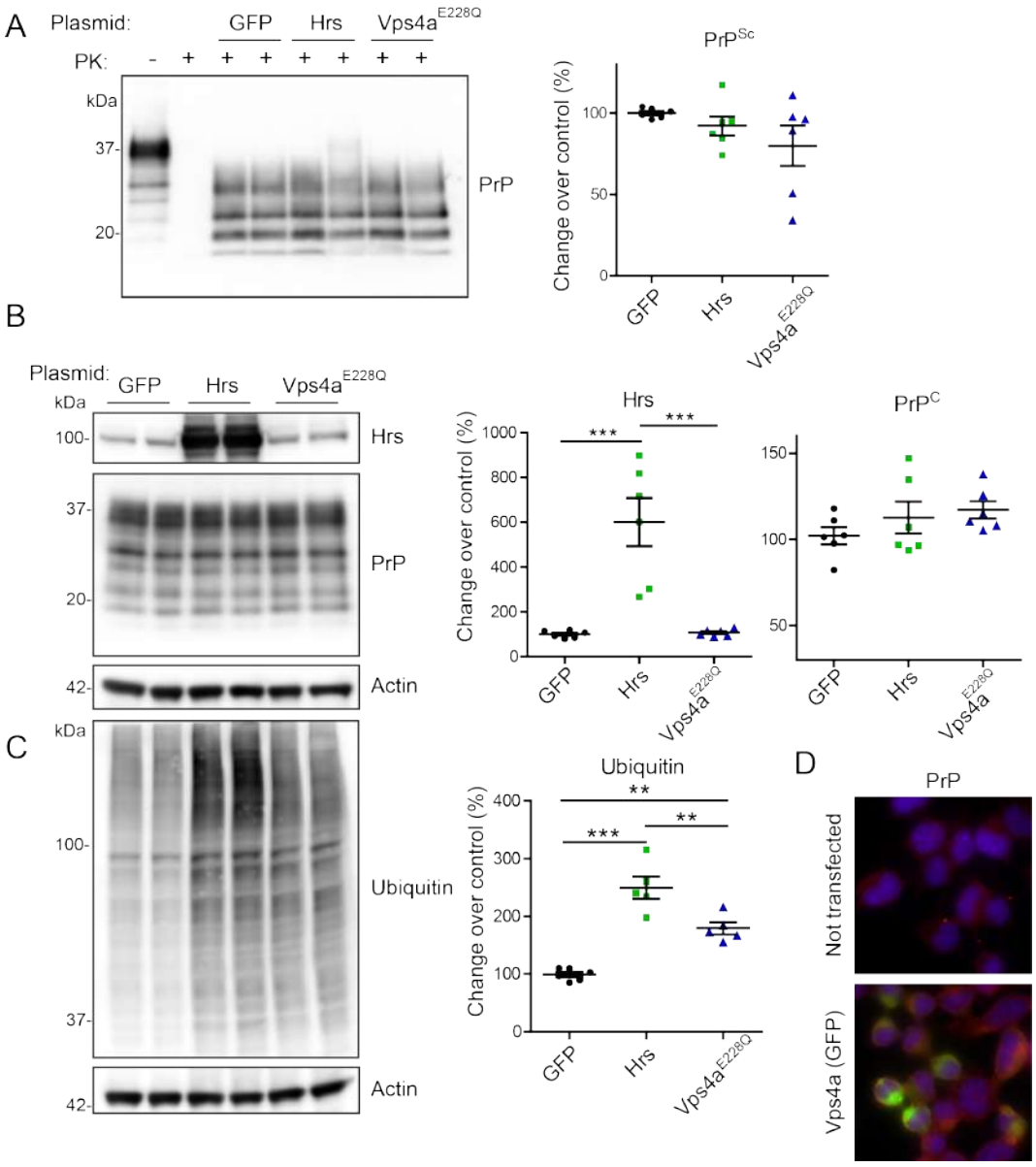

Figure 5.3: Hrs overexpression or dominant negative Vps4a has no impact on PrP^{Sc} levels. (A) Transfection of the plasmids Hrs, GFP, or Vps4a^{E228Q} into prion-infected N2a cells had no effect on PrP^{Sc} levels measured in cell lysates by proteinase K digestion and quantified by western blot. n=3 experiments in technical duplicate. No significance, student t test. (B) Western blots of Hrs and PrP^{C} levels in N2a cells transfected with either Hrs, GFP, or Vps4a^{E228Q} and quantified. n=3 experiments in technical duplicate. ***p$<<$0.001, One-way ANOVA, followed by Tukey multiple comparison test. (C) Western blots of ubiquitinated protein levels in N2a cells transfected with either Hrs, GFP, or Vps4a^{E228Q} and quantified. n=3 experiments in technical duplicate. ***p$<<$0.001, One-way ANOVA, followed by Tukey multiple comparison test. (D) Fluorescent images reveal the low transfection efficiency of Vps4a plasmid tagged with GFP compared to not transfected cells, both stained for PrP (Cy3).

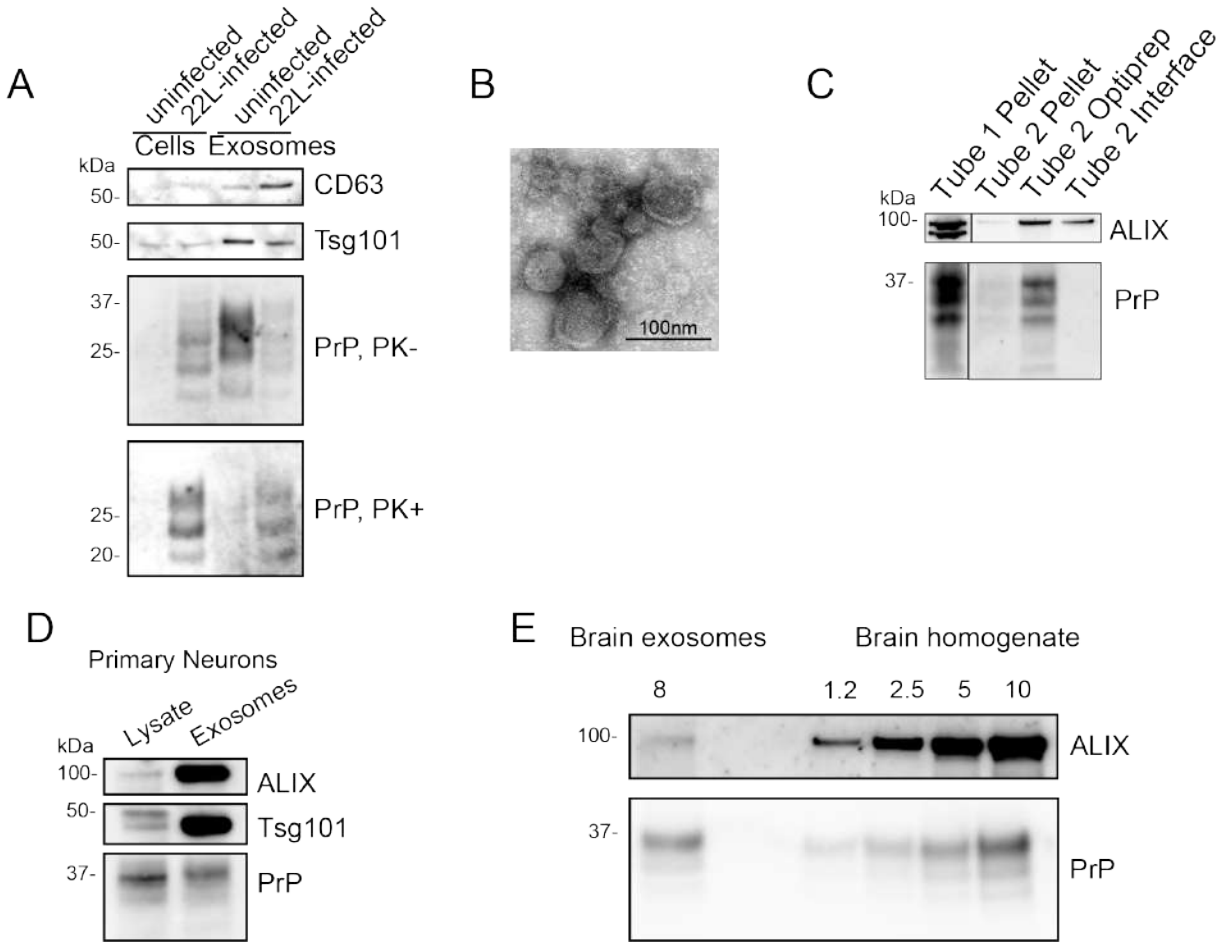

Figure 5.4: Exosomes are a justifiable mechanism of prion spread in the brain. (A) Western blots reveal exosomal markers CD63 and Tsg101 are enriched in exosomes isolated from the media compared to cell lysate of both uninfected and 22L-infected cell lines (lanes 3 & 4). Western blots of PrP and proteinase K (PK) digested PrP shows PrP^{Sc} is contained in exosomes of 22L-infected cells. (B) Transmission electron microscopy of isolated exosomes. Scale bar = 100nm. (C) Western blots of exosomal markers ALIX and PrP^{C} from purification of exosomes from protein aggregates assay. Tube 1: 100,000g spin of exosomes with PrP^{Sc} in PBS only. Tube 2: Separation of PrP^{Sc} aggregates and exosomes by ultracentrifugation over a 20% Optiprep™ cushion. (D) Western blots of Exosomes isolated from primary neurons showing enrichment of exosome markers ALIX, Tsg101, and PrP compared to neuron lysate. (E) Western blots of exosome markers ALIX and PrP in brain homogenate and exosomes isolated from brain. Exosome protein concentration was compared to a curve of brain homogenate concentrations, in nanograms.

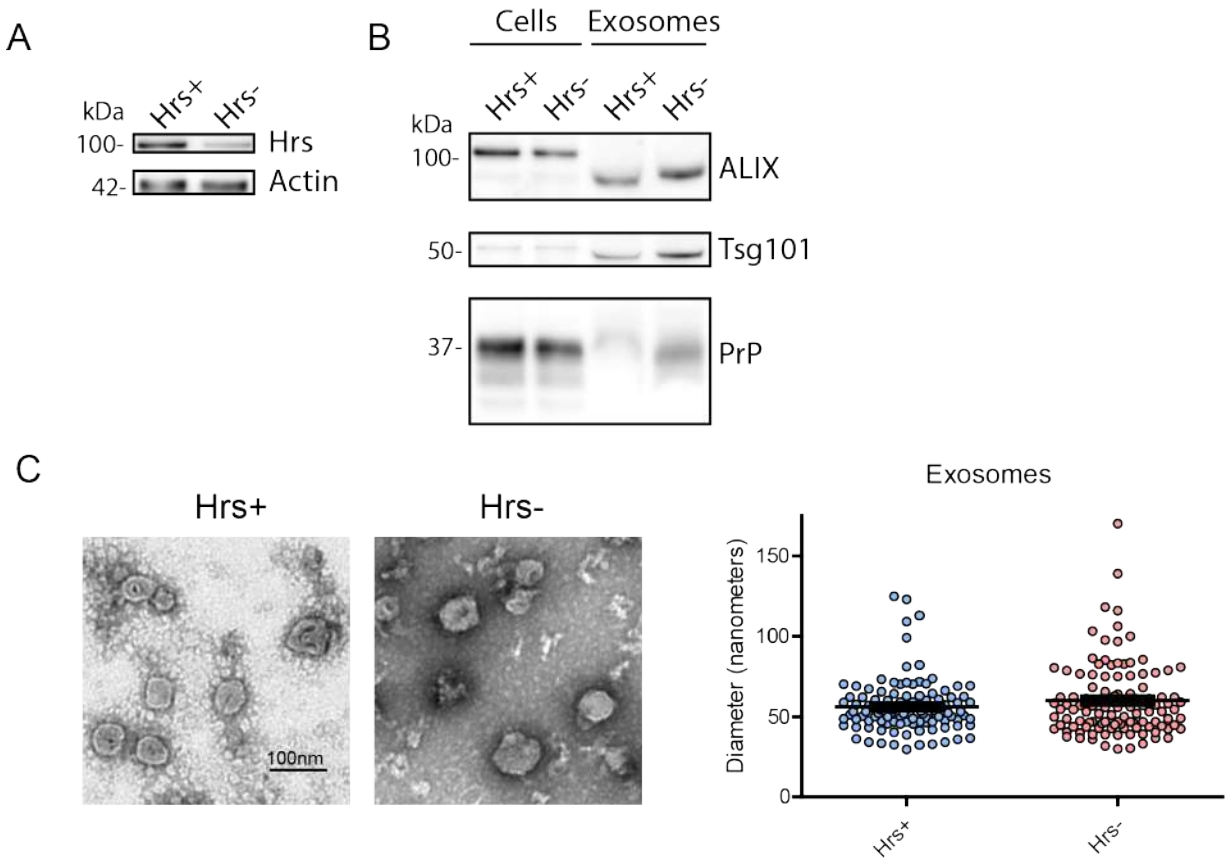

Figure 5.5: Hrs depletion does not decrease EVs released in primary neuron culture. (A) Western blots of Hrs levels compared to the loading control actin in Hrsf/f primary neurons transduced with Cre-lentivirus, resulting in either Hrs+ or Hrs- neurons. (B) Western blots of the crude exosome analysis by ExoQuic, revealing that Hrs depletion caused a slight increase in EV proteins ALIX, Tsg101, and PrP compared to the Hrs+ neuron media. Tsg101 was highly enriched in the EV fraction. Experiment was repeated 4 times, all with an increase in exosomal proteins in the Hrs- EV fraction. (C) Analysis of the size of exosomes by transmission electron microscopy reveals no difference in the average diameter of the EVs isolated from the media of Hrs+ or Hrs- neurons. Scale bar =100 nm. n=110. No significant difference, Student's t test.

Chapter 6

Conclusion

In conclusion, we have identified (i) properties of prion strains that enable prion neuroinvasion, (ii) pathways involved in prion spread, and (iii) novel mechanisms of prion toxicity. We have highlighted how detrimental soluble oligomers are in prion disease, as oligomers readily neuroinvade, likely through axonal transport, and rapidly cause disease. We have identified a crucial role for the ESCRT pathway in both prion disease and synapse health. Exciting new pathways involved in prion pathogenesis have been unearthed, such as the increase in Arc and the immediate early genes to prion infection. However, these discoveries have also unmasked additional questions, as much remains to be explored.

6.1 Properties of prion strains promoting neuroinvasion

Prion strains, while identical in amino acid sequence, have many differing biochemical properties that affect disease incubation time, brain lesions, and plaque morphology. Subfibrillar strains are efficient at replicating PrP^{Sc}, are non-congophilic, form diffuse aggregates in the

brain, and are unstable in denaturing conditions, contrary to fibrillar strains (Bett et al., 2012). Additionally, subfibrillar strains rapidly neuroinvade upon either intra-tongue (IT) or intravenous inoculation (IV), while fibrillar strains have reduced capacity to neuroinvade (Aguilar-Calvo et al., 2018; Bett et al., 2012; Bett et al., 2017). Here, we found that the solubility of prion strains differs between fibrillar and subfibrillar strains and were able to manipulate the solubility of one subfibrillar strain (87V) by sonication. This led to an increase in neuroinvasion of 87V by the IT route. Additionally, increasing the inoculum by 10-fold also increased neuroinvasive capacity of 87V. We hypothesize that the increase in neuroinvasion of 87V is due to the increase in soluble particles available to enter the CNS. Conversely, sonicating the fibrillar strain mCWD had no effect on solubility or neuroinvasion, and neither did increasing the concentration, suggesting mCWD is too conformationally stable and large to neuroinvade and be solubilized.

Supporting our conclusions from Chapter 2 is another study from our lab that examined the neuroinvasion of diverse prion strains from the IV route. The attack rate of neuroinvasion for all the subfibrillar strains was 100%, whereas the fibrillar strains were significantly lower (60% for 87V and 17% for mCWD). However, after further analysis, the mCWD prions that entered the brain after IV analysis had altered biochemical properties, resulting in a novel strain, again supporting that mCWD is too conformationally stable and large to neuroinvade and be solubilized. Our lab has also investigated the effects of post-translation modifications of PrP^C on plaque formation, finding that glycans on PrP^C prevent plaque formation, increase solubility, reduce heparan sulfate binding, accelerate spongiform changes and disease (Sevillano et al., 2020), highlighting that increasing the solubility of prion strains accelerates spread and disease.

Our studies implicate the lethality of small, soluble particles in misfolded protein aggregate diseases. The subfibrillar strains neuroinvade much more frequently and more rapidly, yet

do not form plaques in the brain, suggesting that plaques are not the biggest threat to neurodegenerative diseases, rather soluble oligomers are. Studies in Alzheimer's disease have also proposed soluble forms of Aβ to be much more toxic than the plaques formed in the brain (Ferreira and Klein, 2011; Funke, 2011; Lacor et al., 2004; Li and Selkoe, 2020; Price et al., 2014; Rijal Upadhaya et al., 2012). Therapeutics targeting soluble oligomers, rather than disassociating plaques in the brain, are what will prevent the toxicity of misfolded proteins.

6.2 Pathways involved in prion spread

We found that depletion of Hrs in neurons, astrocytes, or microglia did not noticeably affect prion conversion in vivo. Depleting components of the ESCRT pathway has previously been shown to reduce prion conversion in immortalized cells (Vilette et al., 2015; Yim et al., 2015). We show that in addition to Hrs reduction resulting in a decrease in PrP^{Sc} in N2a cells, depleting Hrs in primary neurons also results in a decrease in PrP^{Sc} levels. However, this decrease was not was due to an increase in autophagic degradation, as autophagic flux was impaired in both Hrs-depleted N2a cells and primary neurons.

As Hrs is involved in endosomal sorting, we examined how this could affect both localization and degradation of PrP^{C}. There were no differences in the total levels of PrP^{C}, confirming that we were not altering levels of substrate for prion conversion. However, we discovered an increase in PrP^{C} on the cell surface, suggesting that losing the function of the ESCRT pathway and endosomal sorting ultimately affects the levels of surface PrP^{C}. These results led us to believe that the lack of internalization of PrP^{C} and PrP^{Sc} contributed to the decrease in prion conversion, supported by previous studies identifying PrP^{Sc} within the endosomal pathways conversion (Borchelt et al., 1992). Additionally, we observed an increase in PrP^{Sc} levels upon

depletion of Vps35 in prion-infected N2a cells, a component of the retromer pathway that recycles PrP^{C} to the Golgi body and cell surface. Depletion of Vps35 also caused an increase in total levels of PrP^{C}, and presumably, more internalization of PrP^{Sc} into the MVB, further supporting the idea that the MVB is a major site of prion conversion.

Given that previous reports (Vilette et al., 2015; Yim et al., 2015), as well as our own data, concluded that Hrs depletion results in a decrease in PrP^{Sc} conversion in vitro, we were initially surprised that depletion of Hrs in neurons, astrocytes, or microglia did not noticeably affect prion conversion in vivo. The location of prion conversion remains highly controversial, with the field being equally uncertain whether prion conversion occurs intracellularly or on the cell membrane (Goold et al., 2011) (Borchelt et al., 1992), yet in vivo studies of prion conversion are scarce. One in vivo study showed reduced levels of muskelin (Heisler et al., 2018) resulted in increased exosomal and surface PrP^{C} levels. When inoculated with prion disease, muskelin-deficient mice had accelerated disease and increased PrP^{Sc} load, implicating the cell surface as the major site of prion conversion. When depleting Hrs in neurons, we also observed altered subcellular trafficking, resulting in an increase in surface PrP^{C}. Yet, contrary to this study, we did not see accelerated disease due to increased PrP^{Sc} load or increased ADAM-10 cleaved PrP^{Sc}. Taken together, these findings support the need to investigate prion conversion further in vivo. Additionally, glial cells are large contributors to prion propagation and could overshadow any decrease in neuron conversion.

This is not the first time that in vitro data has contradicted in vivo data. Recently, a study reported (Abdelaziz et al., 2019) that manipulating the autophagy pathway in vitro affected prion conversion but had no effects in vivo. While many studies have investigated sites of prion conversion in vitro (Abdelaziz et al., 2019; Beranger et al., 2002; Borchelt et al., 1992; Caughey

et al., 1991; Goold et al., 2013; Guo et al., 2016; Heiseke et al., 2009; Magalhaes et al., 2005; Marijanovic et al., 2009; Veith et al., 2009; Yim et al., 2015), conversion must be further investigated in vivo to be able to conclude the location of conversion.

6.3 Uncovering mechanisms of prion toxicity

In investigating cellular pathways contributing to prion spread, we also discovered novel mechanisms of prion toxicity. We found a loss of mGluR5 and synapsin-I in prion disease, coinciding with an increase in Arc and the immediate early genes, which was accelerated by depletion of ESCRT-0 in neurons. Arc activity can be induced by activation of mGluR5, causing an increase in internalization of synaptic receptors and long-term depression in neurons. Additionally, an increase in Arc is seen within 24 hours of primary neurons incubated with partially purified prions, again indicating activation of Arc activity by prion infection. As Arc induces endocytosis and degradation of receptors, a functional endolysosomal pathway is essential for synapse health. Our data supports the idea of an integrated role of the endolysosomal pathway and synapse health in prion disease. Furthermore, we observed an accumulation of ubiquitin inclusions early in prion disease, also accelerated by loss of ESCRT-0, implicating improper function of degradative pathways in the brain during prion disease. Prion disease has been shown to impair the function and localization, but not the levels, of Rab7 (Shim et al., 2016), posing another potential mechanism for how the endolysosomal pathway is dysfunctional during prion disease and contributes to synapse damage. Yet the activity of many other endolysosomal proteins during prion infection has not been thoroughly examined and may provide further insight into the biology of synapse health and mechanisms of prion toxicity.

Ultrastructural analysis of brains at different time points in disease highlights the signifi-

cant damage acquired in synapses from prion disease and illustrates Hrs depletion accelerating this damage. We observed an increase in concave synapses, thickened and irregular post synaptic densities, and a decrease in synaptic vesicle docking at terminal prion disease. The mechanisms underlying these ultrastructural synapse changes remain unclear but are thought to be through increased signaling at the synapse (Desmond and Levy, 1983; Fischer et al., 2000; Marrone and Petit, 2002; Siskova et al., 2009; Tao-Cheng, 2019), implicating excitotoxicity as a possible mechanism of prion toxicity. Understanding how changes to synapse structure occur will provide potential therapeutic targets for not only prion disease, but other neurodegenerative diseases.

6.4 Future directions

While all prion strains exhibit neurotoxicity and disease, understanding prion strains will uncover more insight into the role of protein aggregation in neurodegeneration. We have repeatedly found that soluble prion oligomers are more neuroinvasive and cause disease at a much faster rate. Factors contributing to the solubility of prion strains remain elusive. However, recent work suggests that the glycans on the prion protein can greatly affect plaque formation and spread, likely due to the capacity to bind heparan sulfate. Differences in glycan composition between prion strains are currently being investigated and will potentially explain the variability in biochemical properties and selective cell vulnerability.

We need to further explore the effects of prion infection on endolysosomal pathway function. Profiling the activity of Rabs and LRRK2 during prion infection will uncover where and how the pathways are impaired. Additionally, the UPS is a degradative system which has been reported to be dysregulated by prion disease (McKinnon et al., 2016). We have not investigated

how depletion of Hrs affects the UPS pathway, but that is one obvious question that could be answered. We would also like to know how Hrs accelerates damage to synapses by studying toxicity assays in primary neuron culture. The role of Arc in prion disease also remains of interest. How do prions affect neuroplasticity? How do prions alter the transcription profile in a neuron? Single cell RNAseq will be essential for understanding prion toxicity. This could perhaps provide insight as to the normal function of PrP^{C} as well. We have in vitro systems to identify how Arc is increased upon prion infection through both biochemical and microscopic techniques, which could uncover biomarkers and therapeutic targets for prion disease. The biology behind prion disease is fascinating, but ultimately our goals are to prevent the disease altogether.

Bibliography

1 Abdelaziz, D.H., S. Thapa, B. Abdulrahman, L. Vankuppeveld, and H.M. Schatzl. 2019. Metformin reduces prion infection in neuronal cells by enhancing autophagy. *Biochem Biophys Res Commun*

2 Abdulrahman, B.A., D. Abdelaziz, S. Thapa, L. Lu, S. Jain, S. Gilch, S. Proniuk, A. Zukiwski, and H.M. Schatzl. 2017. The celecoxib derivatives AR-12 and AR-14 induce autophagy and clear prion-infected cells from prions. *Sci Rep* 7:17565.

3 Abdulrahman, B.A., D.H. Abdelaziz, and H.M. Schatzl. 2018. Autophagy regulates exosomal release of prions in neuronal cells. *J Biol Chem* 293:8956-8968.

4 Abdulrahman, B.A., W. Tahir, K. Doh-Ura, S. Gilch, and H.M. Schatzl. 2019. Combining autophagy stimulators and cellulose ethers for therapy against prion disease. *Prion* 13:185-196.

5 Afghah, Z., X. Chen, and J.D. Geiger. 2020. Role of endolysosomes and inter-organellar signaling in brain disease. *Neurobiol Dis* 134:104670.

6 Aguib, Y., A. Heiseke, S. Gilch, C. Riemer, M. Baier, H.M. Schatzl, and A. Ertmer. 2009. Autophagy induction by trehalose counteracts cellular prion infection. *Autophagy* 5:361-369.

7 Aguilar-Calvo, P., C. Bett, A.M. Sevillano, T.D. Kurt, J. Lawrence, K. Soldau, P. Hammarstrom, K.P.R. Nilsson, and C.J. Sigurdson. 2018. Generation of novel neuroinvasive prions following intravenous challenge. *Brain Pathol* 28:999-1011.

8 Allen, N.J., and C. Eroglu. 2017. Cell Biology of Astrocyte-Synapse Interactions. *Neuron* 96:697-708.

9 Almeida, C.G., R.H. Takahashi, and G.K. Gouras. 2006. Beta-amyloid accumulation impairs multivesicular body sorting by inhibiting the ubiquitin-proteasome system. *J Neurosci* 26:4277-4288.

10 Almeida, C.G., D. Tampellini, R.H. Takahashi, P. Greengard, M.T. Lin, E.M. Snyder, and G.K. Gouras. 2005. Beta-amyloid accumulation in APP mutant neurons reduces PSD-95 and GluR1 in synapses. *Neurobiol Dis* 20:187-198.

11 Alpers, M.P. 2005. The epidemiology of kuru in the period 1987 to 1995. *Communicable diseases intelligence quarterly report* 29:391-399.

12 Arellano-Anaya, Z.E., A. Huor, P. Leblanc, S. Lehmann, M. Provansal, G. Raposo, O. Andreoletti, and D. Vilette. 2015. Prion strains are differentially released through the exosomal pathway. *Cell Mol Life Sci* 72:1185-1196.

13 Arnold, J.E., C. Tipler, L. Laszlo, J. Hope, M. Landon, and R.J. Mayer. 1995. The abnormal isoform of the prion protein accumulates in late-endosome-like organelles in scrapie-infected mouse brain. *The Journal of pathology* 176:403-411.

14 Ayers, J.I., C.R. Schutt, R.A. Shikiya, A. Aguzzi, A.E. Kincaid, and J.C. Bartz. 2011. The strain-encoded relationship between PrP replication, stability and processing in neurons is predictive of the incubation period of disease. *PLoS Pathog* 7:e1001317.

15 Bache, K.G., A. Brech, A. Mehlum, and H. Stenmark. 2003. Hrs regulates multivesicular body formation via ESCRT recruitment to endosomes. *J Cell Biol* 162:435-442.

16 Banks, W.A., M.L. Niehoff, C. Adessi, and C. Soto. 2004. Passage of murine scrapie prion protein across the mouse vascular blood-brain barrier. *Biochem Biophys Res Commun* 318:125-130.

17 Baral, P.K., J. Yin, A. Aguzzi, and M.N.G. James. 2019. Transition of the prion protein from a structured cellular form (PrP(C)) to the infectious scrapie agent (PrP(Sc)). *Protein Sci* 28:2055-2063.

18 Baron, T. 2002. Mouse models of prion disease transmission. *Trends in molecular medicine* 8:495-500.

19 Bartoletti-Stella, A., P. Corrado, N. Mometto, S. Baiardi, P.F. Durrenberger, T. Arzberger, R. Reynolds, H. Kretzschmar, S. Capellari, and P. Parchi. 2019. Analysis of RNA Expression Profiles Identifies Dysregulated Vesicle Trafficking Pathways in Creutzfeldt-Jakob Disease. *Mol Neurobiol* 56:5009-5024.

20 Bartz, J.C., A.E. Kincaid, and R.A. Bessen. 2003. Rapid prion neuroinvasion following tongue infection. *J Virol* 77:583-591.

21 Baumann, F., M. Tolnay, C. Brabeck, J. Pahnke, U. Kloz, H.H. Niemann, M. Heikenwalder, T. Rülicke, A. Bürkle, and A. Aguzzi. 2007. Lethal recessive myelin toxicity of prion protein lacking its central domain. *Embo j* 26:538-547.

22 Beekes, M., and P.A. McBride. 2000. Early accumulation of pathological PrP in the enteric nervous system and gut-associated lymphoid tissue of hamsters orally infected with scrapie. *Neurosci Lett* 278:181-184.

23 Belichenko, P.V., D. Brown, M. Jeffrey, and J.R. Fraser. 2000. Dendritic and synaptic alterations of hippocampal pyramidal neurones in scrapie-infected mice. *Neuropathol Appl Neurobiol* 26:143-149.

24 Beranger, F., A. Mange, B. Goud, and S. Lehmann. 2002. Stimulation of PrP(C) retrograde transport toward the endoplasmic reticulum increases accumulation of PrP(Sc) in prion-infected cells. *J Biol Chem* 277:38972-38977.

25 Beringue, V., A. Le Dur, P. Tixador, F. Reine, L. Lepourry, A. Perret-Liaudet, S. Haik, J.L. Vilotte, M. Fontes, and H. Laude. 2008. Prominent and persistent extraneural infection in human PrP transgenic mice infected with variant CJD. *PLoS ONE* 3:e1419.

26 Bett, C., S. Joshi-Barr, M. Lucero, M. Trejo, P. Liberski, J.W. Kelly, E. Masliah, and C.J. Sigurdson. 2012. Biochemical properties of highly neuroinvasive prion strains. *PLoS Pathogens* 8:e1002522.

27 Bett, C., J. Lawrence, T.D. Kurt, C. Orru, P. Aguilar-Calvo, A.E. Kincaid, W.K. Surewicz, B. Caughey, C. Wu, and C.J. Sigurdson. 2017. Enhanced neuroinvasion by smaller, soluble prions. *Acta Neuropathol Commun* 5:32.

28 Bi, R., L.-L. Kong, M. Xu, G.-D. Li, D.-F. Zhang, I. Alzheimer's Disease Neuroimaging, T. Li, Y. Fang, C. Zhang, B. Zhang, and Y.-G. Yao. 2018. The Arc Gene Confers Genetic Susceptibility to Alzheimer's Disease in Han Chinese. *Molecular neurobiology* 55:1217-1226.

29 Bobrie, A., S. Krumeich, F. Reyal, C. Recchi, L.F. Moita, M.C. Seabra, M. Ostrowski, and C. Thery. 2012. Rab27a supports exosome-dependent and -independent mechanisms that modify the tumor microenvironment and can promote tumor progression. *Cancer Res* 72:4920-4930.

30 Boellaard, J.W., M. Kao, W. Schlote, and H. Diringer. 1991. Neuronal autophagy in experimental scrapie. *Acta Neuropathol* 82:225-228.

31 Bolton, D.C., M.P. McKinley, and S.B. Prusiner. 1982. Identification of a protein that purifies with the scrapie prion. *Science* 218:1309-1311.

32 Boon, J.Y., J. Dusonchet, C. Trengrove, and B. Wolozin. 2014. Interaction of LRRK2 with kinase and GTPase signaling cascades. *Front Mol Neurosci* 7:64.

33 Borchelt, D.R., A. Taraboulos, and S.B. Prusiner. 1992. Evidence for synthesis of scrapie prion proteins in the endocytic pathway. *J Biol Chem* 267:16188-16199.

34 Brandner, S., S. Isenmann, A. Raeber, M. Fischer, A. Sailer, Y. Kobayashi, S. Marino, C. Weissmann, and A. Aguzzi. 1996. Normal host prion protein necessary for scrapie-induced neurotoxicity. *Nature* 379:339-343.

35 Brown, D., P. Belichenko, J. Sales, M. Jeffrey, and J.R. Fraser. 2001. Early loss of dendritic spines in murine scrapie revealed by confocal analysis. *Neuroreport* 12:179-183.

36 Büeler, H., M. Fischer, Y. Lang, H. Bluethmann, H.P. Lipp, S.J. DeArmond, S.B. Prusiner, M. Aguet, and C. Weissmann. 1992. Normal development and behaviour of mice lacking the neuronal cell-surface PrP protein. *Nature* 356:577-582.

37 Büeler, H., A. Raeber, A. Sailer, M. Fischer, A. Aguzzi, and C. Weissmann. 1994. High prion and PrPSc levels but delayed onset of disease in scrapie-inoculated mice heterozygous for a disrupted PrP gene. *Mol Med* 1:19-30.

38 Burgoyne, R.D., and A. Morgan. 2015. Cysteine string protein (CSP) and its role in preventing neurodegeneration. *Semin Cell Dev Biol* 40:153-159.

39 Campeau, J.L., G. Wu, J.R. Bell, J. Rasmussen, and V.L. Sim. 2013. Early increase and late decrease of purkinje cell dendritic spine density in prion-infected organotypic mouse cerebellar cultures. *PLoS One* 8:e81776.

40 Castle, A.R., and A.C. Gill. 2017. Physiological Functions of the Cellular Prion Protein. *Frontiers in molecular biosciences* 4:19.

41 Cataldo, A.M., C.M. Peterhoff, J.C. Troncoso, T. Gomez-Isla, B.T. Hyman, and R.A. Nixon. 2000. Endocytic pathway abnormalities precede amyloid beta deposition in sporadic Alzheimer's disease and Down syndrome: differential effects of APOE genotype and presenilin mutations. *Am J Pathol* 157:277-286.

42 Caughey, B., G.J. Raymond, D. Ernst, and R.E. Race. 1991. N-terminal truncation of the scrapie-associated form of PrP by lysosomal protease(s): implications regarding the site of conversion of PrP to the protease-resistant state. *J Virol* 65:6597-6603.

43 Chiesa, R., P. Piccardo, B. Ghetti, and D.A. Harris. 1998. Neurological illness in transgenic mice expressing a prion protein with an insertional mutation. *Neuron* 21:1339-1351.

44 Clague, M.J., and S. Urbé. 2001. The interface of receptor trafficking and signalling. *J Cell Sci* 114:3075-3081.

45 Clayton, E.L., S. Mizielinska, J.R. Edgar, T.T. Nielsen, S. Marshall, F.E. Norona, M. Robbins, H. Damirji, I.E. Holm, P. Johannsen, J.E. Nielsen, E.A. Asante, J. Collinge, F.R. consortium, and A.M. Isaacs. 2015. Frontotemporal dementia caused by CHMP2B mutation is characterised by neuronal lysosomal storage pathology. *Acta Neuropathol* 130:511-523.

46 Clinton, J., C. Forsyth, M.C. Royston, and G.W. Roberts. 1993. Synaptic degeneration is the primary neuropathological feature in prion disease: a preliminary study. *Neuroreport* 4:65-68.

47 Cocucci, E., and J. Meldolesi. 2015. Ectosomes and exosomes: shedding the confusion between extracellular vesicles. *Trends Cell Biol* 25:364-372.

48 Coleman, B.M., E. Hanssen, V.A. Lawson, and A.F. Hill. 2012. Prion-infected cells regulate the release of exosomes with distinct ultrastructural features. *FASEB J* 26:4160-4173.

49 Collinge, J. 2001. Prion diseases of humans and animals: their causes and molecular basis. *Annual review of neuroscience* 24:519-550.

50 Collinge, J., A.E. Harding, F. Owen, M. Poulter, R. Lofthouse, A.M. Boughey, T. Shah, and T.J. Crow. 1989. Diagnosis of Gerstmann-Straussler syndrome in familial dementia with prion protein gene analysis. *Lancet* 2:15-17.

51 Collinge, J., M.A. Whittington, K.C. Sidle, C.J. Smith, M.S. Palmer, A.R. Clarke, and J.G. Jefferys. 1994. Prion protein is necessary for normal synaptic function. *Nature* 370:295-297.

52 Collis, S.C., and R.H. Kimberlin. 1985. Long-term persistence of scrapie infection in mouse spleens in the absence of clinical disease. *FEMS Microbiology Letters* 29:111-114.

53 Corbett, G.T., Z. Wang, W. Hong, M. Colom-Cadena, J. Rose, M. Liao, A. Asfaw, T.C. Hall, L. Ding, A. DeSousa, M.P. Frosch, J. Collinge, D.A. Harris, M.S. Perkinton, T.L. Spires-Jones, T.L. Young-Pearse, A. Billinton, and D.M. Walsh. 2019. PrP is a central player in toxicity mediated by soluble aggregates of neurodegeneration-causing proteins. *Acta Neuropathol*

54 Cui, H.L., B. Guo, B. Scicluna, B.M. Coleman, V.A. Lawson, L. Ellett, P.J. Meikle, M. Bukrinsky, N. Mukhamedova, D. Sviridov, and A.F. Hill. 2014. Prion infection impairs cholesterol metabolism in neuronal cells. *The Journal of biological chemistry* 289:789-802.

55 Cunningham, C., R. Deacon, H. Wells, D. Boche, S. Waters, C.P. Diniz, H. Scott, J.N. Rawlins, and V.H. Perry. 2003. Synaptic changes characterize early behavioural signs in the ME7 model of murine prion disease. *Eur J Neurosci* 17:2147-2155.

56 Cunningham, C., R. Deacon, H. Wells, D. Boche, S. Waters, C.P. Diniz, H. Scott, J.N.P. Rawlins, and V.H. Perry. 2003. Synaptic changes characterize early behavioural signs in the ME7 model of murine prion disease. *Eur J Neurosci* 17:2147-2155.

57 Daneman, R., and A. Prat. 2015. The blood-brain barrier. *Cold Spring Harbor perspectives in biology* 7:a020412.

58 Davenport, K.A., D.M. Henderson, J. Bian, G.C. Telling, C.K. Mathiason, and E.A. Hoover. 2015. Insights into Chronic Wasting Disease and Bovine Spongiform Encephalopathy Species Barriers by Use of Real-Time Conversion. *J Virol* 89:9524-9531.

59 DeArmond, S.J., and S.B. Prusiner. 1995. Etiology and pathogenesis of prion diseases. *Am J Pathol* 146:785-811.

60 Deleault, A.M., N.R. Deleault, B.T. Harris, J.R. Rees, and S. Supattapone. 2008. The effects of prion protein proteolysis and disaggregation on the strain properties of hamster scrapie. *The Journal of general virology* 89:2642-2650.

61 Deng, H., P. Wang, and J. Jankovic. 2018. The genetics of Parkinson disease. *Ageing research reviews* 42:72-85.

62 Desmond, N.L., and W.B. Levy. 1983. Synaptic correlates of associative potentiation/depression: an ultrastructural study in the hippocampus. *Brain Res* 265:21-30.

63 Detwiler, L.A. 1992. Scrapie. *Rev Sci Tech* 11:491-537.

64 Du, X., A.S. Kazim, A.J. Brown, and H. Yang. 2012. An essential role of Hrs/Vps27 in endosomal cholesterol trafficking. *Cell Rep* 1:29-35.

65 Eleuteri, S., and A. Albanese. 2019. VPS35-Based Approach: A Potential Innovative Treatment in Parkinson's Disease. *Front Neurol* 10:1272.

66 Ermolayev, V., T. Cathomen, J. Merk, M. Friedrich, W. Härtig, G.S. Harms, M.A. Klein, and E. Flechsig. 2009. Impaired axonal transport in motor neurons correlates with clinical prion disease. *PLoS pathogens* 5:e1000558-e1000558.

67 Ersdal, C., C.M. Goodsir, M.M. Simmons, G. McGovern, and M. Jeffrey. 2009. Abnormal prion protein is associated with changes of plasma membranes and endocytosis in bovine spongiform encephalopathy (BSE)-affected cattle brains. *Neuropathol Appl Neurobiol* 35:259-271.

68 Esposito, G., F. Ana Clara, and P. Verstreken. 2012. Synaptic vesicle trafficking and Parkinson's disease. *Developmental neurobiology* 72:134-144.

69 Falsig, J., T. Sonati, U.S. Herrmann, D. Saban, B. Li, K. Arroyo, B. Ballmer, P.P. Liberski, and A. Aguzzi. 2012. Prion pathogenesis is faithfully reproduced in cerebellar organotypic slice cultures. *PLoS Pathog* 8:e1002985.

70 Fang, C., T. Imberdis, M.C. Garza, H. Wille, and D.A. Harris. 2016. A Neuronal Culture System to Detect Prion Synaptotoxicity. *PLoS Pathog* 12:e1005623.

71 Fang, C., B. Wu, N.T.T. Le, T. Imberdis, R.C.C. Mercer, and D.A. Harris. 2018. Prions activate a p38 MAPK synaptotoxic signaling pathway. *PLoS Pathog* 14:e1007283.

72 Fernandes, A.C., V. Uytterhoeven, S. Kuenen, Y.C. Wang, J.R. Slabbaert, J. Swerts, J. Kasprowicz, S. Aerts, and P. Verstreken. 2014. Reduced synaptic vesicle protein degradation at lysosomes curbs TBC1D24/sky-induced neurodegeneration. *J Cell Biol* 207:453-462.

73 Fernández-Alfonso, T., and T.A. Ryan. 2006. The efficiency of the synaptic vesicle cycle at central nervous system synapses. *Trends Cell Biol* 16:413-420.

74 Ferreira, S.T., and W.L. Klein. 2011. The Aβ oligomer hypothesis for synapse failure and memory loss in Alzheimer's disease. *Neurobiology of learning and memory* 96:529-543.

75 Ferrer, I. 2002. Synaptic pathology and cell death in the cerebellum in Creutzfeldt-Jakob disease. *Cerebellum* 1:213-222.

76 Fevrier, B., D. Vilette, F. Archer, D. Loew, W. Faigle, M. Vidal, H. Laude, and G. Raposo. 2004. Cells release prions in association with exosomes. *Proceedings of the National Academy of Sciences of the United States of America* 101:9683-9688.

77 Filimonenko, M., S. Stuffers, C. Raiborg, A. Yamamoto, L. Malerod, E.M. Fisher, A. Isaacs, A. Brech, H. Stenmark, and A. Simonsen. 2007. Functional multivesicular bodies are required for autophagic clearance of protein aggregates associated with neurodegenerative disease. *J Cell Biol* 179:485-500.

78 Fiorino, A.S. 1996. Sleep, genes and death: fatal familial insomnia. *Brain Res Brain Res Rev* 22:258-264.

79 Fischer, M., S. Kaech, U. Wagner, H. Brinkhaus, and A. Matus. 2000. Glutamate receptors regulate actin-based plasticity in dendritic spines. *Nat Neurosci* 3:887-894.

80 Fraser, H., and A.G. Dickinson. 1968. The sequential development of the brain lesion of scrapie in three strains of mice. *J Comp Pathol* 78:301-311.

81 Frost, B., and M.I. Diamond. 2010. Prion-like mechanisms in neurodegenerative diseases. *Nature reviews. Neuroscience* 11:155-159.

82 Fukuda, M. 2013. Rab27 effectors, pleiotropic regulators in secretory pathways. *Traffic* 14:949-963.

83 Funke, S.A. 2011. Detection of Soluble Amyloid-β Oligomers and Insoluble High-Molecular-Weight Particles in CSF: Development of Methods with Potential for Diagnosis and Therapy Monitoring of Alzheimer's Disease. *International journal of Alzheimer's disease* 2011:151645.

84 Giese, A., D.R. Brown, M.H. Groschup, C. Feldmann, I. Haist, and H.A. Kretzschmar. 1998. Role of microglia in neuronal cell death in prion disease. *Brain Pathol* 8:449-457.

85 Gilch, S., C. Bach, G. Lutzny, I. Vorberg, and H.M. Schätzl. 2009. Inhibition of cholesterol recycling impairs cellular PrP(Sc) propagation. *Cellular and molecular life sciences : CMLS* 66:3979-3991.

86 Gill, O.N., Y. Spencer, A. Richard-Loendt, C. Kelly, R. Dabaghian, L. Boyes, J. Linehan, M. Simmons, P. Webb, P. Bellerby, N. Andrews, D.A. Hilton, J.W. Ironside, J. Beck, M. Poulter, S. Mead, and S. Brandner. 2013. Prevalent abnormal prion protein in human appendixes after bovine spongiform encephalopathy epizootic: large scale survey. *Bmj* 347:f5675.

87 Ginsberg, S.D., M.J. Alldred, S.E. Counts, A.M. Cataldo, R.L. Neve, Y. Jiang, J. Wuu, M.V. Chao, E.J. Mufson, R.A. Nixon, and S. Che. 2010. Microarray analysis of hippocampal CA1 neurons implicates early endosomal dysfunction during Alzheimer's disease progression. *Biol Psychiatry* 68:885-893.

88 Ginsberg, S.D., E.J. Mufson, S.E. Counts, J. Wuu, M.J. Alldred, R.A. Nixon, and S. Che. 2010. Regional selectivity of rab5 and rab7 protein upregulation in mild cognitive impairment and Alzheimer's disease. *J Alzheimers Dis* 22:631-639.

89 Girard, E., D. Chmiest, N. Fournier, L. Johannes, J.L. Paul, B. Vedie, and C. Lamaze. 2014. Rab7 is functionally required for selective cargo sorting at the early endosome. *Traffic* 15:309-326.

90 Glatzel, M., and A. Aguzzi. 2000. PrP(C) expression in the peripheral nervous system is a determinant of prion neuroinvasion. *The Journal of general virology* 81:2813-2821.

91 Gomez-Nicola, D., N.L. Fransen, S. Suzzi, and V.H. Perry. 2013. Regulation of microglial proliferation during chronic neurodegeneration. *J Neurosci* 33:2481-2493.

92 Goniotaki, D., A.K.K. Lakkaraju, A.N. Shrivastava, P. Bakirci, S. Sorce, A. Senatore, R. Marpakwar, S. Hornemann, F. Gasparini, A. Triller, and A. Aguzzi. 2017. Inhibition of group-I metabotropic glutamate receptors protects against prion toxicity. *PLoS Pathog* 13:e1006733.

93 Goold, R., C. McKinnon, S. Rabbanian, J. Collinge, G. Schiavo, and S.J. Tabrizi. 2013. Alternative fates of newly formed PrPSc upon prion conversion on the plasma membrane. *J Cell Sci* 126:3552-3562.

94 Goold, R., C. McKinnon, and S.J. Tabrizi. 2015. Prion degradation pathways: Potential for therapeutic intervention. *Mol Cell Neurosci* 66:12-20.

95 Gousset, K., E. Schiff, C. Langevin, Z. Marijanovic, A. Caputo, D.T. Browman, N. Chenouard, F. de Chaumont, A. Martino, J. Enninga, J.C. Olivo-Marin, D. Mannel, and C. Zurzolo. 2009. Prions hijack tunnelling nanotubes for intercellular spread. *Nature cell biology* 11:328-336.

96 Gray, B.C., Z. Siskova, V.H. Perry, and V. O'Connor. 2009. Selective presynaptic degeneration in the synaptopathy associated with ME7-induced hippocampal pathology. *Neurobiol Dis* 35:63-74.

97 Grimsey, N.J., L.J. Coronel, I.C. Cordova, and J. Trejo. 2016. Recycling and Endosomal Sorting of Protease-activated Receptor-1 Is Distinctly Regulated by Rab11A and Rab11B Proteins. *J Biol Chem* 291:2223-2236.

98 Guo, B.B., S.A. Bellingham, and A.F. Hill. 2015. The neutral sphingomyelinase pathway regulates packaging of the prion protein into exosomes. *J Biol Chem* 290:3455-3467.

99 Guo, B.B., S.A. Bellingham, and A.F. Hill. 2016. Stimulating the Release of Exosomes Increases the Intercellular Transfer of Prions. *J Biol Chem* 291:5128-5137.

100 Hannaoui, S., L. Maatouk, N. Privat, E. Levavasseur, B.A. Faucheux, and S. Haïk. 2013. Prion propagation and toxicity occur in vitro with two-phase kinetics specific to strain and neuronal type. *J Virol* 87:2535-2548.

101 Harrathi, C., N. Fernandez-Borges, H. Erana, S.R. Elezgarai, V. Venegas, J.M. Charco, and J. Castilla. 2019. Insights into the Bidirectional Properties of the Sheep-Deer Prion Transmission Barrier. *Mol Neurobiol* 56:5287-5303.

102 Hasegawa, T., M. Konno, T. Baba, N. Sugeno, A. Kikuchi, M. Kobayashi, E. Miura, N. Tanaka, K. Tamai, K. Furukawa, H. Arai, F. Mori, K. Wakabayashi, M. Aoki, Y. Itoyama, and A. Takeda. 2011. The AAA-ATPase VPS4 regulates extracellular secretion and lysosomal targeting of alpha-synuclein. *PLoS One* 6:e29460.

103 Hausser, A., and K. Schlett. 2019. Coordination of AMPA receptor trafficking by Rab GTPases. *Small GTPases* 10:419-432.

104 Heikenwalder, M., C. Julius, and A. Aguzzi. 2007. Prions and peripheral nerves: A deadly rendezvous. *Journal of neuroscience research*

105 Heiseke, A., Y. Aguib, C. Riemer, M. Baier, and H.M. Schatzl. 2009. Lithium induces clearance of protease resistant prion protein in prion-infected cells by induction of autophagy. *J Neurochem* 109:25-34.

106 Heisler, F.F., Y. Pechmann, I. Wieser, H.C. Altmeppen, L. Veenendaal, M. Muhia, M. Schweizer, M. Glatzel, S. Krasemann, and M. Kneussel. 2018. Muskelin Coordinates PrP(C) Lysosome versus Exosome Targeting and Impacts Prion Disease Progression. *Neuron* 99:1155-1169 e1159.

107 Herrmann, U.S., T. Sonati, J. Falsig, R.R. Reimann, P. Dametto, T. O'Connor, B. Li, A. Lau, S. Hornemann, S. Sorce, U. Wagner, D. Sanoudou, and A. Aguzzi. 2015. Prion infections and anti-PrP antibodies trigger converging neurotoxic pathways. *PLoS Pathog* 11:e1004662.

108 Hilfiker, S., V.A. Pieribone, A.J. Czernik, H.T. Kao, G.J. Augustine, and P. Greengard. 1999. Synapsins as regulators of neurotransmitter release. *Philos Trans R Soc Lond B Biol Sci* 354:269-279.

109 Hilton, K.J., C. Cunningham, R.A. Reynolds, and V.H. Perry. 2013. Early Hippocampal Synaptic Loss Precedes Neuronal Loss and Associates with Early Behavioural Deficits in Three Distinct Strains of Prion Disease. *PloS one* 8:e68062-e68062.

110 Houston, F., and O. Andréoletti. 2018. The zoonotic potential of animal prion diseases. *Handbook of clinical neurology* 153:447-462.

111 Houston, F., S. McCutcheon, W. Goldmann, A. Chong, J. Foster, S. Siso, L. Gonzalez, M. Jeffrey, and N. Hunter. 2008. Prion diseases are efficiently transmitted by blood transfusion in sheep. *Blood* 112:4739-4745.

112 Hu, Y.B., E.B. Dammer, R.J. Ren, and G. Wang. 2015. The endosomal-lysosomal system: from acidification and cargo sorting to neurodegeneration. *Transl Neurodegener* 4:18.

113 Hurley, J.H. 2015. ESCRTs are everywhere. *Embo j* 34:2398-2407.

114 Hwang, D., I.Y. Lee, H. Yoo, N. Gehlenborg, J.H. Cho, B. Petritis, D. Baxter, R. Pitstick, R. Young, D. Spicer, N.D. Price, J.G. Hohmann, S.J. Dearmond, G.A. Carlson, and L.E. Hood. 2009. A systems approach to prion disease. *Molecular systems biology* 5:252.

115 Iguchi, Y., L. Eid, M. Parent, G. Soucy, C. Bareil, Y. Riku, K. Kawai, S. Takagi, M. Yoshida, M. Katsuno, G. Sobue, and J.P. Julien. 2016. Exosome secretion is a key pathway for clearance of pathological TDP-43. *Brain* 139:3187-3201.

116 Inoshita, T., T. Arano, Y. Hosaka, H. Meng, Y. Umezaki, S. Kosugi, T. Morimoto, M. Koike, H.Y. Chang, Y. Imai, and N. Hattori. 2017. Vps35 in cooperation with LRRK2

regulates synaptic vesicle endocytosis through the endosomal pathway in Drosophila. *Hum Mol Genet* 26:2933-2948.

117 Jeffrey, M., W.G. Halliday, J. Bell, A.R. Johnston, N.K. MacLeod, C. Ingham, A.R. Sayers, D.A. Brown, and J.R. Fraser. 2000. Synapse loss associated with abnormal PrP precedes neuronal degeneration in the scrapie-infected murine hippocampus. *Neuropathol Appl Neurobiol* 26:41-54.

118 Jeffrey, M., J.R. Scott, A. Williams, and H. Fraser. 1992. Ultrastructural features of spongiform encephalopathy transmitted to mice from three species of bovidae. *Acta Neuropathol* 84:559-569.

119 Kaatz, M., C. Fast, U. Ziegler, A. Balkema-Buschmann, B. Hammerschmidt, M. Keller, A. Oelschlegel, L. McIntyre, and M.H. Groschup. 2012. Spread of Classic BSE Prions from the Gut via the Peripheral Nervous System to the Brain. *Am J Pathol* 181:515-524.

120 Katzmann, D.J., M. Babst, and S.D. Emr. 2001. Ubiquitin-dependent sorting into the multivesicular body pathway requires the function of a conserved endosomal protein sorting complex, ESCRT-I. *Cell* 106:145-155.

121 Kerrigan, T.L., and A.D. Randall. 2013. A new player in the "synaptopathy" of Alzheimer's disease - arc/arg 3.1. *Front Neurol* 4:9.

122 Kim, Y.S., R.I. Carp, S.M. Callahan, M. Natelli, and H.M. Wisniewski. 1990. Vacuolization, incubation period and survival time analyses in three mouse genotypes injected stereotactically in three brain regions with the 22L scrapie strain. *J Neuropathol Exp Neurol* 49:106-113.

123 Kim, Y.S., R.I. Carp, S.M. Callahan, and H.M. Wisniewski. 1990. Pathogenesis and pathology of scrapie after stereotactic injection of strain 22L in intact and bisected cerebella. *J Neuropathol Exp Neurol* 49:114-121.

124 Korb, E., and S. Finkbeiner. 2011. Arc in synaptic plasticity: from gene to behavior. *Trends Neurosci* 34:591-598.

125 Kovács, G.G., E. Gelpi, T. Ströbel, G. Ricken, J.R. Nyengaard, H. Bernheimer, and H. Budka. 2007. Involvement of the endosomal-lysosomal system correlates with regional pathology in Creutzfeldt-Jakob disease. *Journal of neuropathology and experimental neurology* 66:628-636.

126 Kranich, J., N.J. Krautler, J. Falsig, B. Ballmer, S. Li, G. Hutter, P. Schwarz, R. Moos, C. Julius, G. Miele, and A. Aguzzi. 2010. Engulfment of cerebral apoptotic bodies controls the course of prion disease in a mouse strain-dependent manner. *J Exp Med* 207:2271-2281.

127 Kuczius, T., and M.H. Groschup. 1999. Differences in Proteinase K Resistance and Neuronal Deposition of Abnormal Prion Proteins Characterize Bovine Spongiform Encephalopathy (BSE) and Scrapie Strains. *Mol Med* 5:406-418.

128 Kümmel, D., and C. Ungermann. 2014. Principles of membrane tethering and fusion in endosome and lysosome biogenesis. *Current opinion in cell biology* 29:61-66.

129 Kuroki, T., S. Osari, K. Nagata, and A. Kawaguchi. 2018. Influenza A Virus NS1 Protein Suppresses JNK1-Dependent Autophagosome Formation Mediated by Rab11a Recycling Endosomes. *Front Microbiol* 9:3120.

130 Kurt, T.D., C. Bett, N. Fernandez-Borges, S. Joshi-Barr, S. Hornemann, T. Rulicke, J. Castilla, K. Wuthrich, A. Aguzzi, and C.J. Sigurdson. 2014. Prion transmission prevented by modifying the beta2-alpha2 loop structure of host PrPC. *J Neurosci* 34:1022-1027.

131 Kuwahara, T., and T. Iwatsubo. 2020. The Emerging Functions of LRRK2 and Rab GTPases in the Endolysosomal System. *Frontiers in neuroscience* 14:227.

132 Lacor, P.N., M.C. Buniel, L. Chang, S.J. Fernandez, Y. Gong, K.L. Viola, M.P. Lambert, P.T. Velasco, E.H. Bigio, C.E. Finch, G.A. Krafft, and W.L. Klein. 2004. Synaptic targeting by Alzheimer's-related amyloid beta oligomers. *J Neurosci* 24:10191-10200.

133 Le, N.T.T., B. Wu, and D.A. Harris. 2019. Prion neurotoxicity. *Brain Pathol* 29:263-277.

134 Lee, J.A., A. Beigneux, S.T. Ahmad, S.G. Young, and F.B. Gao. 2007. ESCRT-III dysfunction causes autophagosome accumulation and neurodegeneration. *Curr Biol* 17:1561-1567.

135 Li, D., S. Huang, J. Zhu, T. Hu, Z. Han, S. Zhang, J. Zhao, F. Chen, and P. Lei. 2019. Exosomes from MiR-21-5p-Increased Neurons Play a Role in Neuroprotection by Suppressing Rab11a-Mediated Neuronal Autophagy In Vitro After Traumatic Brain Injury. *Med Sci Monit* 25:1871-1885.

136 Li, S., and D.J. Selkoe. 2020. A mechanistic hypothesis for the impairment of synaptic plasticity by soluble Ab oligomers from Alzheimer brain. *J Neurochem*

137 Liberski, P.P., D.R. Brown, B. Sikorska, B. Caughey, and P. Brown. 2008. Cell death and autophagy in prion diseases (transmissible spongiform encephalopathies). *Folia Neuropathol* 46:1-25.

138 Liberski, P.P., B. Sikorska, J.J. Hauw, N. Kopp, N. Streichenberger, P. Giraud, J. Boellaard, H. Budka, G.G. Kovacs, J. Ironside, and P. Brown. 2010. Ultrastructural characteristics (or evaluation) of Creutzfeldt-Jakob disease and other human transmissible spongiform encephalopathies or prion diseases. *Ultrastruct Pathol* 34:351-361.

139 Linden, R. 2017. The Biological Function of the Prion Protein: A Cell Surface Scaffold of Signaling Modules. *Front Mol Neurosci* 10:77.

140 Linsenmeier, L., B. Mohammadi, S. Wetzel, B. Puig, W.S. Jackson, A. Hartmann, K. Uchiyama, S. Sakaguchi, K. Endres, J. Tatzelt, P. Saftig, M. Glatzel, and H.C. Altmeppen. 2018. Structural and mechanistic aspects influencing the ADAM10-mediated shedding of the prion protein. *Mol Neurodegener* 13:18.

141 Liu, L., D. Jiang, A. McDonald, Y. Hao, G.L. Millhauser, and F. Zhou. 2011. Copper redox cycling in the prion protein depends critically on binding mode. *J Am Chem Soc* 133:12229-12237.

142 Lopez-Perez, O., R. Bolea, B. Marin, J.J. Badiola, and I. Martin-Burriel. 2019. Autophagy impairment in highly prion-affected brain areas of sheep experimentally infected with atypical scrapie. *Vet Microbiol* 233:78-84.

143 Lopez-Perez, O., A. Otero, H. Filali, D. Sanz-Rubio, J.M. Toivonen, P. Zaragoza, J.J. Badiola, R. Bolea, and I. Martin-Burriel. 2019. Dysregulation of autophagy in the central nervous system of sheep naturally infected with classical scrapie. *Sci Rep* 9:1911.

144 Lopez-Perez, O., J.M. Toivonen, A. Otero, L. Solanas, P. Zaragoza, J.J. Badiola, R. Osta, R. Bolea, and I. Martin-Burriel. 2020. Impairment of autophagy in scrapie-infected transgenic mice at the clinical stage. *Lab Invest* 100:52-63.

145 Magalhaes, A.C., G.S. Baron, K.S. Lee, O. Steele-Mortimer, D. Dorward, M.A. Prado, and B. Caughey. 2005. Uptake and neuritic transport of scrapie prion protein coincident with infection of neuronal cells. *J Neurosci* 25:5207-5216.

146 Mahley, R.W. 2016. Central Nervous System Lipoproteins: ApoE and Regulation of Cholesterol Metabolism. *Arterioscler Thromb Vasc Biol* 36:1305-1315.

147 Majer, A., S.J. Medina, Y. Niu, B. Abrenica, K.J. Manguiat, K.L. Frost, C.S. Philipson, D.L. Sorensen, and S.A. Booth. 2012. Early mechanisms of pathobiology are revealed by transcriptional temporal dynamics in hippocampal CA1 neurons of prion infected mice. *PLoS Pathog* 8:e1003002.

148 Makarava, N., J.C. Chang, R. Kushwaha, and I.V. Baskakov. 2019. Region-Specific Response of Astrocytes to Prion Infection. *Frontiers in neuroscience* 13:1048.

149 Makarava, N., J.C. Chang, K. Molesworth, and I.V. Baskakov. 2020. Region-specific glial homeostatic signature in prion diseases is replaced by a uniform neuroinflammation signature, common for brain regions and prion strains with different cell tropism. *Neurobiol Dis* 137:104783.

150 Mallucci, G., A. Dickinson, J. Linehan, P.C. Klöhn, S. Brandner, and J. Collinge. 2003. Depleting neuronal PrP in prion infection prevents disease and reverses spongiosis. *Science* 302:871-874.

151 Mallucci, G.R., M.D. White, M. Farmer, A. Dickinson, H. Khatun, A.D. Powell, S. Brandner, J.G. Jefferys, and J. Collinge. 2007. Targeting cellular prion protein reverses early cognitive deficits and neurophysiological dysfunction in prion-infected mice. *Neuron* 53:325-335.

152 Manson, J.C., A.R. Clarke, M.L. Hooper, L. Aitchison, I. McConnell, and J. Hope. 1994. 129/Ola mice carrying a null mutation in PrP that abolishes mRNA production are developmentally normal. *Mol Neurobiol* 8:121-127.

153 Marijanovic, Z., A. Caputo, V. Campana, and C. Zurzolo. 2009. Identification of an intracellular site of prion conversion. *PLoS Pathog* 5:e1000426.

154 Marrone, D.F., and T.L. Petit. 2002. The role of synaptic morphology in neural plasticity: structural interactions underlying synaptic power. *Brain Res Brain Res Rev* 38:291-308.

155 Massignan, T., E. Biasini, E. Lauranzano, P. Veglianese, M. Pignataro, L. Fioriti, D.A. Harris, M. Salmona, R. Chiesa, and V. Bonetto. 2010. Mutant prion protein expression is associated with an alteration of the Rab GDP dissociation inhibitor alpha (GDI)/Rab11 pathway. *Mol Cell Proteomics* 9:611-622.

156 Mathiason, C.K. 2017. Scrapie, CWD, and Transmissible Mink Encephalopathy. *Progress in molecular biology and translational science* 150:267-292.

157 Mattei, V., M.G. Barenco, V. Tasciotti, T. Garofalo, A. Longo, K. Boller, J. Lower, R. Misasi, F. Montrasio, and M. Sorice. 2009. Paracrine diffusion of PrP(C) and propagation of prion infectivity by plasma membrane-derived microvesicles. *PLoS One* 4:e5057.

158 Matus, A. 2000. Actin-based plasticity in dendritic spines. *Science* 290:754-758.

159 McBride, P.A., W.J. Schulz-Schaeffer, M. Donaldson, M. Bruce, H. Diringer, H.A. Kretzschmar, and M. Beekes. 2001. Early spread of scrapie from the gastrointestinal tract to the central nervous system involves autonomic fibers of the splanchnic and vagus nerves. *J Virol* 75:9320-9327.

160 McInnes, J., K. Wierda, A. Snellinx, L. Bounti, Y.C. Wang, I.C. Stancu, N. Apóstolo, K. Gevaert, I. Dewachter, T.L. Spires-Jones, B. De Strooper, J. De Wit, L. Zhou, and P. Verstreken. 2018. Synaptogyrin-3 Mediates Presynaptic Dysfunction Induced by Tau. *Neuron* 97:823-835.e828.

161 McKinnon, C., R. Goold, R. Andre, A. Devoy, Z. Ortega, J. Moonga, J.M. Linehan, S. Brandner, J.J. Lucas, J. Collinge, and S.J. Tabrizi. 2016. Prion-mediated neurodegeneration is associated with early impairment of the ubiquitin-proteasome system. *Acta Neuropathol* 131:411-425.

162 Mead, S., J. Uphill, J. Beck, M. Poulter, T. Campbell, J. Lowe, G. Adamson, H. Hummerich, N. Klopp, I.M. Ruckert, H.E. Wichmann, D. Azazi, V. Plagnol, W.H. Pako, J. Whitfield, M.P. Alpers, J. Whittaker, D.J. Balding, I. Zerr, H. Kretzschmar, and J. Collinge. 2012. Genome-wide association study in multiple human prion diseases suggests genetic risk factors additional to PRNP. *Hum Mol Genet* 21:1897-1906.

163 Miura, E., T. Hasegawa, M. Konno, M. Suzuki, N. Sugeno, N. Fujikake, S. Geisler, M. Tabuchi, R. Oshima, A. Kikuchi, T. Baba, K. Wada, Y. Nagai, A. Takeda, and M. Aoki. 2014. VPS35 dysfunction impairs lysosomal degradation of alpha-synuclein and exacerbates neurotoxicity in a Drosophila model of Parkinson's disease. *Neurobiol Dis* 71:1-13.

164 Morin, J.P., G. Ceron-Solano, G. Velazquez-Campos, G. Pacheco-Lopez, F. Bermudez-Rattoni, and S. Diaz-Cintra. 2016. Spatial Memory Impairment is Associated with Intraneural Amyloid-beta Immunoreactivity and Dysfunctional Arc Expression in the Hippocampal-CA3 Region of a Transgenic Mouse Model of Alzheimer's Disease. *J Alzheimers Dis* 51:69-79.

165 Moya-Alvarado, G., A. Gonzalez, N. Stuardo, and F.C. Bronfman. 2018. Brain-Derived Neurotrophic Factor (BDNF) Regulates Rab5-Positive Early Endosomes in Hippocampal Neurons to Induce Dendritic Branching. *Front Cell Neurosci* 12:493.

166 Nathanson, N., J. Wilesmith, and C. Griot. 1997. Bovine spongiform encephalopathy (BSE): causes and consequences of a common source epidemic. *American journal of epidemiology* 145:959-969.

167 Ng, E.L., B.Q. Gan, F. Ng, and B.L. Tang. 2012. Rab GTPases regulating receptor trafficking at the late endosome-lysosome membranes. *Cell biochemistry and function* 30:515-523.

168 Ng, E.L., and B.L. Tang. 2008. Rab GTPases and their roles in brain neurons and glia. *Brain research reviews* 58:236-246.

169 Nishida, N., P. Tremblay, T. Sugimoto, K. Shigematsu, S. Shirabe, C. Petromilli, S.P. Erpel, R. Nakaoke, R. Atarashi, T. Houtani, M. Torchia, S. Sakaguchi, S.J. DeArmond, S.B. Prusiner, and S. Katamine. 1999. A mouse prion protein transgene rescues mice deficient for the prion protein gene from purkinje cell degeneration and demyelination. *Lab Invest* 79:689-697.

170 Nixon, R.A. 2013. The role of autophagy in neurodegenerative disease. *Nat Med* 19:983-997.

171 Norris, A., P. Tammineni, S. Wang, J. Gerdes, A. Murr, K.Y. Kwan, Q. Cai, and B.D. Grant. 2017. SNX-1 and RME-8 oppose the assembly of HGRS-1/ESCRT-0 degradative microdomains on endosomes. *Proceedings of the National Academy of Sciences of the United States of America* 114:E307-E316.

172 Numrich, J., and C. Ungermann. 2014. Endocytic Rabs in membrane trafficking and signaling. *Biological chemistry* 395:327-333.

173 Nuvolone, M., M. Hermann, S. Sorce, G. Russo, C. Tiberi, P. Schwarz, E. Minikel, D. Sanoudou, P. Pelczar, and A. Aguzzi. 2016. Strictly co-isogenic C57BL/6J-Prnp-/- mice: A rigorous resource for prion science. *J Exp Med* 213:313-327.

174 Nuvolone, M., M. Paolucci, S. Sorce, V. Kana, R. Moos, T. Matozaki, and A. Aguzzi. 2017. Prion pathogenesis is unaltered in the absence of SIRPα-mediated "don't-eat-me" signaling. *PLoS One* 12:e0177876.

175 Oshima, M., T. Seki, Y. Kurauchi, A. Hisatsune, and H. Katsuki. 2019. Reciprocal Regulation of Chaperone-Mediated Autophagy/Microautophagy and Exosome Release. *Biol Pharm Bull* 42:1394-1401.

176 Ostrowski, M., N.B. Carmo, S. Krumeich, I. Fanget, G. Raposo, A. Savina, C.F. Moita, K. Schauer, A.N. Hume, R.P. Freitas, B. Goud, P. Benaroch, N. Hacohen, M. Fukuda, C. Desnos, M.C. Seabra, F. Darchen, S. Amigorena, L.F. Moita, and C. Thery. 2010. Rab27a and Rab27b control different steps of the exosome secretion pathway. *Nature cell biology* 12:19-30; sup pp 11-13.

177 Owen, F., M. Poulter, R. Lofthouse, J. Collinge, T.J. Crow, D. Risby, H.F. Baker, R.M. Ridley, K. Hsiao, and S.B. Prusiner. 1989. Insertion in prion protein gene in familial Creutzfeldt-Jakob disease. *Lancet* 1:51-52.

178 Parry, H.B. 1960. Scrapie: a transmissible hereditary disease of sheep. *Nature* 185:441-443.

179 Peebles, C.L., J. Yoo, M.T. Thwin, J.J. Palop, J.L. Noebels, and S. Finkbeiner. 2010. Arc regulates spine morphology and maintains network stability in vivo. *Proceedings of the National Academy of Sciences of the United States of America* 107:18173-18178.

180 Peggion, C., R. Stella, F. Chemello, M.L. Massimino, G. Arrigoni, S. Cagnin, G. Biancotto, C. Franchin, M.C. Sorgato, and A. Bertoli. 2019. The Prion Protein Regulates Synaptic Transmission by Controlling the Expression of Proteins Key to Synaptic Vesicle Recycling and Exocytosis. *Mol Neurobiol* 56:3420-3436.

181 Peng, L., H. Liu, H. Ruan, W.H. Tepp, W.H. Stoothoff, R.H. Brown, E.A. Johnson, W.D. Yao, S.C. Zhang, and M. Dong. 2013. Cytotoxicity of botulinum neurotoxins reveals a direct role of syntaxin 1 and SNAP-25 in neuron survival. *Nat Commun* 4:1472.

182 Perdigão, C., M.A. Barata, M.N. Araújo, F.S. Mirfakhar, J. Castanheira, and C. Guimas Almeida. 2020. Intracellular Trafficking Mechanisms of Synaptic Dysfunction in Alzheimer's Disease. *Front Cell Neurosci* 14:72.

183 Peretz, D., M.R. Scott, D. Groth, R.A. Williamson, D.R. Burton, F.E. Cohen, and S.B. Prusiner. 2001. Strain-specified relative conformational stability of the scrapie prion protein. *Protein Sci* 10:854-863.

184 Perez-Gonzalez, R., S.A. Gauthier, A. Kumar, and E. Levy. 2012. The exosome secretory pathway transports amyloid precursor protein carboxyl-terminal fragments from the cell into the brain extracellular space. *J Biol Chem* 287:43108-43115.

185 Pfeffer, S.R. 2010. Two Rabs for exosome release. *Nature cell biology* 12:3-4.

186 Price, K.A., M. Varghese, A. Sowa, F. Yuk, H. Brautigam, M.E. Ehrlich, and D.L. Dickstein. 2014. Altered synaptic structure in the hippocampus in a mouse model of Alzheimer's disease with soluble amyloid-β oligomers and no plaque pathology. *Mol Neurodegener* 9:41.

187 Properzi, F., M. Logozzi, H. Abdel-Haq, C. Federici, L. Lugini, T. Azzarito, I. Cristofaro, D. di Sevo, E. Ferroni, F. Cardone, M. Venditti, M. Colone, E. Comoy, V. Durand, S. Fais, and M. Pocchiari. 2015. Detection of exosomal prions in blood by immunochemistry techniques. *The Journal of general virology* 96:1969-1974.

188 Prusiner, S.B. 1982. Novel proteinaceous infectious particles cause scrapie. *Science* 216:136-144.

189 Prusiner, S.B., R.A. Barry, M.P. McKinley, C.G. Bellinger, R.K. Meyer, S.J. DeArmond, and D.T. Kingsbury. 1985. Scrapie and Creutzfeldt-Jakob disease prions. *Microbiological sciences* 2:33-39.

190 Prusiner, S.B., W.J. Hadlow, C.M. Eklund, and R.E. Race. 1977. Sedimentation properties of the scrapie agent. *Proceedings of the National Academy of Sciences of the United States of America* 74:4656-4660.

191 Prusiner, S.B., and D.T. Kingsbury. 1985. Prions--infectious pathogens causing the spongiform encephalopathies. *CRC critical reviews in clinical neurobiology* 1:181-200.

192 Puri, C., M. Vicinanza, A. Ashkenazi, M.J. Gratian, Q. Zhang, C.F. Bento, M. Renna, F.M. Menzies, and D.C. Rubinsztein. 2018. The RAB11A-Positive Compartment Is a Primary Platform for Autophagosome Assembly Mediated by WIPI2 Recognition of PI3P-RAB11A. *Dev Cell* 45:114-131 e118.

193 Rezaie, P., and P.L. Lantos. 2001. Microglia and the pathogenesis of spongiform encephalopathies. *Brain Res Brain Res Rev* 35:55-72.

194 Rijal Upadhaya, A., E. Capetillo-Zarate, I. Kosterin, D. Abramowski, S. Kumar, H. Yamaguchi, J. Walter, M. Fändrich, M. Staufenbiel, and D.R. Thal. 2012. Dispersible amyloid β-protein oligomers, protofibrils, and fibrils represent diffusible but not soluble aggregates: their role in neurodegeneration in amyloid precursor protein (APP) transgenic mice. *Neurobiology of aging* 33:2641-2660.

195 Robinson, S.W., M.L. Nugent, D. Dinsdale, and J.R. Steinert. 2014. Prion protein facilitates synaptic vesicle release by enhancing release probability. *Hum Mol Genet* 23:4581-4596.

196 Rozas, J.L., L. Gómez-Sánchez, J. Mircheski, P. Linares-Clemente, J.L. Nieto-González, M.E. Vázquez, R. Luján, and R. Fernández-Chacón. 2012. Motorneurons require cysteine string protein-α to maintain the readily releasable vesicular pool and synaptic vesicle recycling. *Neuron* 74:151-165.

197 Sadoul, R., M.H. Laporte, R. Chassefeyre, K.I. Chi, Y. Goldberg, C. Chatellard, F.J. Hemming, and S. Fraboulet. 2018. The role of ESCRT during development and functioning of the nervous system. *Semin Cell Dev Biol* 74:40-49.

198 Saman, S., W. Kim, M. Raya, Y. Visnick, S. Miro, B. Jackson, A.C. McKee, V.E. Alvarez, N.C. Lee, and G.F. Hall. 2012. Exosome-associated tau is secreted in tauopathy models and is selectively phosphorylated in cerebrospinal fluid in early Alzheimer disease. *J Biol Chem* 287:3842-3849.

199 Sandberg, M.K., H. Al-Doujaily, C.J. Sigurdson, M. Glatzel, C. O'Malley, C. Powell, E.A. Asante, J.M. Linehan, S. Brandner, J.D. Wadsworth, and J. Collinge. 2010. Chronic wasting disease prions are not transmissible to transgenic mice overexpressing human prion protein. *The Journal of general virology* 91:2651-2657.

200 Sarasa, R., A. Martínez, E. Monleón, R. Bolea, A. Vargas, J.J. Badiola, and M. Monzón. 2012. Involvement of astrocytes in transmissible spongiform encephalopathies: a confocal microscopy study. *Cell and tissue research* 350:127-134.

201 Schmidt, O., and D. Teis. 2012. The ESCRT machinery. *Curr Biol* 22:R116-120.

202 Scott, D.A., I. Tabarean, Y. Tang, A. Cartier, E. Masliah, and S. Roy. 2010. A pathologic cascade leading to synaptic dysfunction in alpha-synuclein-induced neurodegeneration. *J Neurosci* 30:8083-8095.

203 Scott, M.R., S. Supattapone, H.O. Nguyen, S.J. DeArmond, and S.B. Prusiner. 2000. Transgenic models of prion disease. *Archives of virology. Supplementum* 113-124.

204 Sevillano, A.M., P. Aguilar-Calvo, T.D. Kurt, J.A. Lawrence, K. Soldau, T.H. Nam, T. Schumann, D.P. Pizzo, S. Nystrom, B. Choudhury, H. Altmeppen, J.D. Esko, M. Glatzel, K.P.R. Nilsson, and C.J. Sigurdson. 2020. Prion protein glycans reduce intracerebral fibril formation and spongiosis in prion disease. *J Clin Invest* 130:1350-1362.

205 Sharma, M., J. Burré, P. Bronk, Y. Zhang, W. Xu, and T.C. Südhof. 2012. CSPα knockout causes neurodegeneration by impairing SNAP-25 function. *Embo j* 31:829-841.

206 Sharma, M., J. Burré, and T.C. Südhof. 2012. Proteasome inhibition alleviates SNARE-dependent neurodegeneration. *Science translational medicine* 4:147ra113.

207 Sheehan, P., M. Zhu, A. Beskow, C. Vollmer, and C.L. Waites. 2016. Activity-Dependent Degradation of Synaptic Vesicle Proteins Requires Rab35 and the ESCRT Pathway. *J Neurosci* 36:8668-8686.

208 Shim, S.Y., S. Karri, S. Law, H.M. Schatzl, and S. Gilch. 2016. Prion infection impairs lysosomal degradation capacity by interfering with rab7 membrane attachment in neuronal cells. *Sci Rep* 6:21658.

209 Shimizu, H., S. Kawamura, and K. Ozaki. 2003. An essential role of Rab5 in uniformity of synaptic vesicle size. *J Cell Sci* 116:3583-3590.

210 Shimojo, M., J. Madara, S. Pankow, X. Liu, J. Yates, 3rd, T.C. Südhof, and A. Maximov. 2019. Synaptotagmin-11 mediates a vesicle trafficking pathway that is essential for development and synaptic plasticity. *Genes & development* 33:365-376.

211 Sikorska, B., P.P. Liberski, and P. Brown. 2007. Neuronal autophagy and aggresomes constitute a consistent part of neurodegeneration in experimental scrapie. *Folia Neuropathol* 45:170-178.

212 Silveira, J.R., G.J. Raymond, A.G. Hughson, R.E. Race, V.L. Sim, S.F. Hayes, and B. Caughey. 2005. The most infectious prion protein particles. *Nature* 437:257-261.

213 Simpson, J.C., and A.T. Jones. 2005. Early endocytic Rabs: functional prediction to functional characterization. *Biochemical Society symposium* 99-108.

214 Siskova, Z., A. Page, V. O'Connor, and V.H. Perry. 2009. Degenerating synaptic boutons in prion disease: microglia activation without synaptic stripping. *Am J Pathol* 175:1610-1621.

215 Siso, S., L. Gonzalez, and M. Jeffrey. 2010. Neuroinvasion in prion diseases: the roles of ascending neural infection and blood dissemination. *Interdisciplinary perspectives on infectious diseases* 2010:747892.

216 Siso, S., M. Jeffrey, and L. Gonzalez. 2009. Neuroinvasion in sheep transmissible spongiform encephalopathies: the role of the haematogenous route. *Neuropathol Appl Neurobiol* 35:232-246.

217 Skibinski, G., N.J. Parkinson, J.M. Brown, L. Chakrabarti, S.L. Lloyd, H. Hummerich, J.E. Nielsen, J.R. Hodges, M.G. Spillantini, T. Thusgaard, S. Brandner, A. Brun, M.N. Rossor, A. Gade, P. Johannsen, S.A. Sørensen, S. Gydesen, E.M. Fisher, and J. Collinge. 2005. Mutations in the endosomal ESCRTIII-complex subunit CHMP2B in frontotemporal dementia. *Nature genetics* 37:806-808.

218 Smith, H.L., O.J. Freeman, A.J. Butcher, S. Holmqvist, I. Humoud, T. Schatzl, D.T. Hughes, N.C. Verity, D.P. Swinden, J. Hayes, L. de Weerd, D.H. Rowitch, R.J.M. Franklin, and G.R. Mallucci. 2020. Astrocyte Unfolded Protein Response Induces a Specific Reactivity State that Causes Non-Cell-Autonomous Neuronal Degeneration. *Neuron*

219 Snyder, E.M., Y. Nong, C.G. Almeida, S. Paul, T. Moran, E.Y. Choi, A.C. Nairn, M.W. Salter, P.J. Lombroso, G.K. Gouras, and P. Greengard. 2005. Regulation of NMDA receptor trafficking by amyloid-beta. *Nat Neurosci* 8:1051-1058.

220 Sonati, T., R.R. Reimann, J. Falsig, P.K. Baral, T. O'Connor, S. Hornemann, S. Yaganoglu, B. Li, U.S. Herrmann, B. Wieland, M. Swayampakula, M.H. Rahman, D. Das, N. Kav, R. Riek, P.P. Liberski, M.N. James, and A. Aguzzi. 2013. The toxicity of antiprion antibodies is mediated by the flexible tail of the prion protein. *Nature* 501:102-106.

221 Sorce, S., M. Nuvolone, G. Russo, A. Chincisan, D. Heinzer, M. Avar, M. Pfammatter, P. Schwarz, M. Delic, M. Muller, S. Hornemann, D. Sanoudou, C. Scheckel, and A. Aguzzi. 2020. Genome-wide transcriptomics identifies an early preclinical signature of prion infection. *PLoS Pathog* 16:e1008653.

222 Spagnolli, G., M. Rigoli, S. Orioli, A.M. Sevillano, P. Faccioli, H. Wille, E. Biasini, and J.R. Requena. 2019. Full atomistic model of prion structure and conversion. *PLoS Pathog* 15:e1007864.

223 Spencer, B., C. Kim, T. Gonzalez, A. Bisquertt, C. Patrick, E. Rockenstein, A. Adame, S.J. Lee, P. Desplats, and E. Masliah. 2016. alpha-Synuclein interferes with the ESCRT-III complex contributing to the pathogenesis of Lewy body disease. *Hum Mol Genet* 25:1100-1115.

224 Star, E.N., A.J. Newton, and V.N. Murthy. 2005. Real-time imaging of Rab3a and Rab5a reveals differential roles in presynaptic function. *J Physiol* 569:103-117.

225 Stuffers, S., A. Brech, and H. Stenmark. 2009. ESCRT proteins in physiology and disease. *Experimental cell research* 315:1619-1626.

226 Sunyach, C., A. Jen, J. Deng, K.T. Fitzgerald, Y. Frobert, J. Grassi, M.W. McCaffrey, and R. Morris. 2003. The mechanism of internalization of glycosylphosphatidylinositol-anchored prion protein. *Embo j* 22:3591-3601.

227 Tahir, W., B. Abdulrahman, D.H. Abdelaziz, S. Thapa, R. Walia, and H.M. Schätzl. 2020. An astrocyte cell line that differentially propagates murine prions. *J Biol Chem*

228 Takahashi, R.H., T.A. Milner, F. Li, E.E. Nam, M.A. Edgar, H. Yamaguchi, M.F. Beal, H. Xu, P. Greengard, and G.K. Gouras. 2002. Intraneuronal Alzheimer abeta42

accumulates in multivesicular bodies and is associated with synaptic pathology. *Am J Pathol* 161:1869-1879.

229 Tamai, K., N. Tanaka, A. Nara, A. Yamamoto, I. Nakagawa, T. Yoshimori, Y. Ueno, T. Shimosegawa, and K. Sugamura. 2007. Role of Hrs in maturation of autophagosomes in mammalian cells. *Biochem Biophys Res Commun* 360:721-727.

230 Tamai, K., M. Toyoshima, N. Tanaka, N. Yamamoto, Y. Owada, H. Kiyonari, K. Murata, Y. Ueno, M. Ono, T. Shimosegawa, N. Yaegashi, M. Watanabe, and K. Sugamura. 2008. Loss of hrs in the central nervous system causes accumulation of ubiquitinated proteins and neurodegeneration. *Am J Pathol* 173:1806-1817.

231 Tamguney, G., M.W. Miller, L.L. Wolfe, T.M. Sirochman, D.V. Glidden, C. Palmer, A. Lemus, S.J. DeArmond, and S.B. Prusiner. 2009. Asymptomatic deer excrete infectious prions in faeces. *Nature* 461:529-532.

232 Tanikawa, S., F. Mori, K. Tanji, A. Kakita, H. Takahashi, and K. Wakabayashi. 2012. Endosomal sorting related protein CHMP2B is localized in Lewy bodies and glial cytoplasmic inclusions in α-synucleinopathy. *Neurosci Lett* 527:16-21.

233 Tao-Cheng, J.H. 2019. Stimulation induces gradual increases in the thickness and curvature of postsynaptic density of hippocampal CA1 neurons in slice cultures. *Mol Brain* 12:44.

234 Tixador, P., L. Herzog, F. Reine, E. Jaumain, J. Chapuis, A. Le Dur, H. Laude, and V. Beringue. 2010. The physical relationship between infectivity and prion protein aggregates is strain-dependent. *PLoS Pathog* 6:e1000859.

235 Uchiyama, K., N. Muramatsu, M. Yano, T. Usui, H. Miyata, and S. Sakaguchi. 2013. Prions disturb post-Golgi trafficking of membrane proteins. *Nature communications* 4:1846-1846.

236 Um, J.W., A.C. Kaufman, M. Kostylev, J.K. Heiss, M. Stagi, H. Takahashi, M.E. Kerrisk, A. Vortmeyer, T. Wisniewski, A.J. Koleske, E.C. Gunther, H.B. Nygaard, and S.M. Strittmatter. 2013. Metabotropic glutamate receptor 5 is a coreceptor for Alzheimer abeta oligomer bound to cellular prion protein. *Neuron* 79:887-902.

237 Uytterhoeven, V., S. Kuenen, J. Kasprowicz, K. Miskiewicz, and P. Verstreken. 2011. Loss of skywalker reveals synaptic endosomes as sorting stations for synaptic vesicle proteins. *Cell* 145:117-132.

238 Uytterhoeven, V., S. Kuenen, J. Kasprowicz, K. Miskiewicz, and P. Verstreken. 2011. Loss of skywalker reveals synaptic endosomes as sorting stations for synaptic vesicle proteins. *Cell* 145:117-132.

239 Vazquez-Fernandez, E., M.R. Vos, P. Afanasyev, L. Cebey, A.M. Sevillano, E. Vidal, I. Rosa, L. Renault, A. Ramos, P.J. Peters, J.J. Fernandez, M. van Heel, H.S. Young, J.R. Requena, and H. Wille. 2016. The Structural Architecture of an Infectious Mammalian Prion Using Electron Cryomicroscopy. *PLoS Pathog* 12:e1005835.

240 Vazquez-Sanchez, S., S. Bobeldijk, M.P. Dekker, L. van Keimpema, and J.R.T. van Weering. 2018. VPS35 depletion does not impair presynaptic structure and function. *Sci Rep* 8:2996.

241 Veith, N.M., H. Plattner, C.A. Stuermer, W.J. Schulz-Schaeffer, and A. Burkle. 2009. Immunolocalisation of PrPSc in scrapie-infected N2a mouse neuroblastoma cells by light and electron microscopy. *Eur J Cell Biol* 88:45-63.

242 Vella, L.J., B.J. Scicluna, L. Cheng, E.G. Bawden, C.L. Masters, C.S. Ang, N. Willamson, C. McLean, K.J. Barnham, and A.F. Hill. 2017. A rigorous method to enrich for exosomes from brain tissue. *J Extracell Vesicles* 6:1348885.

243 Vella, L.J., R.A. Sharples, V.A. Lawson, C.L. Masters, R. Cappai, and A.F. Hill. 2007. Packaging of prions into exosomes is associated with a novel pathway of PrP processing. *The Journal of pathology* 211:582-590.

244 Vicinanza, M., C. Puri, and D.C. Rubinsztein. 2019. Coincidence detection of RAB11A and PI(3)P by WIPI2 directs autophagosome formation. *Oncotarget* 10:2579-2580.

245 Vidyadhara, D.J., J.E. Lee, and S.S. Chandra. 2019. Role of the endolysosomal system in Parkinson's disease. *J Neurochem* 150:487-506.

246 Vilette, D., K. Laulagnier, A. Huor, S. Alais, S. Simoes, R. Maryse, M. Provansal, S. Lehmann, O. Andreoletti, L. Schaeffer, G. Raposo, and P. Leblanc. 2015. Efficient inhibition of infectious prions multiplication and release by targeting the exosomal pathway. *Cell Mol Life Sci* 72:4409-4427.

247 Vincenti, J.E., L. Murphy, K. Grabert, B.W. McColl, E. Cancellotti, T.C. Freeman, and J.C. Manson. 2015. Defining the Microglia Response during the Time Course of Chronic Neurodegeneration. *J Virol* 90:3003-3017.

248 Wadsworth, J.D., E.A. Asante, and J. Collinge. 2010. Review: contribution of transgenic models to understanding human prion disease. *Neuropathol Appl Neurobiol* 36:576-597.

249 Watson, J.A., B.J. Bhattacharyya, J.H. Vaden, J.A. Wilson, M. Icyuz, A.D. Howard, E. Phillips, T.M. DeSilva, G.P. Siegal, A.J. Bean, G.D. King, S.E. Phillips, R.J. Miller, and S.M. Wilson. 2015. Motor and Sensory Deficits in the teetering Mice Result from Mutation of the ESCRT Component HGS. *PLoS Genet* 11:e1005290.

250 Watts, J.C., M.E.C. Bourkas, and H. Arshad. 2018. The function of the cellular prion protein in health and disease. *Acta Neuropathol* 135:159-178.

251 Waung, M.W., B.E. Pfeiffer, E.D. Nosyreva, J.A. Ronesi, and K.M. Huber. 2008. Rapid translation of Arc/Arg3.1 selectively mediates mGluR-dependent LTD through persistent increases in AMPAR endocytosis rate. *Neuron* 59:84-97.

252 Wells, G.A., and J.W. Wilesmith. 1995. The neuropathology and epidemiology of bovine spongiform encephalopathy. *Brain Pathol* 5:91-103.

253 Welz, T., J. Wellbourne-Wood, and E. Kerkhoff. 2014. Orchestration of cell surface proteins by Rab11. *Trends Cell Biol* 24:407-415.

254 Wilham, J.M., C.D. Orru, R.A. Bessen, R. Atarashi, K. Sano, B. Race, K.D. Meade-White, L.M. Taubner, A. Timmes, and B. Caughey. 2010. Rapid end-point quantitation of prion seeding activity with sensitivity comparable to bioassays. *PLoS Pathog* 6:e1001217.

255 Wilkerson, J.R., J.P. Albanesi, and K.M. Huber. 2018. Roles for Arc in metabotropic glutamate receptor-dependent LTD and synapse elimination: Implications in health and disease. *Semin Cell Dev Biol* 77:51-62.

256 Wilkerson, J.R., N.P. Tsai, M.A. Maksimova, H. Wu, N.P. Cabalo, K.W. Loerwald, J.B. Dictenberg, J.R. Gibson, and K.M. Huber. 2014. A role for dendritic mGluR5-mediated local translation of Arc/Arg3.1 in MEF2-dependent synapse elimination. *Cell Rep* 7:1589-1600.

257 Will, R.G., J.W. Ironside, M. Zeidler, S.N. Cousens, K. Estibeiro, A. Alperovitch, S. Poser, M. Pocchiari, A. Hofman, and P.G. Smith. 1996. A new variant of Creutzfeldt-Jakob disease in the UK. *Lancet* 347:921-925.

258 Williamson, L.C., and E.A. Neale. 1998. Syntaxin and 25-kDa synaptosomal-associated protein: differential effects of botulinum neurotoxins C1 and A on neuronal survival. *Journal of neuroscience research* 52:569-583.

259 Wu, J., R.S. Petralia, H. Kurushima, H. Patel, M.Y. Jung, L. Volk, S. Chowdhury, J.D. Shepherd, M. Dehoff, Y. Li, D. Kuhl, R.L. Huganir, D.L. Price, R. Scannevin, J.C. Troncoso, P.C. Wong, and P.F. Worley. 2011. Arc/Arg3.1 regulates an endosomal pathway essential for activity-dependent beta-amyloid generation. *Cell* 147:615-628.

260 Wucherpfennig, T., M. Wilsch-Brauninger, and M. Gonzalez-Gaitan. 2003. Role of Drosophila Rab5 during endosomal trafficking at the synapse and evoked neurotransmitter release. *J Cell Biol* 161:609-624.

261 Wulf, M.A., A. Senatore, and A. Aguzzi. 2017. The biological function of the cellular prion protein: an update. *BMC biology* 15:34.

262 Xu, W., A.M. Weissmiller, J.A. White, 2nd, F. Fang, X. Wang, Y. Wu, M.L. Pearn, X. Zhao, M. Sawa, S. Chen, S. Gunawardena, J. Ding, W.C. Mobley, and C. Wu. 2016. Amyloid precursor protein-mediated endocytic pathway disruption induces axonal dysfunction and neurodegeneration. *J Clin Invest* 126:1815-1833.

263 Xu, Y., C. Tian, S.B. Wang, W.L. Xie, Y. Guo, J. Zhang, Q. Shi, C. Chen, and X.P. Dong. 2012. Activation of the macroautophagic system in scrapie-infected experimental animals and human genetic prion diseases. *Autophagy* 8:1604-1620.

264 Yamasaki, T., A. Suzuki, R. Hasebe, and M. Horiuchi. 2018. Retrograde Transport by Clathrin-Coated Vesicles is Involved in Intracellular Transport of PrP(Sc) in Persistently Prion-Infected Cells. *Sci Rep* 8:12241.

265 Yi, J.J., and M.D. Ehlers. 2007. Emerging roles for ubiquitin and protein degradation in neuronal function. *Pharmacological reviews* 59:14-39.

266 Yim, Y.I., B.C. Park, R. Yadavalli, X. Zhao, E. Eisenberg, and L.E. Greene. 2015. The multivesicular body is the major internal site of prion conversion. *J Cell Sci* 128:1434-1443.

267 Young, J.E., L.K. Fong, H. Frankowski, G.A. Petsko, S.A. Small, and L.S.B. Goldstein. 2018. Stabilizing the Retromer Complex in a Human Stem Cell Model of Alzheimer's Disease Reduces TAU Phosphorylation Independently of Amyloid Precursor Protein. *Stem Cell Reports* 10:1046-1058.

268 Zabeo, D., A. Cvjetkovic, C. Lasser, M. Schorb, J. Lotvall, and J.L. Hoog. 2017. Exosomes purified from a single cell type have diverse morphology. *J Extracell Vesicles* 6:1329476.

269 Zhang, J., J. Liu, A. Norris, B.D. Grant, and X. Wang. 2018. A novel requirement for ubiquitin-conjugating enzyme UBC-13 in retrograde recycling of MIG-14/Wntless and Wnt signaling. *Molecular biology of the cell* 29:2098-2112.

270 Zhu, C., U.S. Herrmann, J. Falsig, I. Abakumova, M. Nuvolone, P. Schwarz, K. Frauenknecht, E.J. Rushing, and A. Aguzzi. 2016. A neuroprotective role for microglia in prion diseases. *J Exp Med* 213:1047-1059.

271 Zou, W., M. Lai, Y. Zhang, L. Zheng, Z. Xing, T. Li, Z. Zou, Q. Song, X. Zhao, L. Xia, J. Yang, A. Liu, H. Zhang, Z.K. Cui, Y. Jiang, and X. Bai. 2019. Exosome Release Is Regulated by mTORC1. *Adv Sci (Weinh)* 6:1801313.

272 Zulkefli, K.L., F.J. Houghton, P. Gosavi, and P.A. Gleeson. 2019. A role for Rab11 in the homeostasis of the endosome-lysosomal pathway. *Experimental cell research* 380:55-68.